Modeling and Optimization of Multiple Access for 5G Networks and Beyond

by

Joao Victor DE CARVALHO EVANGELISTA

MANUSCRIPT-BASED THESIS PRESENTED TO ÉCOLE DE TECHNOLOGIE SUPÉRIEURE IN PARTIAL FULFILLMENT FOR THE DEGREE OF DOCTOR OF PHILOSOPHY
Ph.D.

MONTREAL, OCTOBER 29, 2021

ÉCOLE DE TECHNOLOGIE SUPÉRIEURE
UNIVERSITÉ DU QUÉBEC

BOARD OF EXAMINERS

THIS THESIS HAS BEEN EVALUATED

BY THE FOLLOWING BOARD OF EXAMINERS

Mr. Georges Kaddoum, Thesis supervisor
Department of Electrical Engineering, École de technologie supérieure

Mr. Segla Kpodjedo, President of the board of examiners
Department of Software Engineering, École de technologie supérieure

Mr. Naïm Batani, Member of the jury
Department of Electrical Engineering, École de technologie supérieure

Mr. Chadi Assi, External examiner
Concordia Institute for Information Systems Engineering, Concordia University

THIS THESIS WAS PRESENTED AND DEFENDED

IN THE PRESENCE OF A BOARD OF EXAMINERS AND THE PUBLIC

ON OCTOBER 21, 2021

AT ÉCOLE DE TECHNOLOGIE SUPÉRIEURE

FOREWORD

The work contained in this thesis consists of the research outcomes accomplished during my doctoral degree under the supervision of Dr. Georges Kaddoum from August 2016 to August 2021. This work was financially supported by the Mitacs Globalink Graduate Fellowship, the FRQNT B2X Fellowship and the Mitacs Accelerate Fellowship.

The main topic of this thesis is the modelling and optimization of multiple access technologies for 5G networks and beyond. During my Ph.D. studies, I composed one accepted conference paper, one accepted journal paper and two journal papers currently under review. Additionally, I was a co-author on five journal papers, one conference paper and one magazine article.

The first two chapters of the thesis include the background of multiple access technologies and an in-depth review of the state-of-the-art. The remaining chapters are based on the publications authored during my doctorate. Finally, chapter six presents the conclusions of the thesis and presents future research directions.

ACKNOWLEDGEMENTS

Firstly, I would like to acknowledge my gratitude to Dr. Georges Kaddoum for his mentorship and supervision. He has been a constant source of encouragement, guidance and inspiration throughout the whole duration of my Ph.D. I appreciate his patience and comprehension immensely during the COVID-19 pandemic that delayed the progress of my research due to personal issues I faced. I sincerely hope we can continue our work collaborations in the future, and I am happy to call him a friend.

Besides my supervisor, I would like to thank my collaborators, Dr. Francisco Escribano, Dr. Alexandre Wagemakers, Dr. Aydin Sarraf and Dr. Basile Agba. I am deeply grateful to all my labmates from the LaCIME group who made the Ph.D. experience less lonesome, including Elie, Dr. Bassant, Dawa, Dr. Long, Dr. Vu, Dat, Jung, Ibrahim, Hamza and Ali. I dedicate a special thanks to Dr. Zeeshan Sattar, who was my main collaborator and with whom I became close friends. I am also thankful to my master supervisors, Dr. Daniel Chaves and Dr. Cecilio Pimentel. Their mentorship was fundamental for becoming the professional and person I am today.

I am forever indebted to my parents, Ricardo and Elcyene, who instilled in me a deep appreciation for my education and helped shape me into the man I am today. Without their sacrifices, I would not have the opportunities I had in life and would never have reached this far.

Finally, I'd like to show my appreciation to my partner Julia. She was fundamental in helping me keep my sanity during the 18 months and counting of isolation and social distancing during the COVID-19 pandemic.

Modélisation et Optimisation des Accès Multiples sur les Réseaux 5G et Au-Delà

Joao Victor DE CARVALHO EVANGELISTA

RÉSUMÉ

Au cours des cinq dernières années, la 5G est passée d'un ensemble d'exigences à une norme de communication cellulaire entièrement spécifiée. Les objectifs de conception de la 5G ont suivi la tendance des normes LTE et ont ajouté la prise en charge de nouveaux services parallèlement aux améliorations des communications voix et données. Naturellement, ces nouveaux services ont des exigences de qualité de service différentes de celles des applications voix et données. Pour prendre en charge une myriade d'applications différentes avec des exigences distinctes, la conception des spécifications 5G doit être très flexible, prenant en charge plusieurs numérologies, structures de trames et procédures d'accès aléatoire. Ces changements ont exigé une refonte radicale de plusieurs technologies utilisées dans les réseaux précédents, notamment en repensant l'accès multiple.

Les nouveaux services pris en charge par la 5G sont regroupés en trois ensembles d'applications en fonction de leurs besoins : l'évolution du haut-débit mobile (eMBB), les communications machine massives (mMTC) et les communications à ultra haute fiabilité et faible latence (URLLC). Alors que les services eMBB font principalement référence à l'amélioration des applications de données actuelles, les applications mMTC et URLLC n'étaient auparavant pas prises en charge par les anciennes normes cellulaires.

Au moment de la rédaction de cette thèse, la spécification de la 5G non autonome, essentiellement la 5G fonctionnant au-dessus des réseaux LTE existants, est terminée. La spécification de la 5G autonome devrait être finalisée dans l'année à venir. Néanmoins, le développement de nouvelles normes cellulaires est un processus progressif, et il reste encore beaucoup à faire pour répondre aux exigences stipulées pour les réseaux 5G et au-delà. Par conséquent, le sujet principal de ce travail est de proposer de nouveaux modèles mathématiques pour permettre l'évaluation théorique des performances des réseaux 5G en ce qui concerne l'accès multiple et de proposer de nouvelles méthodes d'optimisation pour garantir les performances nécessaires aux services 5G. Dans ce contexte, le deuxième chapitre de cette thèse s'intéresse à l'optimisation de l'accès multiple à code clairsemé (SCMA). Le SCMA permet au réseau de servir plus d'utilisateurs que de ressources orthogonales, et émerge donc comme un catalyseur de connectivité massive. Nous formulons deux problèmes d'optimisation : l'un cherchant à maximiser le débit total du réseau et l'autre l'équité. Nous prouvons formellement la complexité des deux problèmes et proposons deux algorithmes d'optimisation sous-optimaux et comparons leurs performances avec d'autres algorithmes de la littérature. De plus, nous analysons l'impact des informations d'état de canal non à jour sur les performances des algorithmes.

Le troisième chapitre de cette thèse se concentre sur la modélisation des réseaux d'accès en liaison montante sans autorisation habilité par le SCMA. Nous modélisons ce système dans le cadre de la géométrie stochastique et dérivons des expressions analytiques de pour la densité

spectrale de surface et la probabilité de réussite de la transmission. Enfin, nous comparons les performances et l'évolutivité du SCMA avec un système d'accès multiple orthogonal.

Dans le quatrième chapitre, nous concentrons nos efforts sur les aspects du service URLLC. Nous considérons un système d'accès en liaison montante sans autorisation fonctionnant sur le spectre des ondes millimétriques avec des stations de base équipées de réseaux d'antennes massifs pour effectuer une formation de faisceau conjuguée afin de séparer les signaux de differents utilisateurs. Nous utilisons un modèle géométrique stochastique spatio-temporel pour dériver des expressions pour la fiabilité du système et la probabilité de défaillance d'accès, et du délai. Enfin, nous étudions l'impact du nombre d'antennes de stations de base sur les performances et évaluons l'adéquation de ce schéma pour satisfaire les exigences strictes de qualité de service des applications URLLC.

Le cinquième chapitre de cette thèse concerne le problème d'adaptation de la liaison distribuée dans le cadre d'une transmission sans autorisation en liaison montante dans un système mMTC. Comme les applications mMTC sont limitées en puissance, nous modélisons le problème comme une minimisation intercouche de puissance moyenne sous des contraintes de délai spécifiques à l'utilisateur. Nous formulons le problème sous la forme d'un jeu stochastique partiellement observable et proposons trois algorithmes distribués différents basés sur l'apprentissage par renforcement. Nous évaluons les performances des algorithmes concernant la consommation électrique moyenne et le délai du réseau. De plus, nous comparons les performances des algorithmes avec une solution de base basée sur un protocole de demande de répétition automatique hybride réactif augmentant la puissance. Nous concluons le chapitre en analysant les compromis impliquant les performances des algorithmes et la surcharge de signalisation qu'ils nécessitent.

Mots-clés: 5G, réseaux d'accès de liaison montante sans autorisation, accès multiple, mMTC, URLLC

Modeling and Optimization of Multiple Access for 5G Networks and Beyond

Joao Victor DE CARVALHO EVANGELISTA

ABSTRACT

5G has evolved from a set of requirements to a fully specified cellular communication standard in the last five years. 5G's design goals followed the trend in LTE standards and added support to new services alongside voice and data communications improvements. Naturally, these new services have different quality of service requirements than voice and data applications. To support a myriad of different services with distinct requirements, the design of 5G specifications must be highly flexible, supporting multiple numerologies, frame structures, and random access procedures. These changes demanded a radical redesign of several technologies used in previous networks, including rethinking multiple access.

The new services supported by 5G are grouped into three sets of applications based on their requirements: enhanced Mobile Broadband (eMBB), massive Machine Type Communication (mMTC), and Ultra-Reliable Low-Latency Communications (URLLC). While eMBB services mainly refer to the enhancement of current data applications, both mMTC and URLLC address applications not supported by past cellular standards.

At the time of writing this thesis, the specification of non-standalone 5G, basically 5G operating on top of legacy LTE networks, is finished. The specification for standalone 5G should be finalized in the coming year. Nonetheless, the development of new cellular standards is a gradual process, and there is much work to be done to fulfill the requirements stipulated for 5G networks. Therefore, the main topic of this work is to propose novel mathematical models to allow the theoretical evaluation of the performance of 5G networks with regards to the multiple access and propose novel optimization methods to guarantee the performance needed for the 5G service.

In this setting, the second chapter of this thesis is concerned with optimizing sparse code multiple access (SCMA). SCMA allows the network to schedule more users than orthogonal resources, emerging as an enabler of massive connectivity. We formulate two optimization problems: one seeking to maximize the sum rate of the network and the other the fairness. We formally prove the complexity of both problems and propose two sub-optimal optimization algorithms and compare their performances with available algorithms from the literature. Moreover, we analyze the impact of outdated channel state information on the algorithms performance.

The third chapter of this thesis focuses on the modelling of SCMA enabled grant-free access networks. We model this system within the stochastic geometry framework and derive closed-form analytical expressions for the area spectral density and the probability of transmission success. Finally, we compare SCMA's performance and scalability with an orthogonal multiple access system.

In the fourth chapter, we focus our efforts on the multiple access aspects of the uplink URLLC service. We consider a grant-free access system operating on the millimetre-wave spectrum

with base stations equipped with massive antenna arrays to perform conjugate beamforming to separate the signal from distinct users. We use a spatiotemporal stochastic geometric model to derive closed-form expressions for the system's reliability and latent access failure probability. Finally, we investigate the impact of the number of base station antennas on the performance and evaluate the suitability of this scheme to satisfy the stringent URLLC quality of service requirements.

The fifth chapter of this thesis concerns the distributed link adaptation problem of the uplink transmissions in a grant-free mMTC system. As mMTC applications are power limited, we model the problem as a cross-layer average power minimization under user-specific delay constraints. We formulate the problem as a partially observable stochastic game and propose three different distributed algorithms based on reinforcement learning. We evaluate the performance of the algorithms concerning the network's average power consumption and delay. Furthermore, we compare the algorithms' performance with a baseline solution based on a power-boosting reactive hybrid automatic repeat request protocol. We conclude the chapter by analyzing the tradeoffs involving the algorithms' performance and the signalling overhead they require.

Keywords: 5G, grant-free access, multiple access, mMTC, URLLC

TABLE OF CONTENTS

Page

LIST OF TABLES

LIST OF FIGURES

LIST OF ALGORITHMS

Page

LIST OF ABBREVIATIONS

3GPP	3rd Generation Partnership Project
5G	Fifth Generation
ACK	Acknowledgement
ADAM	Adaptive Moment Estimation
AMC	Adaptive Modulation And Coding
ANN	Artificial Neural Network
AR	Augmented Reality
ASE	Area Spectral Efficiency
AWGN	Additive White Gaussian Noise
BER	Bit Error Rate
BLER	Block Error Rate
BP	Belief Propagation
BS	Base Station
BSUM	Block Successive Upper-Bound Minimization
BSLM	Block Successive Lower-Bound Maximization
CBA	Contention-Based Access
CCDF	Complementary Cumulative Distribution Function
CDMA	Code Division Multiple Access
CD-NOMA	Code-Division Non-Orthogonal Multiple Access

CERT	Concurrent Experience Replay Trajectories
cIoT	Critical Internet Of Things
CLDI	Centralized Learning With Decentralized Inference
CMDP	Constrained Markov Decision Process
CNN	Convolutional Neural Network
CSI	Channel State Information
CSMA/CA	Subcarrier Sensing Multiple Access/collision Avoidance
CSMA	Subcarrier Sensing Multiple Access
CW	Congestion Window
D2D	Device-to-Device
DACC	Distributed Actors With Centralized Critic
DC	Difference of Convex
DCQN	Deep Convolutional Q Network
Dec-POMDP	Decentralized Partially Observable Markov Decision Process
DER	Damped Exploration Renewal
DFS	Dynamic Frequency Selection
DNN	Deep Neural Network
DPM	Dynamic Power Management
DQL	Deep Q-learning
DQN	Deep Q-network

DRL	Deep Reinforcement Learning
eMBB	Enhanced Mobile Broadband
FIFO	First-in First-out
FUO	Fixed User Order
FR1	Frequency Range 1
FR2	Frequency Range 2
GFRA	Grant-free Random Access
GRU	Gated Recurrent Unit
H2H	Human-to-human
HARQ	Hybrid Automatic Repeat Request
HPPP	Homogeneous Poisson Point Process
ICI	Inter-Carrier Interference
i.i.d.	Independent And Identically Distributed
IL	Independent Learners
IoT	Internet Of Things
IQL	Independent Q-learning
ISI	Inter-Symbol Interference
JAL	Joint Action Learners
KPI	Key Performance Indicator
LAFP	Latent Access Failure Probability

LOS	Line-of-sight
LSD	List Spherical Decoding
LSTM	Long Short Term Memory
LTE	Long Term Evolution
M2M	Machine-to-machine
MAC	Medium Access Control
MAP	Maximum A Posteriori
MARL	Multiagent Reinforcement Learning
MC-CDMA	Multicarrier Code-Division Multiple Access
MDP	Markov Decision Process
MIMO	Multiple Input Multiple Output
MINLP	Mixed-Integer Nonlinear Programming
ML	Maximum Likelihood
mMTC	Massive Machine-type Communication
MPA	Message Passing Algorithm
MUD	Multi-user Decoding
MUST	Multiuser Superposition Transmission
mmWave	Millimeter Wave
MTD	Machine-type Device
NACK	Negative Acknowledgement

NB-IoT	Narrowband Internet Of Things
NLOS	Non Line-of-sight
NOMA	Non-orthogonal Multiple Access
NR	New Radio
OA	Opportunistic Allocation
OFDMA	Orthogonal Frequency Division Multiple Access
OFDM	Orthogonal Frequency Division Multiplexing
OMA	Orthogonal Multiple Access
PAPR	Peak Average Power Ratio
PDF	Probability Density Function
PD-NOMA	Power-Division Non-Orthogonal Multiple Access
PF	Proportional Fair
PGFL	Probability Generating Functional
PMF	Probability Mass Function
PHY	Physical Layer
PLR	Packet Loss Rate
PMF	Probability Mass Function
POSG	Partially Observable Stochastic Game
PPO	Proximal Policy Optimization
PRACH	Physical Random Access Channel

PSMA	Power Domain Sparse Code Multiple Access
PUSCH	Physical Uplink Shared Channel
QAM	Quadrature Amplitude Modulation
QoS	Quality Of Service
RACH	Random Access Channel
RAR	Random Access Request
RA	Random Access
RE	Resource Element
RL	Reinforcement Learning
RSMA	Rate-Splitting Multiple Access
RTT	Round-trip Time
SCMA	Sparse Code Multiple Access
SDMA	Space-Division Multiple Access
SER	Symbol Error Rate
SGD	Stochastic Gradient Descent
SIC	Successive Interference Cancellation
SIR	Signal-to-Interference Ratio
SINR	Signal To Interference Plus Noise Ratio
SPS	Semi-persistent Scheduling
TDMA	Time Division Multiple Access

TFE	Trajectory Feature Extraction
TRPO	Trust Region Policy Optimization
TTI	Transmission Time Interval
UE	User Equipment
ULA	Uniform Linear Array
URLLC	Ultra Reliable Low-latency Communication
V2X	Vehicle-to-everything
VR	Virtual Reality
WAP	Wireless Access Point
ZF	Zero-Forcing

LIST OF SYMBOLS AND UNITS OF MEASUREMENTS

x	Scalar
$\mathbf{x}$	Vector
$\mathbf{X}$	Matrix
$\mathbf{x}^T$	Transpose
$\mathbf{x}^H$	Hermitian transpose
$\mathcal{X}$	Set
$\|\mathcal{X}\|$	Cardinality of a set
$\mathbb{R}$	Set of real numbers
$\mathbb{C}$	Set of complex numbers
$\mathbb{B}$	Set of binary numbers
$\mathbf{\Phi}$	Point process
$\mathbf{\Phi}(\cdot)$	Counting measure of a point process
$\mathcal{N}(\cdot,\cdot)$	Normal distribution
$\mathcal{CN}(\cdot,\cdot)$	Circularly symmetric complex normal distribution
$Binomial(\cdot)$	Binomial distribution
$Uniform(\cdot,\cdot)$	Uniform distribution
$E(\cdot)$	Expectation operator
$\mathbb{P}(\cdot)$	Probability function
$\mathbf{1}(\cdot)$	Indicator function

$\exp(\cdot)$	Exponential function
$\mathrm{tr}(\cdot)$	Trace function
$\det(\cdot)$	Determinant function
$\ln(\cdot)$	Natural logarithm
$\log_2(\cdot)$	Base-2 logarithm
$\Gamma(\cdot)$	Gamma function
$\gamma(\cdot,\cdot)$	Upper-incomplete gamma function
$\tanh(\cdot)$	Hyperbolic tangent function

INTRODUCTION

0.1 Motivation

In the past decades, wireless communications have significantly impacted several industries and shaped how people interact nowadays. Military goals drove the first efforts on wireless communication development, and for a long time, access to this technology remained out of the reach of the general public. First-generation systems (1G) were introduced in the early eighties and introduced the public to the possibility of communication without the need for wires. Second-generation systems (2G) switched from the analog modulated signals of 1G to digitally modulated ones, where the voice was quantized, modulated and transmitted as a continuous stream of bits. This transition was motivated by the higher capacity, improved cost, efficiency, and speed of digital systems. Data applications were gradually introduced in 2G systems and were consolidated on third-generation systems (3G). 3G maintained voice support and added support for data transmission over circuit-switched systems. The evolution of electronic hardware made handheld devices with huge computing power possible. This resulted in a higher demand for widespread connectivity and new data-hungry services, which required similar performance as wired broadband systems. This new demand gave birth to fourth-generation systems (4G) purely focused on data services. Voice over internet protocol (VoIP) and voice over long term evolution (VoLTE) were introduced to provide voice and multimedia services using packet data to replace the previous circuit-switched format. Despite the increased data rates brought by 4G, there are new consumer demands that this technology cannot satisfy. For instance, the introduction of augmented reality (AR), the increase of multimedia over voice services, and the massive connectivity required by the internet of things (IoT).

In this context, fifth-generation (5G) cellular networks are designed with the ambitious goals of satisfying multiple emergent use-cases with conflicting requirements. Thus, 5G services are split into three categories according to their quality of service (QoS) requirements:

- **Enhanced Mobile Broadband (eMBB)**: This category consists of most of the services previously offered by LTE. So, eMBB service targets traditional human-to-human (H2H) communications, transmitting both voice and data. Thus, the mission of the 5G eMBB technologies is to enhance the QoS by supporting larger data volumes, better user experience, higher data rates, and higher mobility.
- **Massive Machine-Type Communication (mMTC)**: This category consists of services aimed at applications consisting on a massive number of machine type devices (MTDs), such as remote sensors and smart city monitoring. This type of applications have fundamentally different QoS requirements from traditional services under the eMBB umbrella. MTDs usually have to transmit small packets sporadically and usually do not require high data rates and large data volumes. Moreover, these devices must operate with very little power consumption, enabling extremely long battery life (up to tens of years).
- **Ultra Reliable Low-Latency Communications (URLLC)**: This category encompasses critical services that require low-latency and very high reliability, such as critical IoT (cIoT) systems, vehicular networks, urban safety and critical industrial automation.

Despite the development of 5G, LTE networks are not going anywhere. Therefore, the integration and coexistence of LTE and 5G is another topic of concern to radio engineers and researchers alike.

In order to meet the ambitious goals set by 5G specifications, the third generation partnership project (3GPP), a consortium of worldwide telecommunication standards organizations, decided that a complete redesign of the radio access technology (RAT) was necessary. In the fall of 2015, the first steps towards this goal were taken to introduce a new RAT standard, namely 5G New Radio (NR). The standardization process of NR is done in steps marked by 3GPP releases. In December 2020, 3GPP release 17 (the third release of 5G standards) was unveiled, and currently, the standards organizations and telecom companies are working on the specifications for release

18. So far, the leading technologies introduced by 5G NR are (Dahlman, Parkvall & Skold, 2018):

- Higher frequency operation and spectrum flexibility.
- Ultra-lean design.
- Flexible orthogonal frequency division multiplexing (OFDM) numerology.
- Flexible frame structure with slots of different durations.
- Flexible duplex schemes, with frequency division duplexing (FDD) and time division duplexing (TDD) being used in different frequency bands.
- Advanced antenna systems enabled by a massive number of antennas.
- Streamlined initial access and addition of two-step random access.
- Carrier aggregation and dual connectivity support between NR and LTE.
- Dual active protocol stack to reduce handover overhead.
- Crosslink interference mitigation and remote interference management.
- Integrated access backhaul.
- NR operation in unlicensed spectra.

The introduction of new technologies demands for new mathematical models to characterize the performance of 5G networks. Additionally, the goal of servicing new classes of applications has shifted the sole focus from improving the network data rates to more complex QoS requirements, such as low-latency and high reliability in URLLC applications and massive scalability in mMTC.

0.2 Problem Statement

In this thesis, we focus our efforts on the role of multiple access technologies in enabling the QoS requirements of 5G services. Traditionally, cellular networks follow an orthogonal multiple access (OMA) approach to user scheduling. Each user must request a channel, and the base station (BS) must resolve the requests and allocate dedicated orthogonal channels

(also referred to as grants) to these users to finally transmit their data. This method works pretty well to satisfy the QoS requirements of voice and data services. However, it has severe limitations to fulfill novel applications that 5G networks must serve. In this context, the adoption of non-orthogonal multiple access (NOMA) schemes has become a hot research topic within the wireless communications community (Vaezi *et al.*, 2019). In NOMA, multiple devices are allowed to share the same network resources (Ding, Yang, Fan & Poor, 2014). As the wireless spectrum is both finite and expensive, this enables the network to overload its resources, serving a larger number of users than in OMA, which is perfectly aligned with 5G applications that require massive connectivity. Additionally, NOMA can enhance the uplink ergodic sum rate of the network by benefiting from the near-far effect experienced by users near the BS and on the cell edge, and from the small scale fading (Wei, Yang, Ng, Yuan & Hanzo, 2019). However, users sharing the same resources will naturally interfere with each other, so careful optimization of the subcarrier scheduling, the user grouping, and the power allocation is essential to reap the benefits promised by NOMA technologies. Therefore, one of the objectives of this thesis is to study novel optimization strategies that optimize resource allocation in NOMA.

Furthermore, we consider the role of grant-free, as opposed to grant-based, uplink data transmission in fulfilling the QoS requirements of mMTC and URLLC services. In grant-based multiple access, the users must send a request for a dedicated channel before initiating data transmission. After receiving requests from all active users, the BS resolves conflicts and schedules dedicated network resources to receive the data transmission of selected users. This access paradigm is particularly suitable for eMBB services, primarily for H2H voice and data applications. LTE standards adopt it in a four-step random access procedure (Vilgelm, Schiessl, Al-Zubaidy, Kellerer & Gross, 2018). However, mMTC applications need to serve a massive number of user devices that transmit small packets sporadically, using the least amount of power possible. In this scenario, the devices might spend more power requesting a dedicated channel than transmitting data (Au *et al.*, 2014). In this setting, grant-free access presents

itself as an attractive solution. In grant-free access, the device transmits its data directly on the random access channel, potentially saving the power that would be spent requesting dedicated resources and even increasing its throughput (Gao & Dai, 2019). It is worth highlighting that grant-free access is subjected to collisions, requiring data retransmissions. Thus, grant-free access systems need to be well designed to obtain power savings in comparison to grant-based. This poses a challenging problem of optimizing the channel access in grant-free systems with little coordination from a central BS. Hence, in this thesis, we investigate aspects related to the decentralized optimization of grant-free access networks and their scalability with respect to the number of supported users.

On top of the power spent in the resource request procedure, grant-based access also incurs an additional latency. In LTE networks, it takes at least 10 ms to transmit a single packet from the moment it arrives at the physical layer queue. Therefore, grant-free access is a promising path to reach the stringent latency constraints required in URLLC networks. The analysis of URLLC applications required the development of new mathematical models. Typically, physical layer researchers would analyze the performance of cellular systems with detailed models for the wireless channel, user location and transmitted signals with little to no regard to the temporal aspects of the network. On the other hand, medium access control (MAC) and network layer research would analyze the systems' temporal aspects through detailed queuing models while abstracting most of the radio signals and propagation aspects. However, both physical and temporal aspects are of utmost importance to fully characterize the performance of URLLC services. This fomented the development of novel spatiotemporal models based on the integration of stochastic geometry with the temporal modeling of the network (Chisci, ElSawy, Conti, Alouini & Win, 2019). In this work, we are also concerned with developing mathematical models for the spatiotemporal analysis of the impact of new 5G technologies in URLLC services.

0.3 Research Objectives

The set of services expected to be supported by 5G and next-generation networks is exceptionally diverse. Thus, a one-size-fits-all approach to the network design is doom to fail. In this context, 5G NR is designed to be highly flexible and future-proof. As a consequence, distinct mathematical models are required to characterize the performance of different classes of services.

The broad objective of this thesis is to propose novel mathematical models and optimization algorithms to different multiple access technologies while incorporating the particularities of the service constraints and QoS requirements. More specifically, we focus on the following four objectives:

- Power-division multiplexing NOMA (PDM-NOMA), previously known as superposition coding, is superior to OMA (Wei *et al.*, 2019; Chen, Ding, Dai & Zhang, 2017; Zeng, Yadav, Dobre, Tsiropoulos & Poor, 2017; Liu, Pan, Zhang & Song, 2016) concerning its sum-rate and ergodic capacity. Moreover, from an information-theoretic perspective, SCMA can achieve better performance than PDM-NOMA (Moltafet, Yamchi, Javan & Azmi, 2018b). Therefore, this thesis aims to propose novel optimization methods for uplink SCMA in eMBB applications and the tradeoff between throughput maximization and fairness.
- When using NOMA, the network can overload its resources by scheduling more users than there are orthogonal resources available. This property makes NOMA a potential technology to enable massive connectivity in mMTC. Hence, this thesis aims to develop a mathematical model to characterize the performance of uplink grant-free SCMA in mMTC networks concerning its area spectral efficiency and scalability.
- When investigating novel access technologies, it is essential to characterize its interplay with other established 5G NR methods. So, the third objective of this research is to model the latency and scalability of uplink grant-free access using massive multiple-input

multiple-output (MIMO) BSs in millimetre wave (mmWave) frequencies serving URLLC applications.

- Grant-free access eliminates the overhead of requesting a dedicated channel, thus reducing the power and latency of a transmission attempt; however, it is susceptible to collisions. Accordingly, the optimization of the transmitted power, channel access attempt and modulation and coding selection (MCS) is crucial to avoid collisions when many users are contending for the same resources. As there is no central coordination to select these parameters, optimizing such networks is a challenging problem. Therefore, the fourth objective of this thesis is to propose decentralized optimization algorithms for grant-free mMTC networks.

0.4 Contributions and Outline

The thesis is structured according to the graph shown in Figure 0.1.

Chapter 1 includes a comprehensive literature review of NOMA, grant-free access, and their roles in 5G. We focus on the aspects and mathematical tools most relevant to the topics covered in the thesis.

In Chapter 2, we formulate the optimization problems to maximize the sum rate and the fairness of uplink SCMA systems. We prove that both problems are non-deterministic polynomial-time hard (NP-hard), and we propose two novel algorithms, based on the successive convex approximation (SCA) method (Razaviyayn, 2014). We show that these algorithms can find locally optimal solutions to the sub-problems and that they can perform algorithms designed through heuristics (Dabiri & Saeedi, 2018). Additionally, we establish the convergence rate of the algorithms and analyze their performance when only outdated channel state information (CSI) is available.

In Chapter 3, we consider a grant-free uplink SCMA network serving mMTC applications. We model both the users and the BSs in the system as homogeneous Poisson point processes (HPPPs) (Haenggi, 2013), and we obtain closed-form analytical expressions for both the probability of

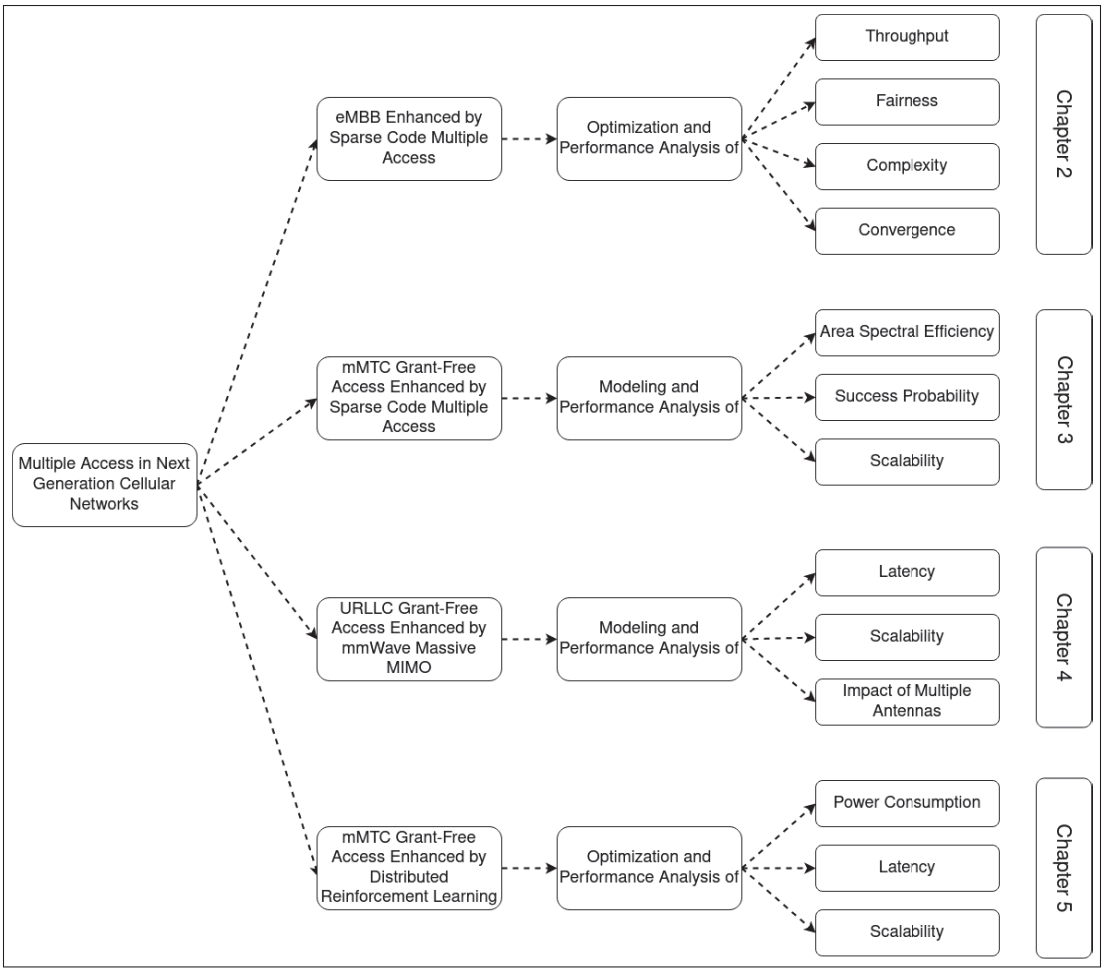

Figure 0.1 Diagram summarizing the thesis structure

success and the area spectral efficiency of this system. We do the same for OMA systems and compare their performance concerning the scalability and area spectral efficiency, showing the gains obtained by using SCMA.

In Chapter 4, we formulate a spatiotemporal model to characterize the performance of an uplink grant-free system serving URLLC applications. In this model, we consider that the BS is equipped with a massive antenna array and that the transmissions use the mmWave band of the spectrum. Also, we include the hybrid automatic repeat request (HARQ) mechanism in the performance analysis of the system. We analyze the network's performance with respect to the

reliability and latency while characterizing the impact of the number of antennas in the BS has on the performance for different URLLC QoS requirements.

In Chapter 5, we consider the problem of uplink MCS and channel access attempts in a cellular network designed to provide mMTC service. We formulate this problem as a power minimization under latency constraints. We show that this problem is intractable and propose three novel distributed solutions based on multiagent reinforcement learning (MARL). These distributed solutions differ from the overhead needed for exchanging information so the users can coordinate their access. We compare these algorithms with a baseline solution concerning the average power consumption, average latency, average collisions, and overhead.

Finally, we conclude this thesis by summarizing the conclusions from the main chapters and presenting recommendations for future works on the same subject.

CHAPTER 1

LITERATURE REVIEW

1.1 The 5G Standard

The standardization procedure of new cellular networks is a continuous process as new releases introduce new technologies to support a constantly developing class of services. Since the fall of 2015, the 3GPP started developing the 5G NR standards. So far, releases 15 and 16 have covered the basic specifications for non-standalone and standalone 5G, respectively. The 3GPP member organizations are currently developing the specifications of release 17, which is expected to be finalized and published in June 2022. In this section, we provide a literature review of the novel technologies introduced in 5G NR, and the supporting research literature, that are of relevance to the theme covered in this thesis.

1.1.1 Spectrum

Distinct frequency bands have distinct propagation characteristics. As a rule of thumb, electromagnetic waves in the higher end of the spectrum (tens of GHz) suffer from higher propagation, penetration, and blockage losses in comparison to waves on the lower-ends (hundreds of MHz) (Americas, 2020). From the Friis equation, the free space path loss of an electromagnetic wave is derived as

$$L_{FS} = \frac{P_T}{P_R} = \left(\frac{4\pi d}{\lambda}\right)^2, \tag{1.1}$$

where P_T and P_R are the transmitted and received powers, respectively, d is the distance between the transmitter and the receiver, and λ is the wavelength. Consequently, as the wave frequency increases (and the wavelength decreases), the received power decreases following an inverse square law. Moreover, objects in the wave's propagation path are relatively large compared to the wave's wavelength, resulting in more diffused scattering and higher attenuation of the signal.

Hence, the signal strength of reflected waves is significantly lower. Due to the severe signal strength loss experienced by these reflected signals, mmWave typically requires a line-of-sight (LOS) link.

For this reason, cellular standards up to LTE have used the spectrum bands from 450 MHz to 6 GHz to provide wide area coverage. On the other hand, electromagnetic signals on the higher end of the spectrum can transmit way more information. Two of the requirements of 5G networks are the hundred-fold and ten-fold increase in the area spectral efficiency and in the connection density, respectively, when compared to LTE (ITU, 2015) are impossible to be achieved without expanding the spectrum usage. Hence, to support such ambitious requirements, 5G NR release 15 standardized the spectrum usage in the mmWave range. The spectrum is divided into two regions (3GPP, 2021a):

- Frequency range 1 (FR1): from 410 MHz to 7125 MHz.
- Frequency range 2 (FR2): from 24.25 GHz to 52.6 GHz.

This spurred the need to adapt current wireless communications mathematical models and protocols to the particularities of mmWave propagation.

The importance of mmWave in 5G NR has attracted much attention from the wireless research community to the modelling of mmWave networks. In (Rappaport *et al.*, 2013), the authors present the motivation for mmWave systems, and the methodology and hardware required to analyze communications signals on the mmWave spectrum. They collect propagation measurements and propose statistical models to characterize the propagation characteristics of mmWave signals in urban environments in the 28 GHz and 38 GHz bands. In (Mezzavilla *et al.*, 2018), Mezzavilla *et al* introduce a discrete-event mmWave network simulator that enables the development of cross-layer simulations of 5G protocols. In (Thornburg, Bai & Heath, 2016), the authors propose several blockage models based on stochastic geometry to effectively model the impact of blockers in an extensive wireless network in a mathematically tractable way.

Besides modelling mmWave, a rich body of literature investigating mmWave as an enabling technology for various 5G services has been developed. In (Ford *et al.*, 2017), the authors

present a survey of the challenges and possible solutions involved in delivering end-to-end, reliable, ultra low-latency services in mmWave cellular systems. In (Roh *et al.*, 2014), the authors use collected measurements and theoretical propagation models to develop novel hybrid beamforming schemes. The authors perform link-level and system-level simulations and indoor and outdoor measurements to demonstrate the performance gains obtained by the proposed schemes.

1.1.2 Numerology and Transmission Structure

The (3GPP, 2021b) document defines 5G NR's transmission structure. Similar to LTE, 5G NR also uses an OFDM waveform for its time dispersion characteristics and the easiness of exploiting time and frequency domains when structuring different signals and channels, both in the uplink and downlink. However, while LTE has a fixed OFDM numerology (subcarrier spacing, cyclic prefix length and symbol duration), 5G NR employs a scalable numerology, designed to accomodate the requirementes of different services and operation on distinct frequency bands. Table 1.1 shows the five numerology configurations available on 5G NR.

Table 1.1 5G NR scalable numerology

Frequency Band	**Subcarrier Spacing (kHz)**	**Symbol Time (μs)**	**Cyclic Prefix (μs)**
FR1	15	66.7	4.7
FR1	30	33.3	2.3
FR1 & FR2	60	16.7	1.2
FR2	120	8.33	0.59
FR2	240	4.17	0.29

5G NR transmissions are split into frames composed of 10 equally divided subframes in the time domain. The subframes are, in turn, composed of slots, and each slot contains 14 OFDM symbols. One frame lasts 10 ms, and one subframe lasts 1 ms. The length of each slot depends on the numerology selected. Figure 1.1 shows the 5G NR frame structure for different numerologies. As the subframe length is fixed, the larger the subcarrier spacing, the more slots are contained

within the subframe. As each slot accounts for a different transmission opportunity, higher-order numerologies enable low-latency communications.

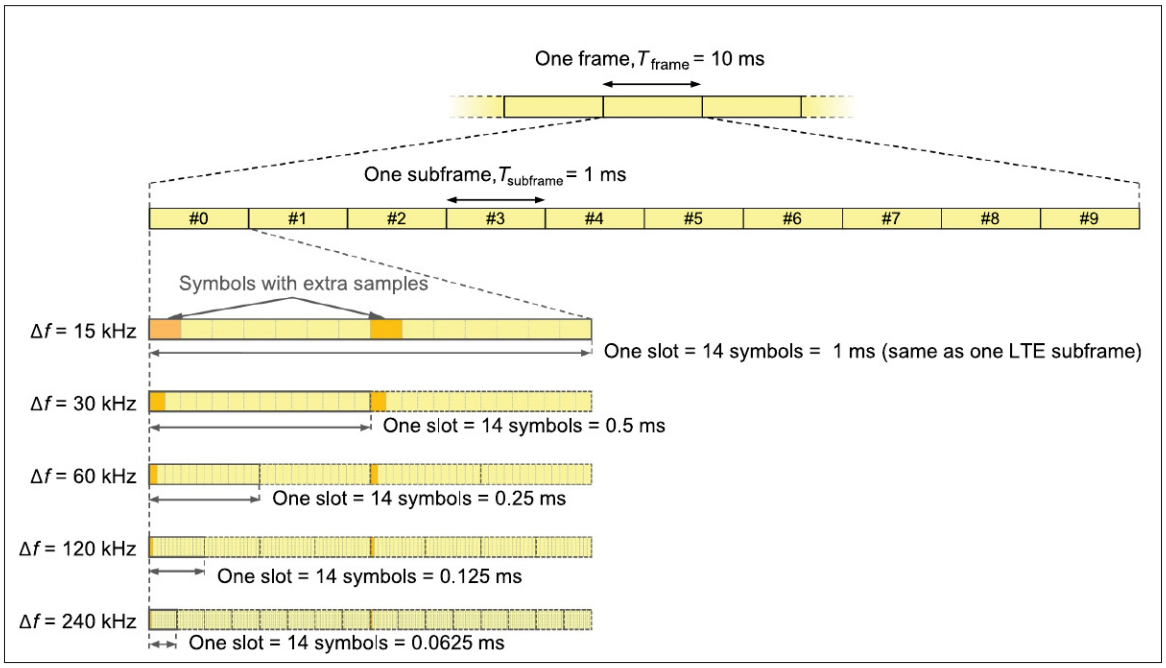

Figure 1.1 5G NR Frame
Taken From Dahlman *et al.* (2018)

1.1.3 Random Access

The 5G NR standards specification concerning random access is defined in (3GPP, 2018a). It offers two access options: four-step random access and two-step random access [1]. As the name suggests, four-step random access requires each user to undergo a four-step process to acquire a dedicated channel to transmits its data. These steps are summarized below:

- **Step 1:** The users who have packets in their queues transmit a randomly chosen orthogonal preamble. The user repeats this step until it receives the feedback indicated in Step 2.
- **Step 2:** The network transmits a random access response (RAR) signal back, indicating the reception of the preambles, along with necessary control information.

[1] The terms two-step random access, packet-based access, contention-based access, and grant-free access denote the same philosophy of random access. Additionally, four-step random access, connection-based access, contention-free access, and grant-based access also mean the same approach. In this thesis, we use all these synonyms interchangeably

- **Step 3:** The users send a message on the uplink to resolve contention (multiple users transmitting the same preamble on Step 1).
- **Step 4:** The network replies to the message sent on Step 3 with a contention resolution message.

This random access procedure must be realized on the initial access, during handover, to reestablish uplink synchronization, and whenever a device needs to transmit but has not been scheduled resources to do so yet.

We outline the steps required to perform two-step random access below:

- **Step 1:** The users who have packets in their queues transmit a randomly chosen orthogonal preamble together with its payload.
- **Step 2:** The network sends back a message indicating successful/failed reception of Step 1 together with any necessary control information.

Figure 1.2 illustrates the differences between the different random access procedures.

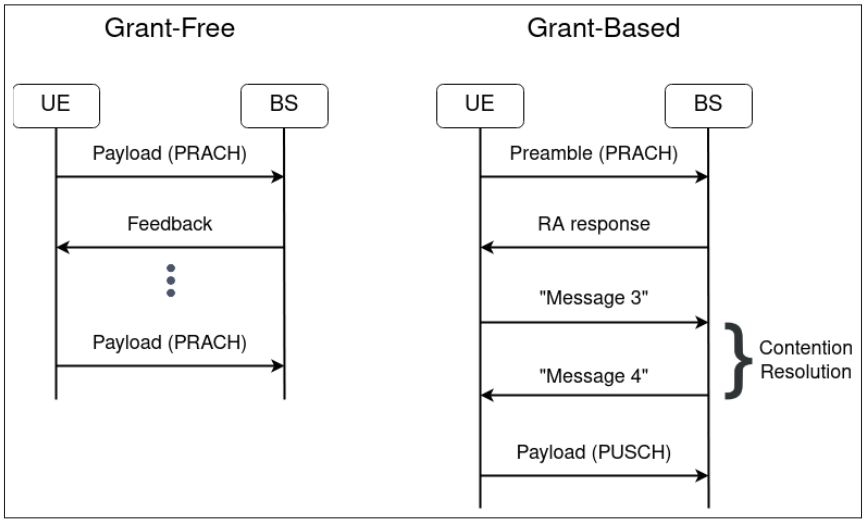

Figure 1.2 Illustration of the access procedure in the two-step random access on the left and four-step random access on the right

There is a clear difference between the two access procedures. The four-step random access mechanism guarantees that the payload transmission happens on a dedicated orthogonal resource, eliminating all sources of intracell interference. However, all users must request a channel before transmitting any data. This configuration is particularly suitable for eMBB services. On the other hand, in the two-step random access scheme, the users skip the resource request stage entirely and transmit their data directly on the random access channel. However, there is a price to pay. Since in this configuration the users transmit their data on the same network resources, the transmissions are vulnerable to collisions. This scheme is suitable for applications requiring ultra-low latency, as there is no time wasted on requesting a network resource and spending power on transmitting small packets sporadically.

Historically, cellular networks have relied on four-step random access systems up to the LTE standards. Hence, the inclusion of two-step random access led to a growing interest by the research community to design and optimize 5G NR networks for the services for which such scheme is suitable.

In (Gao & Dai, 2019), the authors investigate the threshold of the time needed to transmit a packet for which it makes more sense to use grant-based access as opposed to grant-free. They identify that grant-free transmission is more efficient than grant-based concerning the throughput when carrier sensing is present. This result is significant when considering grant-free access for mMTC services. A similar analysis is conducted in (Gharbieh, ElSawy, Yang, Bader & Alouini, 2018). However, instead of using queuing models, Gharbieh *et al* use a spatiotemporal model that incorporates stochastic geometry to model the spatially dependent behaviour of the system, and queuing theory, to model its temporal aspects. Despite arriving at similar results, this work introduces spatiotemporal models as a powerful tool to analyze the latency and throughput in large wireless networks. In (Au *et al.*, 2014) the authors propose a grant-free access network using SCMA to enable massive connectivity. They conduct a link-level analysis of the proposed system and present an interesting observation, when transmitting small packets as much as 30% of the power spent while transmitting one packet is wasted on the grant request.

Much research on grant-free access to enable URLLC service has also been developed. In (Singh, Tirkkonen, Li & Uusitalo, 2018), the authors consider a system where the users need to transmit small packets with high reliability. They propose grant-free access as a mean to achieve low latency and data repetition to achieve reliability. They obtain an analytical expression that, for a given reliability requirement, determines when grant-free access is advantageous compared to grant-based transmission. In (Liu, Wu, Zhang, Fang & Li, 2020), Liu *et al*, develop a sophisticated spatiotemporal model to evaluate the performance of grant-free access for URLLC applications. They compare the latency and reliability of the system with reactive, K-repetition, and proactive HARQ protocols with power-boosting.

1.2 Non-orthogonal Multiple Access

In a multiuser communication system, the system must split resources between the users, a process known as channelization, in order for multiple users to receive and transmit information simultaneously. There are two different types of multiuser channels, the downlink channel and the uplink channel. In the downlink channel, one source is transmitting to many receivers (In a mobile network, a BS is transmitting to users), Figure 1.3 illustrates this concept. Meanwhile, many sources transmit to a single receiver in the uplink channel (In a mobile network, many users transmit to a BS). This concept is illustrated in Figure 1.4. In OMA systems, the channelization procedure splits the networks resources in an orthogonal fashion. Therefore, data streams of different users do not interfere with each other. Hence, the receiver can separate the streams from different users efficiently. On the other hand, in NOMA systems, the resources are split non-orthogonally, resulting in an overlap of the resources allocated to different users. In order to separate data streams from different users, the receiver must apply MUD techniques. OMA systems minimize inter-user interference by allocating non-overlapping resources to each user. However, due to the finite nature of available resources, the number of users allowed to transmit and receive simultaneously is limited. Furthermore, not all users need to transmit/receive at full capacity of their allocated channels at all times. Hence, OMA systems tend to be wasteful with regard to network resources. In this scenario, given the current spectrum scarcity and

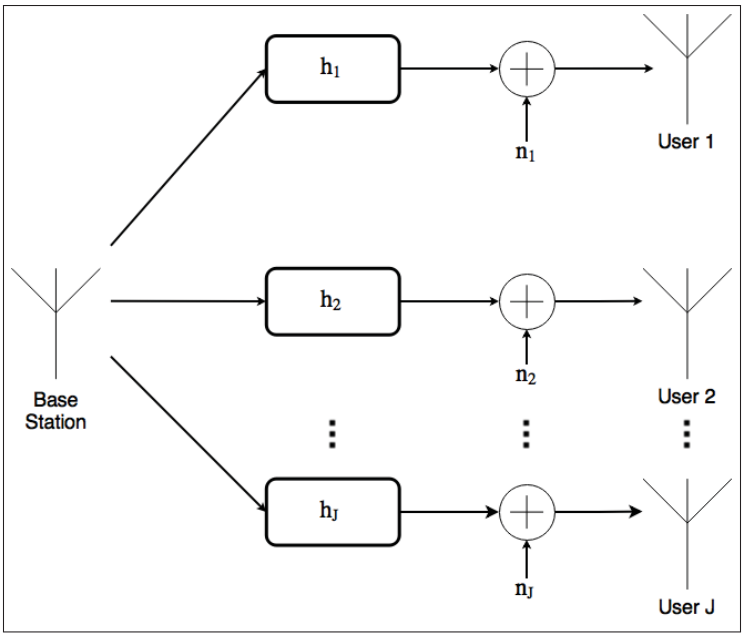

Figure 1.3 Downlink channel diagram

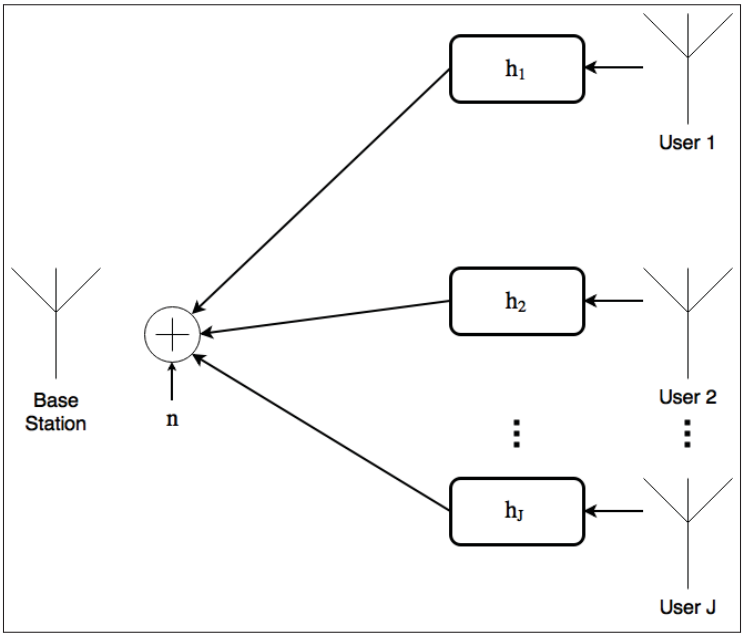

Figure 1.4 Uplink channel diagram

the requirement of massive connectivity imposed by 5G goals, NOMA becomes an attractive solution.

Two main subsets of NOMA schemes are proposed for 5G, power division NOMA (PDM-NOMA), focusing on single-carrier systems, and code division NOMA (CDM-NOMA) on multi-carrier systems. In the following sections, a description of the fundamentals of both subsets, along with a review of the state-of-the-art, is presented.

1.2.1 Power Division Multiplexing NOMA

The main idea of PDM-NOMA is to allocate different power levels for users sharing the same resources such that the receiver can perform successive interference cancellation (SIC) to remove the messages destined to other users and decode their intended message. An illustrative diagram of the distinction between the resource allocation in OMA versus PDM-NOMA networks is shown in Figure 1.5, where blocks of different colours represent different users.

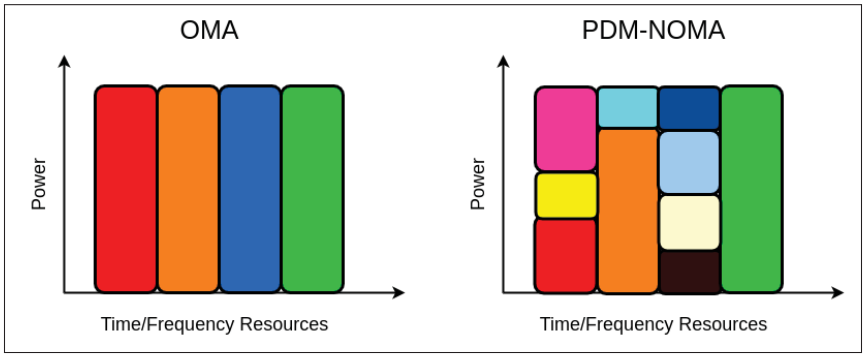

Figure 1.5 Resource allocation in OMA versus PDM-NOMA

In a PDM-NOMA downlink scheme, in which J users share the same resource and their channels are ordered such that $|h_1|^2 \geq |h_2|^2 \geq \cdots \geq |h_J|^2$, the BS transmits the messages to all users on the same resource, with different powers allocated to each message. Thus, the signal received by user j is given by

$$y_j = h_j \sum_{i=1}^{J} \sqrt{\beta_i P} s_i + n_j, \tag{1.2}$$

where β_i is the power ratio allocated to user i, such that $\beta_1 < \beta_2 < \cdots < \beta_J$, P is the total power budget, s_i is the message to the i-th user, h_j is the fading channel gain between the base station

and user j, and n_j is the receiver noise of user j. In the uplink scenario the received signal at the base station is given by

$$y_{BS} = \sum_{i=1}^{J} \sqrt{\beta_i P} h_i s_i + n. \tag{1.3}$$

The symbol transmitted in a NOMA link is the superposition of the symbols transmitted to all users. Figure 1.6 shows the resulting quadrature amplitude modulation (QAM) superposed constellation for a 2-user PDM-NOMA downlink as an example.

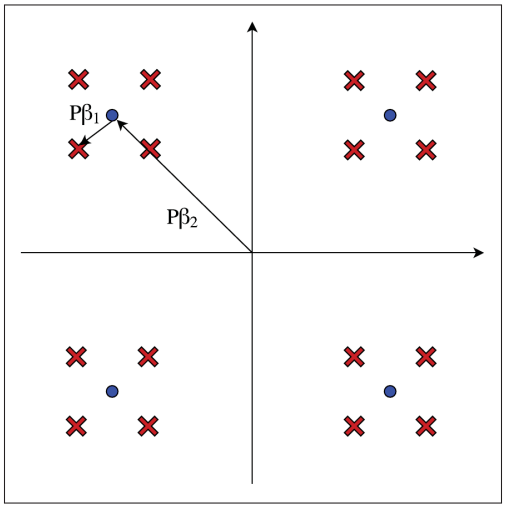

Figure 1.6 Superposed constellation of 2-user PDM-NOMA

In the downlink, each user employs SIC to separate its message. Specifically user j, such that $1 \leq j \leq J$, decodes the messages from users J to $j+1$ (the users with channel quality worse than user j) and remove them from the received signal, sequentially. While decoding a message, the messages from users with better channel quality are treated as interference. A similar decoding procedure is executed in the uplink scenario, with the addition that the BS must go through the messages from all users.

In order to enhance the performance of PDM-NOMA, the combination of NOMA with different technologies has been proposed. Two of these approaches are mentioned in this work: MIMO

PDM-NOMA and cooperative PDM-NOMA. In MIMO PDM-NOMA, the combination of NOMA with MIMO can improve signal diversity and interference reduction in the beamforming mode and spectral efficiency on the spatial multiplexing mode. In cooperative PDM-NOMA, the main goal is to improve the coverage of cell-edge users.

1.2.1.1 MIMO PDM-NOMA

Both MIMO and NOMA technology were proposed to improve the spectral efficiency of a network. Hence, by effectively combining them, even more significant improvements are expected.

In this scenario, both BS and users are equipped with multiple antennas. In downlink transmission, the BS has two options: use its antennas for beamforming in order to improve the signal-to-interference-plus-noise ratio (SINR), or, for spatial multiplexing, increasing the overall throughput.

Considering MIMO PDM-NOMA with beamforming, the users are grouped into clusters, such that users in the same cluster have highly correlated channel vectors. The same beam is used to transmit to users in the same cluster, and they perform SIC to obtain their intended signal. Figure 1.7 illustrates the case considering 4 users. Ideally, the beam intended for one cluster must be orthogonal to the channel vector of users from other clusters to minimize inter-cluster interference. In (Ding, Adachi & Poor, 2016a), the authors propose a beamforming PDM-NOMA scheme supporting $2N$ users served on the same time-frequency resources with N beams, where the beams are obtained through zero-forcing (ZF) (Goldsmith, 2005). An alternative implementation is proposed in (Choi, 2015), where a two-stage beamforming approach based on multicast transmission is presented by the authors.

In contrast to beamforming PDM-NOMA, in spatial multiplexing PDM-NOMA, the goal is to increase the spatial multiplexing gain using multiple antennas. Thus, each antenna transmits an independent data stream, increasing the spectral efficiency of the cell. In spatial multiplexing, PDM-NOMA information transmitted to multiple users are multiplexed in the power domain

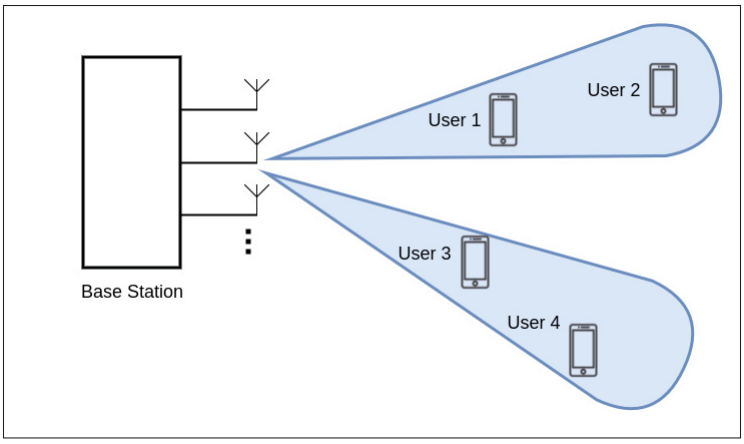

Figure 1.7 Diagram of MIMO PDM-NOMA system

into each independent data stream. Therefore, SIC is performed independently on each data stream to recover the transmitted information. In traditional MIMO systems, the factor of spectral efficiency increase is equal to the minimum between the numbers of transmitting and receiving antennas (Goldsmith, 2005). In (Sun, Han, I & Pan, 2015), the achievable rate of a spatial multiplexing PDM-NOMA system is derived, and two algorithms are proposed for power allocation in this scenario. Results are presented for a two-user scenario, and they show that the achievable rate of spatially multiplexed PDM-NOMA is roughly two times larger than spatially multiplexed OMA.

1.2.1.2 Cooperative PDM-NOMA

Cooperative communications is an effective way to provide spatial diversity and to increase coverage in a wireless network. The main goal of introducing cooperative NOMA is to reduce the outage probability of cell-edge users and improve their overall QoS. As in PDM-NOMA, users with good channel quality must perform SIC to recover their messages, which means that they have prior information about the messages transmitted to users with the worse channel. PDM-NOMA is very well suited for the application of cooperative communications. In this scenario, the users with good channels act as relays to the users with a bad channel. The transmission procedure is divided into two steps, the transmission step and the cooperative step.

During the transmission step, the BS transmits messages to all J users, which perform SIC to decode their information. The cooperative step consists of $J-1$ time slots, during time slot $i \in [2, J]$, user i relays $N-i$ messages to the users with channels worse than his. This scheme is proposed and analyzed in (Ding, Peng & Poor, 2015), and it is shown that it achieves maximum diversity gain for all users. However, this scheme does not scale well, as when the number of users served on the same resources increases, more time slots have to be added to the cooperative step. A possible approach to overcome this issue is to arrange the users into groups, where the cooperative step is performed only within the group. The work in (Ding, Fan & Poor, 2016b) proposes an algorithm for pairing users and evaluates its performance.

1.2.2 Code Domain Multiplexing NOMA

The main difference from PDM-NOMA is that CDM-NOMA was conceived with the multi-carrier transmission in mind. The idea is to assign multiple carriers to each user based on a code. In CDM-NOMA, the transmitter introduces redundancy in the transmitted symbol via code and spreading to enable receivers to perform MUD and separate signals from different users. The MUD procedure is usually performed by a message-passing algorithm (MPA), which is optimal in the maximum a priori (MAP) sense, achieving a good balance between performance and complexity.

In the multi-carrier multiple access schemes presented below, a scenario where J users communicate with a BS over K network resources, which can be OFDM subcarriers, MIMO spatial layers, etc, is assumed.

1.2.2.1 Multi Carrier Low Density Spreading Multiple Access

Multi-carrier OFDM modulation was originally proposed as a way to overcome inter symbol interference (ISI) in wideband communications (Goldsmith, 2005). However, it does not exploit the diversity gain, which can be obtained in multi-carrier transmission over frequency-selective multipath channels. An alternative scheme was proposed (Yee & Linnartz, 1994), named multi-

carrier code division multiple access (MC-CDMA), which provides full diversity gain, but does not preserve orthogonality. Thus, it has to employ MUD to overcome inter-carrier interference (ICI). In this scheme, the transmitted symbols are spread over all available carriers, and the receiver performs MUD to extract its intended message. One of the drawbacks of MC-CDMA is that the decoding complexity increases exponentially with the number of carriers available, rendering this system unfeasible to scale. In (Choi, 2004) a variation of MC-CDMA is proposed, where the transmitted symbols are spread over $N << K$ subcarriers, where N is the degree of spreading and K is the number of available sub-carriers. This scheme achieves a diversity gain of N, but the decoding complexity is reduced. Hence, the degree of spreading N is a tradeoff parameter between decoding complexity and diversity gain. In (van de Beek & Popovic, 2009) a procedure to generate low density spreading sequences, which are referred to as signatures, is proposed and its performance is evaluated. The proposed approach generates low density uniquely decodable signatures with maximum, minimum distance between distinct codewords. In Figure 1.8 a diagram of both downlink and uplink LDSMA systems is presented. In (a), $\mathbf{x} = [x_1 \quad x_2 \quad \cdots x_J]^T$ represents the vector of the symbols transmitted to each user, the matrix $\mathbf{S} = [\mathbf{s}_1 \quad \mathbf{s}_2 \quad \cdots \mathbf{s}_J]$ is the matrix of signatures, where $\mathbf{s}_i$ is the signature of the i-th user. The vectors $\mathbf{n}_i$ and $\mathbf{y}_i$ denote the noise vector and the received signal at user i, respectively. In (b), the scalar x_i is the symbol transmitted by user i, the vectors $\mathbf{n}$ and $\mathbf{y}$ are the noise and the received signal at the BS, respectively.

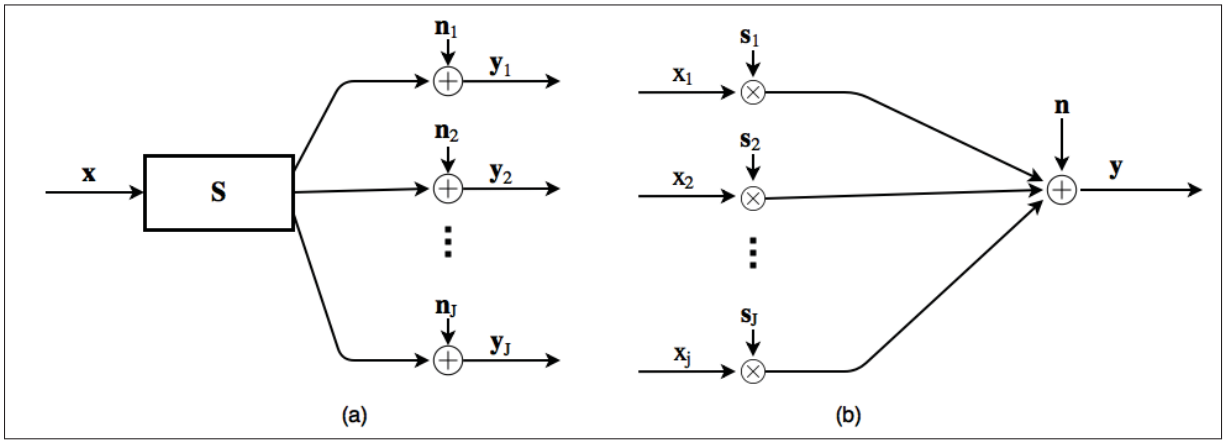

Figure 1.8 (a) Diagram of downlink LDSMA system
(b) Diagram of uplink LDSMA system

1.2.2.2 Sparse Code Multiple Access

The SCMA scheme was first proposed in (Nikopour & Baligh, 2013) as an extension of MC-LDSMA. In the CDMA and the MC-LDSMA schemes, coded bits are first mapped into a symbol, and this symbol is spread through different resources (in the case of CDMA, a quasi-orthogonal spreading sequence is used while in MC-LDSMA, a sparse one is used). On the other hand, the principle of SCMA is to encode the input coded bits into a multi-dimensional constellation sparsely spread onto multiple resources, thus, benefiting from the shaping gain factor of multi-dimensional constellations (Forney Jr. & Wei, 1989). Figure 1.9 compares the structure of the LDS/CDMA modulator with the SCMA one. In an SCMA system, J data layers (users on the downlink scenario) are multiplexed over K resources (OFDM sub-carriers, MIMO spatial layers, ...), where each layer is transmitted over N resources. The overloading factor of the system is given by $\lambda \triangleq \frac{J}{K}$.

The SCMA encoder consists of a mapping $f : \mathbb{B}^{\log_2(M)} \rightarrow \mathcal{X}$, where $\mathcal{X} \subset \mathbb{C}^K$ with cardinality $|\mathcal{X}| = M$, and, M is the order of the modulation being used. Then, we have that $\mathbf{x} = f(\mathbf{b})$, where $\mathbf{x}$ is a K dimensional vector with $N < K$ non-zero entries. The encode function $f(\cdot)$ can be rewritten as the composition of two operations: a constellation mapping $g : \mathbb{B}^{\log_2(M)} \rightarrow C$, where $C \subset \mathbb{C}^N$, and a binary mapping $\mathbf{V} \in \mathbb{B}^{K \times N}$, so, $f \triangleq \mathbf{V}g$. It is worth noting that $\mathbf{V}$ maps an N-dimensional codeword into a K dimensional one and in order to guarantee the sparse structure of the code $\mathbf{V}$ must have $K - N$ all zero rows. So, $\mathbf{V}$ is constructed by inserting $K - N$ all zero rows into $\mathbf{I}_N$, where $\mathbf{I}_N$ is an $N \times N$ identity matrix.

An SCMA system contains J separate layers, each representing one user data layer, defined by $\mathcal{S}_j(\mathbf{V}_j, g_j, M_j, N_j, K) \; \forall \; j \in \{1, \ldots, J\}$. Without loss of generality it is assumed that all users use a constellation of same order and the same number of resources, thus, $M_j = M$ and $N_j = N$ for all $1 \leq j \leq J$. The whole SCMA system can be represented as the set of layers

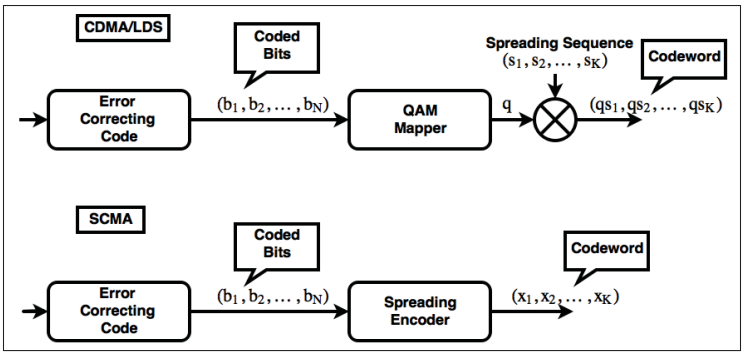

Figure 1.9 Comparison between SCMA and LDS/CDMA

$\mathcal{S}([\mathbf{V}_j]_{j=1}^{J}, [g_j]_{j=1}^{J}, J, M, N, K)$. The received signal is given by

$$\begin{aligned} \mathbf{y} &= \sum_{j=1}^{J} \text{diag}(\mathbf{h}_j)\mathbf{x}_j + \mathbf{n} \\ &= \sum_{j=1}^{J} \text{diag}(\mathbf{h}_j)\mathbf{V}_j g(\mathbf{b}_j) + \mathbf{n}, \end{aligned} \tag{1.4}$$

where $\mathbf{x}_j = (x_{1j}, \ldots, x_{Kj})^T$ is the codeword of layer j, $\mathbf{h}_j = (h_{1j}, \ldots, h_{Kj})^T$ is the channel vector of layer j and $n \sim \mathcal{CN}(0, N_0\mathbf{I}_K)$ is the complex Gaussian noise vector. In a downlink scenario all layers are transmitted by the same transmit point (the BS), thus, the channel for each layer is identical at the receiver, leading to $\mathbf{h_j} = \mathbf{h}$.

The structure of the SCMA code can be neatly conveyed through a factor graph representation. Let $\mathbf{F} \in \mathbb{B}^{K\times J}$ be the factor graph matrix, each element $[\mathbf{F}]_{kj}$ indicates if the layer j transmits information on resource k. $\mathbf{F}$ can be obtained from $\{\mathbf{V}_j\}_{j=1}^{J}$ as $\mathbf{F} = (\mathbf{f}_1, \ldots, \mathbf{f}_J)$, where $\mathbf{f}_j = \text{diag}(\mathbf{V}_j\mathbf{V}_j^T)$. The total number of data layers assigned to each resource is given by the vector $\mathbf{d} = (d_1, \ldots, d_K)^T = \sum_{j=1}^{J} \mathbf{f}_j$. The complexity of decoding a SCMA symbol on each resources is of the order $O(M^d)$. Figure 1.10 shows an example of a factor graph for $K = 4$, $N = 2$ and $J = 6$. The filled squares represent the K resources available, and the empty circles represent the 6 users. The edges of the graph denote that information is being transmitted to or from a user in a resource.

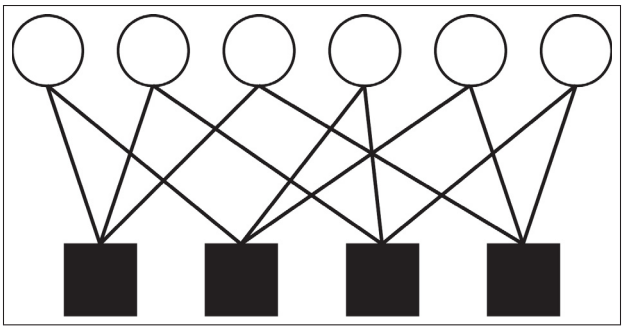

Figure 1.10 Factor graph of an SCMA system with $K = 4$, $N = 2$ and $J = 6$

It was shown in (Nikopour & Baligh, 2013) that the SCMA scheme outperforms the equivalent MC-LDSMA scheme in terms of the block error rate (BLER) while having the same decoding complexity. In (Taherzadeh, Nikopour, Bayesteh & Baligh, 2014) a systematic approach, based on the design principles of lattice constellations, for the design of SCMA codebooks is proposed. A grant-free contention-based uplink transmission scheme for a random access channel, based on SCMA, is proposed in (Au *et al.*, 2014). The motivation for such a scheme is to eliminate the overhead and latency incurred in scheduled uplink transmissions of a small amount of data, which is of particular interest for IoT networks. The primary resource block of the system is a pair of a codebook and a pilot sequence. As long as two users simultaneously transmitting do not use the same codebook and pilot sequence, the receiver can decode both users efficiently. Compared to a grant-free contention-based orthogonal frequency division multiple access (OFDMA) scheme, SCMA enables higher overloading, increased coverage, and lower probability of dropping packets. In (Nikopour *et al.*, 2014) an SCMA downlink system with codebook overloading is proposed. In this system, two users are assigned the same codebook but with different power allocations. Despite having the same codebook, because the users have different power allocations, the MPA decoding algorithm can separate the messages from distinct users. A user pairing algorithm is also proposed. The algorithms pair two users such that the sum rate capacity of the network is maximized. This scheme aligns with the 5G requirement of providing massive connectivity. In (Bao, Ma, Xiao, Ding & Zhu, 2017) the effect of path loss on the uplink MIMO SCMA performance is investigated. An SCMA cell with

randomly deployed users is considered, and maximum likelihood (ML) decoding is assumed on the receiver side. The conclusions of the analysis show that large-scale path loss decreases only the coding gain provided by SCMA, but the diversity order provided by the multiple antenna architecture and the signal-space diversity is preserved.

1.2.3 Resource Management in NOMA

It is foreseen that 5G networks will employ OFDM-like resource division, i.e. the available network resources are divided into time-frequency resource blocks. Hence, to improve spectral efficiency and provide massive connectivity, multiple users can be allocated to the same resource blocks employing NOMA techniques.

The resource allocation problem in OFDM based single-tier NOMA network consists of selecting the sets of users who are scheduled to share the same resources, distribute the power among the multiplexed users on each sub-band and allocating the power across these sub-bands, optimizing some network utility function. This optimization problem is of the non-convex combinatorial type. The authors of (Sun, Ng, Ding & Schober, 2016) analyze the problem of finding the maximum average sum rate in this scenario. An optimal solution employing monotonic optimization (Qian & Zhang, 2010) is obtained. Despite having high computational complexity, rendering this approach unpractical, the optimal solution is an excellent reference to determine the performance of sub-optimal, low complexity algorithms. In the same paper, a sub-optimal approach with lower complexity employing successive convex approximation (Razaviyayn, 2014) is proposed. It is shown that this approach achieves close to optimal results and outperforms the other baseline approaches studied in this work. In (Parida & Das, 2014) a two-step heuristic algorithm to solve the same optimization problem is proposed. Firstly, a greedy user selection scheme is employed, and an iterative power allocation method based on the difference of convex (DC) programming is employed. Afterwards, the same DC algorithm is employed to allocate power across the sub-bands. The algorithm's performance is compared with OFDMA and with similar two-step heuristic algorithms employing a different combination of techniques to obtain a solution. The authors show that the proposed two-step DC-DC

approach outperforms the alternatives in the mean user throughput and the percentage of user pairing in all scenarios under consideration. In (Wei, Ng & Yuan, 2016) a similar problem is considered. However, the authors chose the minimum transmission power to achieve all users' minimum QoS as the network utility function. The authors use a heuristic for user scheduling that results in a sub-carrier allocation satisfying the constraints of the original optimization problem. The original multi-carrier optimization problem can be simplified into a per carrier one. An analytical solution for the simplified problem is provided, and the simulation results show that the proposed scheme outperforms OMA in the power consumption sense. Most of these methods apply a heuristic step to select user sets and assign sub-bands to these sets. Generally, these heuristics do not provide any performance guarantees concerning the optimality of the obtained solutions. Another approach present in the literature is to model the user set and sub-band allocation as a non-cooperative game. In (Di, Bayat, Song & Li, 2015) this problem is solved as a many-to-many two-sided matching game, which provides a low complexity algorithm with good optimality guarantees. The same authors published a similar solution to the channel allocation problem on uplink SCMA networks in (Di, Song & Li, 2016). A two-tier HetNet with small cells using NOMA is considered in (Qian, Wu, Zhou & Shen, 2017). The problem is formulated as two interactive objective functions maximizing the system-wide utility while minimizing the total transmit power. The resulting problem is non-convex and combinatorial, hence, a challenging one. This problem is mapped to a coalition formation game and solved using primal decomposition theory within the framework of simulated annealing. Then, proof of convergence of the proposed algorithm to a global solution in polynomial time is presented.

CHAPTER 2

FAIRNESS AND SUM-RATE MAXIMIZATION VIA JOINT SUBCARRIER AND POWER ALLOCATION IN UPLINK SCMA TRANSMISSION

Joao V.C. Evangelista[1] , Zeeshan Sattar[1] , Georges Kaddoum[1] , Anas Chaaban[2]

[1] Department of Electrical Engineering, École de Technologie Supérieure,
1100 Notre-Dame Ouest, Montréal, Québec, Canada H3C 1K3
[2] School of Engineering, University of British Columbia,
1137 Alumni Avenue, Kelowna, BC, V1Y 1V7 CA

Article published in the IEEE Transactions on Wireless Communications, September, 2019.

2.1 Abstract

In this work, we consider a sparse code multiple access uplink system, where J users simultaneously transmit data over K subcarriers, such that $J > K$, with a constraint on the power transmitted by each user. To jointly optimize the subcarrier assignment and the transmitted power per subcarrier, two new iterative algorithms are proposed, the first one aims to maximize the sum-rate (Max-SR) of the network, while the second aims to maximize the fairness (Max-Min). In both cases, the optimization problem is of the mixed-integer nonlinear programming (MINLP) type, with non-convex objective functions, which are generally not tractable. We prove that both joint allocation problems are NP-hard. To address these issues, we employ a variant of the block successive upper-bound minimization (BSUM) (Razaviyayn, Hong & Luo, 2013) framework, obtaining polynomial-time approximation algorithms to the original problem. Moreover, we evaluate the algorithms' robustness against outdated channel state information (CSI), present an analysis of the convergence of the algorithms, and a comparison of the sum-rate and Jain's fairness index of the novel algorithms with three other algorithms proposed in the literature. The Max-SR algorithm outperforms the others in the sum-rate sense, while the Max-Min outperforms them in the fairness sense.

2.2 Introduction

The fifth generation (5G) of wireless networks is expected to deliver better coverage and a higher capacity to massively connected users. One of the fundamental aspects to achieve this goal is the design of multiple access techniques.

Orthogonal multiple access (OMA) techniques allocate different users into orthogonal network resources, to minimize the interference between users. For instance, time division multiple access (TDMA), code division multiple access (CDMA) and orthogonal frequency division multiple access (OFDMA) assign orthogonal time slots, codes and subcarriers to users, respectively. However, due to the increasing demand for data communications and the introduction of new data-hungry technologies, such as virtual and augmented reality (VR/AR) and massively deployed internet of things (IoT) devices, a tenfold increase in traffic is expected by 2020 (Ericsson, 2015). As the number of orthogonal network resources available is finite, this design paradigm is incompatible with the massive traffic and connectivity requirements of 5G networks. Recently, early information-theoretic works on multi-user communications (Cover, 1972; Ahlswede, 1973) have reemerged under the name non-orthogonal multiple access (NOMA) as a potential solution to deal with this requirement. Although NOMA methods are rooted in the information-theoretic literature, the recent interest has been focused on communication-theoretic aspects such as developing efficient NOMA coding and modulation schemes, with desired error-rate performance and multi-user communication capabilities. Differently from OMA, in NOMA techniques, multiple users are allocated to the same network resources, permitting the allocation of more users and more efficient use of the available resources. In NOMA, each receiver must perform multiuser detection (MUD) to recover the intended transmitted signal. NOMA techniques can be classified into two different groups, power division NOMA (PD-NOMA), code division NOMA (CD-NOMA). Recently, power domain sparse code multiple access (PSMA) (Moltafet, Mokari, Javan, Saeedi & Pishro-Nik, 2018a) has been proposed as a hybrid of PD-NOMA and CD-NOMA. An extensive performance comparison of NOMA methods in a single cell system is found in (Wang, Wang, Lu, Xie & Quan, 2015), while the

comparison between PD-NOMA and CD-NOMA in heterogeneous network is presented in (Moltafet *et al.*, 2018a)

In CD-NOMA, the transmitter introduces redundancy to the transmitted symbol, via code and/or spreading, to enable receivers to perform MUD and separate signals from different users. Furthermore, CD-NOMA has additional advantages in comparison to PD-NOMA (Moltafet *et al.*, 2018b), such as the coding gain and the shaping gain (i.e., methods using multidimensional constellations) (Nikopour & Baligh, 2013).

Motivated by these advantages, this paper is focused on one of the promising CD-NOMA techniques, named sparse code multiple access (SCMA) (Nikopour & Baligh, 2013). In SCMA, sparse multidimensional codebooks are assigned to each user, and each user's data layer is sparsely spread throughout the network resources. In comparison to OFDMA, SCMA allows for more users than subcarriers available to be served simultaneously, while reducing the peak average power ratio (PAPR) due to the sparsity of the subcarrier allocation. SCMA was first proposed in (Nikopour & Baligh, 2013), as a multidimensional generalization of the low density spreading code division multiple access (LDS-CDMA) that yielded better results regarding detection error. In (Taherzadeh *et al.*, 2014), a method to design SCMA codebooks based on lattice coding was proposed. In (Nikopour *et al.*, 2014), a downlink SCMA system is considered, and an algorithm for user pairing along with rate adjustment and a detection strategy is proposed for a multiuser SCMA scheme. It is shown that this scheme can achieve robustness to mobility and high data rates.

2.2.1 Related Work

Regarding resource management and allocation in SCMA networks, an algorithm to maximize the rate of successful accesses on a random access massive machine communications network is suggested in (Xue, Qiu & Li, 2016). In (Luo, Li & Su, 2017), a resource allocation and subcarrier pairing scheme combining OFDMA and SCMA for a dual-hop multiuser relay network is proposed. The problem of assigning SCMA subcarriers to maximize sum rate in uplink

transmission is formulated as matching game in (Di *et al.*, 2016). A grant-free contention based uplink SCMA scheme was proposed in (Au *et al.*, 2014). In (Li *et al.*, 2016), the capacity of an SCMA cell with a Gaussian input is derived and a joint subcarrier and power allocation algorithm is proposed. In (Dabiri & Saeedi, 2018), three algorithms for dynamic subcarrier allocation are presented and their link-level performance is evaluated, one of which takes user fairness in consideration. However, the system-level capacity of these algorithms is not investigated and their fairness is compared in terms of the bit error rate (BER) difference between the best and the worst user. In (Cui, Fan, Lei, Ma & Ding, 2017), a low complexity bisection-based power allocation algorithm, aiming to maximize the capacity of the SCMA system with a finite alphabet is proposed. A stochastic geometry framework to obtain the system-wide area spectral efficiency of underlaid and overlaid device-to-device (D2D) SCMA networks is developed in (Liu, Sheng, Liu, Shi & Li, 2017) and a power allocation strategy to minimize cross-tier interference in underlaid mode and an optimal subcarrier allocation for the overlaid mode are presented. In (Zhu, Qiu & Chen, 2017), a joint subcarrier and power allocation algorithm to maximize the proportional fairness utility function of the downlink SCMA system is proposed. The subcarrier and power allocation are split into two problems. The power allocation problem is transformed to a convex equivalent and the remove-and-reallocate algorithm is proposed to solve the combinatorial subcarrier problem. A similar technique of convexification and alternating optimization is employed in (Abedi, Mokari, Javan & Jorswieck, 2018) to solve a SCMA resource allocation problem taking into account content caching, energy harvesting and physical layer security.

Despite the extensive body of literature regarding the analytical characterization and resource management in SCMA, a few core issues are yet to be properly addressed. Firstly, the network overloading achieved by non-orthogonal scheduling also results in an additional source of interference. Hence, it is fundamental to approach the resource allocation problem from a fairness perspective, as algorithms that maximize the sum-rate do so at the expense of users with poor channel condition. In this vein, one of the algorithms proposed in this paper follows a fairness maximization path. Secondly, as shown in this manuscript, the joint subcarrier and

power allocation problem is NP-hard. The algorithms currently proposed in the literature propose heuristics to achieve sub-optimal solutions. In face of that, we propose a more systematic approach by relaxing the problem and following the BSUM framework.

To the best of our knowledge, no previous works have investigated the fairness in joint subcarrier and power allocation in uplink SCMA transmission in depth. Furthermore, the algorithms proposed in this paper have stronger optimality guarantees in comparison with algorithms proposed in previous works.

2.2.2 Contributions

In this paper, we formulate two optimization problems for joint subcarrier and power allocation in SCMA networks, one aiming to maximize the sum-rate and another one for maximizing the fairness and propose two algorithms to solve them. The first algorithm's goal is to maximize the sum-rate of the network. While this is an essential criterion in cellular networks, fairness between users is equally important. Thus, to include fairness in the optimization, we propose the Max-Min algorithm aimed to maximize the minimum rate among the users. The obtained results demonstrate better performance than the former algorithm in terms of fairness, at the cost of a lowered sum rate.

Both problems are of the non-convex mixed integer nonlinear programming (MINLP) type. We prove that both problems are NP-hard [1]. Then, we propose two algorithms based on the BSUM framework, proposed in (Razaviyayn *et al.*, 2013). The proposed algorithms maximize a lower bound approximation of the objective functions by updating the optimization variables in blocks. As shown in (Razaviyayn *et al.*, 2013), if the lower bound approximation satifies some conditions, this approach has guaranteed convergence to a stationary point, assuring a

[1] As shown in (Moltafet, Azmi, Mokari, Javan & Mokdad, 2018; Mokdad, Azmi, Mokari, Moltafet & Ghaffari-Miab, 2019) for the energy-efficiency and heterogeneous cloud radio access networks in PD-NOMA networks respectively, this problems can be reformulated as a monotonic optimization problem, and the optimal joint allocation can be found using the polyblock outer-approximation algorithm, albeit, the algorithm complexity grows exponentially with the size of the problem.

locally optimal solution. Additionally, we compare both algorithms and the ones proposed in (Dabiri & Saeedi, 2018) in the sum-rate and the Jain's fairness index sense. Results show that the Max-SR algorithm outperforms all other algorithms regarding sum-rate, while the Max-Min algorithm outperforms all others regarding fairness. Furthermore, we evaluate the fairness and sum-rate performance of the algorithms under outdated CSI. Finally, we compare the BER performance of the two proposed algorithms.

To summarize, the list below presents the main accomplishments in this work:

- We prove that the joint power and subcarrier allocation problem is NP-hard.
- We propose a Max-SR algorithm which achieves a better sum-rate in comparison to the ones proposed in (Dabiri & Saeedi, 2018).
- We propose a Max-Min algorithm which achieves better fairness, in terms of the Jain's fairness index, in comparison to the ones proposed in (Dabiri & Saeedi, 2018).
- We evaluate the robustness of the algorithms against outdated channel state information (CSI)

This paper is organized as follows: Section 2.3 contains a brief overview of the SCMA encoder and decoder structure. Also, a description of SCMA signals, and the derivation of its sum-rate is presented. In Section 2.4, the optimization problems are formulated, and an algorithm for sum-rate maximization, and, another for fairness maximization are proposed. Furthermore, in Section 2.5 numerical results are shown, and the performance of the algorithm is evaluated. Also, a numerical analysis of the convergence is presented. Finally, in Section 2.6 the conclusions are presented.

2.2.3 Notation

Throughout this paper, italic lowercase letters denote real and complex scalar values, and x^* denotes the complex conjugate of x. Lower case boldface letters denote vectors, while upper case boldface denote matrices. A lowercase letter with one subscript, x_i, represents the i-th element of the vector $\mathbf{x}$, while both $x_{i,j}$ and $[\mathbf{X}]_{i,j}$ are used to denote the element on the i-th row and j-th column of matrix $\mathbf{X}$. The operators $\mathbf{x}^H$ and $\mathbf{X}^H$ denote the hermitian conjugate

of a vector and of a matrix, respectively. The operator $\det(\mathbf{X})$ is the determinant of the square matrix $\mathbf{X}$ and $\mathrm{tr}(\mathbf{X})$ is its trace. The operator $\mathrm{diag}(\mathbf{x})$ denotes a square matrix with its diagonal components given by $\mathbf{x}$. The operator $E(\cdot)$ denotes the expected value of a random variable. The function $p(\cdot)$ represents the probability density function (PDF) of a random variable and $\mathbf{x} \sim \mathcal{CN}(\boldsymbol{\mu}, \mathbf{K})$, where $\mathbf{K} \in \mathbb{R}^n$, denotes that $\mathbf{x}$ is a complex Gaussian random vector, with mean $\boldsymbol{\mu}$ and covariance matrix $\mathbf{K}$. The sets $\mathbb{R}$, $\mathbb{C}$ and $\mathbb{B}$ are the sets of the real, complex and binary numbers, respectively. A calligraphic uppercase letter, such as $\mathcal{X}$, denotes a set and $|\mathcal{X}|$ is its cardinality. The function $\ln(\cdot)$ denotes the natural logarithm of its argument, while the function $I(\cdot;\cdot)$ is the mutual information between two random variables.

2.3 System Model

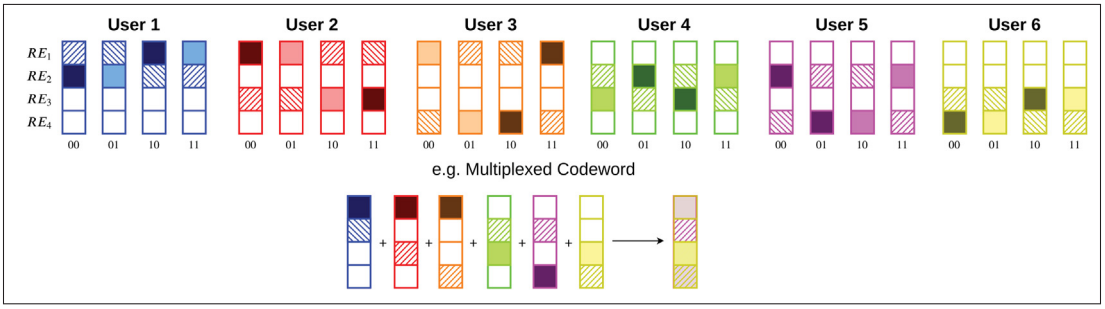

Figure 2.1 Example of an SCMA uplink system with $J = 6$, $K = 4$, $N = 2$ and $d_f = 3$. The square arrays demonstrate the codebook of each user and each square represent the available resource elements (RE). An empty square indicates that no signal is transmitted in the RE and different filling patterns indicate a different complex value

2.3.1 SCMA Overview

Consider a system consisting of one base station (BS), and let $\mathcal{K}$ be the set of available resources (OFDMA subcarriers, MIMO spatial layers and so on), with $|\mathcal{K}| = K$, and $\mathcal{J}$ be the set of users served by the BS, with $|\mathcal{J}| = J$. Each user transmits a symbol from a multidimensional constellation with order M. The SCMA encoder is a mapping $f : \mathbb{B}^{\log_2(M)} \rightarrow \mathcal{S}_j$, with $\mathbf{s}_j = f(\mathbf{b}_j)$, where $\mathbf{b}_j \in \mathbb{B}^{\log_2(M)}$ is a vector of bits taken at the output of a channel encoder,

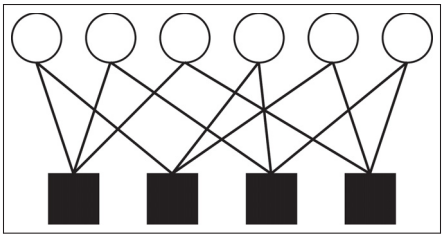

Figure 2.2 Example factor graph with $J = 6$, $K = 4$, $N = 2$ and $d_f = 3$. The circles denote user nodes and the squares denote resource nodes

$\mathcal{S}_j \subset \mathbb{C}^K$, $|\mathcal{S}_j| = M$ and $\mathbf{s}_j$ is a sparse vector with $N < K$ nonzero elements for all $j \in \mathcal{J}$. Each user encodes its transmitted signal from a different multidimensional constellation $\mathcal{S}_j$.

Therefore, the BS serves up to $J = \binom{K}{N}$ users simultaneously and up to $d_f = \binom{K-1}{N-1}$ users are allocated on the same resource. The overloading factor of the cell is given by $\lambda = J/K$. Figure 2.1 shows an example of codebooks and a multiplexed codeword for an SCMA system with $K = 4$, $J = 6$, $N = 2$ and $d_f = 3$. In this figure, each square represents a subcarrier and the different colors represents the codebook of a different user. The texture of the squares is a different symbol from the user's mother constellation, while the blank square indicates that no signal is transmitted at the subcarrier by the user. In the second row, we give an example of the resulting received signal, which is a superposition of the transmitted symbol by each user, for the transmission of an arbitrary pair of bits by each user.

Optimal SCMA decoding is achieved by maximum a posteriori (MAP) decoding. However, due to the complexity of MAP decoding, message passing algorithms (MPA) that achieve near-optimal decoding, such as belief propagation (BP) (McEliece, MacKay & Cheng, 1998) are employed, resulting in a complexity of $O(M^{d_f})$. In order to reduce the decoding complexity of SCMA, alternative receiver architectures have been proposed, such as the SIC-MPA decoder (3GPP, 2016; Zou, Zhao & Zhao, 2015) which is a hybrid of the SIC and MPA procedure, and the list spherical decoding (LSD) algorithm (Wei & Chen, 2017).

The structure of the SCMA code can be neatly conveyed through a factor graph representation. Let $\mathbf{F} \in \mathbb{B}^{K \times J}$ be the factor graph matrix, each element $f_{k,j}$ indicates if any information from the user j is transmitted on resource k. Figure 2.2 illustrates a factor graph with $J = 6$, $K = 4$, $N = 2$ and $d_f = 3$ corresponding to the codebook shown in Figure 2.1, where the circular vertices represent each user, the squared vertices denote the resources and the edges between them the allocation of a user to specific resources.

The reader may refer to (Nikopour & Baligh, 2013) for more details on the encoder/decoder structure of SCMA.

In a SCMA system, the signal received by the BS at the resource k can be written as

$$y_k = \sum_{j \in \mathcal{J}} f_{k,j} h_{k,j} s_{k,j} + n_k, \tag{2.1}$$

where $h_{k,j}$ is the channel coefficient, $s_{k,j}$ is the symbol transmitted from user j on the k-th resource, with average power $p_{k,j} = E(|s_{k,j}|^2)$, and n_k is the k-th component of $\mathbf{n} \sim \mathcal{CN}(0, \sigma_n^2 \mathbf{I})$. Here, we assume that $h_{k,j} = \frac{g_{k,j}}{\sqrt{1+r_j^{\alpha}}}$. Without loss of generality, we assume $g_{k,j}$ is a Rayleigh distributed random variable representing the small scale fading of the channel of user j on subcarrier k, r_j is the distance of user j from the BS and α is the path loss exponent. Throughout this work, it is assumed that the users send a pilot sequence periodically, and, the BS is able to perfectly estimate the CSI. From (2.1), the received signal vector at the BS is written as

$$\mathbf{y} = \mathbf{H}\mathbf{x} + \mathbf{n}, \tag{2.2}$$

where $\mathbf{y} \in \mathbb{C}^K$ is a complex vector, $\mathbf{H} \in \mathbb{C}^{K \times KJ}$ is a matrix composed of submatrices, such that, $\mathbf{H} = [\mathbf{H}_1, \mathbf{H}_2, \cdots, \mathbf{H}_J]$, where, $\mathbf{H}_j = \text{diag}([h_{1,j}, h_{2,j}, \cdots h_{K,j}]^T)\ \forall\ j \in \mathcal{J}$. The vector $\mathbf{x} \in \mathbb{C}^{KJ}$ is given by $\mathbf{x} = \begin{bmatrix} \mathbf{x}_1^T & \mathbf{x}_2^T & \cdots & \mathbf{x}_J^T \end{bmatrix}^T$, where $\mathbf{x}_j = \begin{bmatrix} f_{1,j}s_{1,j} & f_{2,j}s_{2,j} & \cdots & f_{K,j}s_{K,j} \end{bmatrix}^T\ \forall\ j \in \mathcal{J}$.

In this paper, we consider a centralized resource allocation architecture, where K users periodically transmit a pilot signal to the BS. We assume the BS obtains perfect CSI, solves the optimization problem described in Section 2.4, and tells each user which subcarriers, power,

and code-rate to use for the next period of time. We assume the channels are quasi-static, so that users can encode at a fixed rate for a period of time. The process is repeated periodically, where the allocations are changed, and the BS tells users to change their transmission accordingly.

The sum-rate of a SCMA system is defined as the maximum mutual information between the received and transmitted signals. Therefore, assuming channel knowledge at the receiver we have

$$\begin{aligned} R_{\text{SCMA}}^{\text{sum}} &= \max_{p(\mathbf{x})} I(\mathbf{x};\mathbf{y}|\mathbf{H}=\mathbf{H}') \\ &= \max_{p(\mathbf{x})} h(\mathbf{y}|\mathbf{H}=\mathbf{H}') - h(\mathbf{n}) \\ &\overset{(a)}{\leq} \ln[(\pi e)^K \det(\sigma_n^2\mathbf{I}_K + \mathbf{H}'\mathbf{K}_x\mathbf{H}'^H)] - K\ln[\pi e\sigma_n^2] \\ &= \ln\left[\det\left(\mathbf{I}_K + \frac{1}{\sigma_n^2}\mathbf{H}'\mathbf{K}_x\mathbf{H}'^H\right)\right]. \end{aligned} \tag{2.3}$$

In (2.3), the inequality in (a) follows since a Gaussian input maximizes the entropy of a random vector, under a covariance constraint (Cover & Thomas, 2006). In this paper, we are concerned with maximizing this upper bound in the Max-SR algorithm which is referred henceforth as C_{SCMA}. It is worth noting that for an increase on d_f the distribution of $\mathbf{y}$ approaches a multivariate Gaussian, due to the central limit theorem.

Furthermore, $\mathbf{K}_x \in \mathbb{C}^{KJ\times KJ}$ is the covariance matrix of $\mathbf{x}$ and is given by

$$\mathbf{K}_x = \begin{bmatrix} E(\mathbf{x}_1\mathbf{x}_1^H) & E(\mathbf{x}_1\mathbf{x}_2^H) & \cdots & E(\mathbf{x}_1\mathbf{x}_J^H) \\ \vdots & \vdots & \ddots & \vdots \\ E(\mathbf{x}_J\mathbf{x}_1^H) & E(\mathbf{x}_J\mathbf{x}_2^H) & \cdots & E(\mathbf{x}_J\mathbf{x}_J^H) \end{bmatrix}, \tag{2.4}$$

where, each $E(\mathbf{x}_i\mathbf{x}_j^H)$ is given by

$$E(\mathbf{x}_i\mathbf{x}_j^H) = \begin{bmatrix} E\left(x_{1,i}x_{1,j}^*\right) & E\left(x_{1,i}x_{2,j}^*\right) & \cdots & E\left(x_{1,i}x_{K,j}^*\right) \\ \vdots & \vdots & \ddots & \vdots \\ E\left(x_{K,i}x_{1,j}^*\right) & E\left(x_{K,i}x_{2,j}^*\right) & \cdots & E\left(x_{K,i}x_{K,j}^*\right) \end{bmatrix}. \tag{2.5}$$

As concluded in (Li *et al.*, 2016), if each nonzero coordinate of $\mathbf{s}$ is drawn from centrally symmetric constellations, the cross correlation between the multidimensional symbols from different users is equal to zero, hence, $E(\mathbf{x}_i\mathbf{x}_j^H)$ is equal to a $K \times K$ zero matrix for any $i \neq j$. Thus, (2.4) is diagonal. For a more generic derivation, not relying on the central symmetry of the constellation the reader may refer to (Le, Ferrante, Quek & Di Benedetto, 2018; Zaidel, Shental & Shitz, 2018; Shental, Zaidel & Shitz, 2017).

As $\mathbf{H}_j$ is diagonal for all values of j, we have

$$\begin{aligned}\mathbf{H}\mathbf{K}_x\mathbf{H}^H &= \sum_{j=1}^{J}\mathbf{H}_j E\left(\mathbf{x}_j\mathbf{x}_j^H\right)\mathbf{H}_j^H \\ &= \begin{bmatrix} \sum\limits_{j=1}^{J} h_{1,j}E\left(x_{1,j}x_{1,j}^*\right)h_{1,j}^* & \cdots & 0 \\ \vdots & \ddots & \vdots \\ 0 & \cdots & \sum\limits_{j=1}^{J} h_{K,j}E\left(x_{K,j}x_{K,j}^*\right)h_{K,j}^* \end{bmatrix}\end{aligned} \tag{2.6}$$

It is worth noting that such codebook satisfies the design principles established in (Taherzadeh *et al.*, 2014). With that being said, the SCMA sum-rate in (2.3) can be simplified as shown below

$$\begin{aligned} C_{\text{SCMA}} &= \ln\det\left(\mathbf{I}_K + \frac{1}{\sigma_n^2}\mathbf{H}\mathbf{K}_x\mathbf{H}^H\right) = \ln\det\begin{bmatrix} 1+\frac{\sum\limits_{j\in\mathcal{J}}|h_{1,j}|^2E(x_{1,j}^2)}{\sigma_n^2} & \cdots & 0 \\ \vdots & \ddots & \vdots \\ 0 & \cdots & 1+\frac{\sum\limits_{j\in\mathcal{J}}|h_{K,j}|^2E(x_{K,j}^2)}{\sigma_n^2} \end{bmatrix} \\ &= \sum_{k\in\mathcal{K}}\ln\left(1+\frac{\sum\limits_{j\in\mathcal{J}}|h_{k,j}|^2E(x_{k,j}^2)}{\sigma_n^2}\right) = \sum_{k\in\mathcal{K}}\ln\left(1+\frac{\sum\limits_{j\in\mathcal{J}}|h_{k,j}|^2 f_{k,j}p_{k,j}}{\sigma_n^2}\right). \end{aligned} \tag{2.7}$$

Furthermore, by assuming a decoding order starting from user J to user 1 and using the logarithm identity $\log_b(a+c) = \log_b(a) + \log_b(1+\frac{c}{a})$, it is possible to obtain the achievable rate of user

j on resource k, $C_{k,j}$, as

$$\begin{aligned}
&\ln\left(1+\frac{\sum\limits_{j\in\mathcal{J}}|h_{k,j}|^2 f_{k,j}p_{k,j}}{\sigma_n^2}\right)=\ln\left(\frac{\sigma_n^2+\sum\limits_{j\in\mathcal{J}}|h_{k,j}|^2 f_{k,j}p_{k,j}}{\sigma_n^2}\right)\\
=\;&\ln\left(\frac{\sigma_n^2+|h_{k,1}|^2 f_{k,1}p_{k,1}}{\sigma_n^2}\right)+\ln\left(\frac{\sigma_n^2+|h_{k,1}|^2 f_{k,1}p_{k,1}+|h_{k,2}|^2 f_{k,2}p_{k,2}}{\sigma_n^2+|h_{k,1}|^2 f_{k,1}p_{k,1}}\right)+\cdots\\
+\;&\ln\left(\frac{\sigma_n^2+\sum\limits_{i=1}^{J-1}|h_{k,i}|^2 f_{k,i}p_{k,i}+|h_{k,J}|^2 f_{k,J}p_{k,J}}{\sigma_n^2+\sum\limits_{i=1}^{J-1}|h_{k,i}|^2 f_{k,i}p_{k,i}}\right)\\
=\;&\sum_{j\in\mathcal{J}}\ln\left(1+\frac{|h_{k,j}|^2 f_{k,j}p_{k,j}}{\sigma_n^2+\sum\limits_{i=1}^{j-1}|h_{k,i}|^2 f_{k,i}p_{k,i}}\right)=\sum_{j\in\mathcal{J}}C_{k,j}.
\end{aligned}\tag{2.8}$$

Therefore, the achievable rate of each user, C_j, is given by

$$C_j=\sum_{k\in\mathcal{K}}C_{k,j}=\sum_{k\in\mathcal{K}}\ln\left(1+\frac{|h_{k,j}|^2 f_{k,j}p_{k,j}}{\sigma_n^2+\sum\limits_{i=1}^{j-1}|h_{k,i}|^2 f_{k,i}p_{k,i}}\right).\tag{2.9}$$

In the next section, we formulate the joint subcarrier and power allocation problems and present our proposed method to solve them.

2.4 Joint Subcarrier and Power Allocation

We formulate and propose two joint subcarrier and power allocation algorithms to solve two optimization problems: maximizing the sum-rate ($\mathbf{P_{Max\text{-}SR}}$) and maximizing the minimum rate

of users ($\mathbf{P_{Max\text{-}Min}}$). The former can be formulated as

$$\mathbf{P_{Max\text{-}SR}}:$$

$$\max_{\mathbf{P},\mathbf{F}} \quad C_{\text{SCMA}} = \sum_{k\in\mathcal{K}} \ln\left(1 + \frac{\sum\limits_{j\in\mathcal{J}} |h_{k,j}|^2 f_{k,j} p_{k,j}}{\sigma_n^2}\right) \tag{2.10}$$

$$\textbf{s.t.} \quad \sum_{k\in\mathcal{K}} f_{k,j} \leq N \;\forall\; j \in \mathcal{J} \tag{2.11}$$

$$\sum_{j\in\mathcal{J}} f_{k,j} \leq d_f \;\forall\; k \in \mathcal{K} \tag{2.12}$$

$$\sum_{k\in\mathcal{K}} f_{k,j} p_{k,j} \leq P_{\max}^{(j)} \;\forall\; j \in \mathcal{J} \tag{2.13}$$

$$f_{k,j} \in \{0,1\} \;\forall\; k \in \mathcal{K} \text{ and } \forall\; j \in \mathcal{J}, \tag{2.14}$$

where $\mathbf{P} \in \mathbb{R}^{K\times J}$ is the matrix of allocated power, (2.10) is the sum-rate, and (2.11) is the constraint on the number of subcarriers allocated per user. The constraint on the number of users per subcarrier is given by (2.12), while (2.13) is the constraint on the maximum transmitting power available per user. Finally, (2.14) is a binary constraint on the values of $f_{k,j}$.

Furthermore, the problem $\mathbf{P_{Max\text{-}Min}}$ is formulated as

$$\mathbf{P_{Max\text{-}Min}}:$$

$$\max_{\mathbf{P},\mathbf{F}} \quad \min_{j\in\mathcal{J}} \sum_{k\in\mathcal{K}} \ln\left(1 + \frac{|h_{k,j}|^2 f_{k,j} p_{k,j}}{\sigma_n^2 + \sum\limits_{i=1}^{j-1} |h_{k,i}|^2 f_{k,i} p_{k,i}}\right) \tag{2.15}$$

$$\textbf{s.t.} \quad (2.11), (2.12), (2.13), (2.14),$$

where (2.15) is the max-min utility function of the rate per user. The objective function of this problem is non-concave and, similarly to $\mathbf{P_{Max\text{-}SR}}$, also has integer constraints on $\mathbf{F}$. Consequently, we can prove the following statement

Theorem 1. *Both the* $\mathbf{P}_{\textit{Max-SR}}$ *and the* $\mathbf{P}_{\textit{Max-Min}}$ *problems are NP-hard.*

Proof. See Appendix I, Section 1. ■

In order to solve both these problems, we relax the integer constraint on matrix $\mathbf{F}$, given in equation (2.14), to a continuous one. Afterwards, we apply the block successive lower bound maximization (BSLM), which is the maximization variant of the approach proposed in (Razaviyayn *et al.*, 2013), which converges to a local minimum of the relaxed problem (Razaviyayn *et al.*, 2013).

For the sake of clarity, we list the conditions for the convergence of the BSLM algorithm. First consider the problem below

$$\begin{aligned} \max_{\mathbf{x}} \quad & f(\mathbf{x}) \\ \textbf{s.t.} \quad & \mathbf{x} \in \mathcal{X}, \end{aligned}$$

where $f : \mathbb{R}^n \to \mathbb{R}$ is a non-concave and possibly non-smooth function. Let $\mathcal{X}$ be the cartesian product of m closed convex sets: $\mathcal{X} = \mathcal{X}_1 \times \cdots \times \mathcal{X}_m$, with $\mathcal{X}_i \subseteq \mathbb{R}^{n_i}$ and $\sum_i n_i = n$. Furthermore the optimization variable $\mathbf{x} \in \mathbb{R}^n$ can be decomposed into m vectors $\mathbf{x} = (\mathbf{x}_1, \cdots, \mathbf{x}_m)$, such that $\mathbf{x}_i \in \mathcal{X}_i$. At iteration t of the BSLM algorithm, the blocks of optimization variables are updated cyclically, where for each block the following problem is solved

$$\begin{aligned} \max_{\mathbf{x}_i} \quad & \tilde{f}(\mathbf{x}_i, \mathbf{x}^{(t-1)}) \\ \textbf{s.t.} \quad & \mathbf{x}_i \in \mathcal{X}_i, \end{aligned}$$

where $i = t \bmod m$, and $\mathbf{x}^{(t-1)}$ is the previous value of $\mathbf{x}$. The convergence of the BLSM algorithm is guaranteed if the following conditions hold for $\tilde{f}(\mathbf{x}_i, \mathbf{x}^{(t-1)})$:

$$\tilde{f}(\mathbf{x}_i, \mathbf{x}) = f(\mathbf{x}), \quad \forall\, \mathbf{x} \in \mathcal{X}, \forall\, i \tag{2.16}$$

$$\begin{aligned} \tilde{f}(\mathbf{x}_i, \mathbf{y}) \leq\ & f(\mathbf{y}_1, \cdots, \mathbf{y}_{i-1}, \mathbf{x}_i, \mathbf{y}_{i+1}, \cdots, \mathbf{y}_m), \\ & \forall\, \mathbf{x}_i \in \mathcal{X}_i, \forall\, \mathbf{y} \in \mathcal{X}, \forall\, i \end{aligned} \tag{2.17}$$

$$\nabla \tilde{f}(\mathbf{x}_i, \mathbf{x}) = \nabla f(\mathbf{x}) \tag{2.18}$$

$$\tilde{f}(\mathbf{x}_i, \mathbf{y}) \quad \text{is continuous in } (\mathbf{x}_i, \mathbf{y}), \quad \forall\, i \tag{2.19}$$

In the rest of this section, we propose lower bound convex approximations to the objective functions of both $\mathbf{P}_{\text{Max-SR}}$ and $\mathbf{P}_{\text{Max-Min}}$ satisfying conditions (2.16)-(2.19), and finalize by providing a description of the block update algorithm that converges to locally optimal solutions.

2.4.1 Solving $\mathbf{P}_{\text{Max-SR}}$

To solve this problem, we first relax the integer constraint in (2.14), and add a penalty term to the objective function, such that, non-integer solutions to $\mathbf{F}$ are penalized. The $\mathbf{P}_{\text{Max-SR}}$ becomes

$$\mathbf{P}'_{\text{Max-SR}}:$$

$$\max_{\mathbf{P},\mathbf{F}} \quad \sum_{k\in\mathcal{K}} \ln\left(1+\frac{\sum\limits_{j\in\mathcal{J}}|h_{k,j}|^2 f_{k,j}p_{k,j})}{\sigma_n^2}\right)+\gamma\left(\mathbf{F}\right) \tag{2.20}$$

$$\textbf{s.t.} \quad 0\le f_{k,j}\le 1\ \forall\ k\in\mathcal{K} \text{ and } \forall\ j\in\mathcal{J} \tag{2.21}$$

$$(2.11), (2.12), (2.13) \tag{2.22}$$

where $\gamma\left(\mathbf{F}\right)=\lambda\sum\limits_{k\in\mathcal{K}}\sum\limits_{j\in\mathcal{J}}\left(f_{k,j}^2-f_{k,j}\right)$ is the penalty function [2]. Notice that $\gamma\left(\mathbf{F}\right)<0$ for all non-integer solutions and $\gamma\left(\mathbf{F}\right)=0$ for integer ones. This gives incentive for the algorithm to obtain solutions that minimize $\gamma\left(\mathbf{F}\right)$, hence leading to integer solutions of $\mathbf{F}$.

There are two issues that make $\mathbf{P}'_{\text{Max-SR}}$ a hard problem to solve:

- The presence of multi-linear terms of the form $f_{k,j}p_{k,j}$ in (2.20) and (2.13).
- Even if $\mathbf{F}$ and $\mathbf{P}$ are updated cyclically, the objective function in (2.20) is non-concave, due to the addition of $\gamma\left(\mathbf{F}\right)$, which is convex.

[2] By selecting moderately high values for λ (around 20), integer solutions are obtained. As a matter of fact, higher values for λ results in faster convergence to an integer solution, however, it renders the optimization solver iterations more unstable as it contributes to the ill-conditioning of the problem. On the other hand, smaller λ leads to more conservative updates of $\mathbf{F}$ at each BSLM step, resulting in slower convergence, but better optimizers.

Now we present two Lemmas that are instrumental to the algorithm that finds a locally optimal solution to $\mathbf{P'_{Max\text{-}SR}}$ in polynomial time.

Lemma 1. *If* $\mathbf{F}$ *and* $\mathbf{P}$ *are updated cyclically in* $\mathbf{P'_{Max\text{-}SR}}$*, the feasible set of the problem solved in each update step is convex.*

Proof. All constraints in $\mathbf{P'_{Max\text{-}SR}}$ are linear functions of $\mathbf{F}$ and $\mathbf{P}$, with the exception of constraint (2.13) which involves a multi-linear term. However, if $\mathbf{F}$ and $\mathbf{P}$ are updated cyclically, only one of the matrices is updated while the other is kept constant and the multi-linear terms in (2.13) become linear in the variable being updated. Therefore, the feasible sets are convex. ■

Lemma 2. *Let the function*

$$\sum_{k\in\mathcal{K}} \ln\left(1+\frac{\sum\limits_{j\in\mathcal{J}}|h_{k,j}|^2 f_{k,j}p_{k,j}}{\sigma_n^2}\right)+ \gamma\left(\mathbf{F}'\right)+tr\left[\nabla\gamma\left(\mathbf{F}'\right)^T\left(\mathbf{F}-\mathbf{F}'\right)\right], \tag{2.23}$$

where $\nabla\gamma\left(\mathbf{F}'\right)\in\mathbb{R}^{K\times J}$ *is a matrix such that*

$$\left[\nabla\gamma\left(\mathbf{F}'\right)\right]_{k,j}=\left.\frac{\partial\gamma\left(\mathbf{F}\right)}{\partial f_{k,j}}\right|_{\mathbf{F}=\mathbf{F}'}, \tag{2.24}$$

be an approximation to (2.20) in the neighborhood of $\mathbf{F}'$ *for fixed* $\mathbf{P}$*. Notice that (2.23) is a lower bound concave approximation to (2.20) satisfying conditions (2.16)-(2.19).*

Proof. Firstly, notice that $\gamma\left(\mathbf{F}'\right)+\mathrm{tr}\left[\nabla\gamma\left(\mathbf{F}'\right)^T\left(\mathbf{F}-\mathbf{F}'\right)\right]$ is the first order linear approximation of $\gamma\left(\mathbf{F}\right)$ in the neighborhood of $\mathbf{F}'$. So (2.16), (2.18), and (2.19) are satisfied. Furthermore, as $\gamma\left(\mathbf{F}\right)$ is a convex function, we have

$$\gamma(\mathbf{F})\geq\gamma\left(\mathbf{F}'\right)+\mathrm{tr}\left[\nabla\gamma\left(\mathbf{F}'\right)^T\left(\mathbf{F}-\mathbf{F}'\right)\right].$$

As the linear approximation is globally less than $\gamma\left(\mathbf{F}\right)$, we have that (2.23) is a lower bound of (2.10). Thus, (2.16) is also satisfied. ■

With Lemmas 1 and 2 in hand, we can derive the convergence of the relaxed problem $\mathbf{P'_{Max\text{-}SR}}$ to a local optimum, as stated in the Theorem below.

Theorem 2. *By updating* $\mathbf{F}$ *and* $\mathbf{P}$ *cyclically with the solutions to* $\mathbf{P}^{(\mathbf{F})}_{\boldsymbol{Max\text{-}SR}}$ *and* $\mathbf{P}^{(\mathbf{P})}_{\boldsymbol{Max\text{-}SR}}$ *presented below, we can obtain a locally optimal solution to the relaxed problem* $\mathbf{P'}_{\boldsymbol{Max\text{-}SR}}$.

$$\boldsymbol{P}^{(\mathbf{P})}_{\boldsymbol{Max\text{-}SR}}: \quad \max_{\mathbf{P}} \quad (2.10) \quad \boldsymbol{s.t.} \quad (2.13),$$

$$\mathbf{P}^{(\mathbf{F})}_{\boldsymbol{Max\text{-}SR}}: \quad \max_{\mathbf{F}} \quad (2.23) \quad \boldsymbol{s.t.} \quad (2.11), (2.12), (2.13), (2.21),$$

where $\mathbf{F}' = \mathbf{F}^{(t-1)}$*, i.e the previous value of* $\mathbf{F}$.

Proof. From Lemma 1, the feasible set of both $\mathbf{P}^{(\mathbf{F})}_{\mathbf{Max\text{-}SR}}$ and $\mathbf{P}^{(\mathbf{P})}_{\mathbf{Max\text{-}SR}}$ are convex. Moreover, from Lemma 2, we have that (2.23) is a concave lower bound approximation to (2.20) satisfying the conditions in (2.16)-(2.19). Therefore, from the result shown in Theorem 2 in(Razaviyayn *et al.*, 2013), the solution obtained by iteratively updating $\mathbf{F}$ and $\mathbf{P}$ cyclically is a local optimum of $\mathbf{P'}_{\mathbf{Max\text{-}SR}}$. ■

As problems $\mathbf{P}^{(\mathbf{F})}_{\mathbf{Max\text{-}SR}}$ and $\mathbf{P}^{(\mathbf{P})}_{\mathbf{Max\text{-}SR}}$ are concave maximizations over a convex set and are readily solvable. Algorithm 2.1 shows the pseudocode of the Max-SR algorithm, using $\mathbf{P}^{(\mathbf{F})}_{\mathbf{Max\text{-}SR}}$ and $\mathbf{P}^{(\mathbf{P})}_{\mathbf{Max\text{-}SR}}$ as subroutines.

Algorithm 2.1 Maximization of sum-rate

Variable Definition :

1. $\mathbf{F}^{(t)}$ is the subcarrier allocation matrix at the t-th iteration.
2. $\mathbf{P}^{(t)}$ is the power allocation matrix at the t-th iteration.

Initialization :

1. Set the initial values for the power allocation matrix $\mathbf{P}^{(0)}$ randomly.
2. Set the initial values for the subcarrier allocation matrix $\mathbf{F}^{(0)}$.
3. Set the convergence tolerance for the subcarrier allocation ϵ_F.
4. Set the convergence tolerance for the power allocation ϵ_P.
5. $t \leftarrow 0$

Output :

1. Optimized power allocation $\mathbf{P}^*$.
2. Optimized subcarrier allocation $\mathbf{F}^*$.

while $\left\|\mathbf{F}^{(t)} - \mathbf{F}^{(t-1)}\right\| > \epsilon_F$ *and* $\left\|\mathbf{P}^{(t)} - \mathbf{P}^{(t-1)}\right\| > \epsilon_P$ **do**
  $t \leftarrow t + 1$;
  $\mathbf{F^{(t)}} \leftarrow \arg \mathbf{P}^{(\mathbf{F})}_{\textbf{Max-SR}} \left(\mathbf{F}^{(t-1)}, \mathbf{P}^{(t-1)}\right)$; (see Theorem 2)
  $\mathbf{P^{(t)}} \leftarrow \arg \mathbf{P}^{(\mathbf{P})}_{\textbf{Max-SR}} \left(\mathbf{F}^{(t-1)}, \mathbf{P}^{(t-1)}\right)$; (see Theorem 2)
end while
$\mathbf{P}^* \leftarrow \mathbf{P}^{(t)}$;
$\mathbf{F}^* \leftarrow \mathbf{F}^{(t)}$;

2.4.2 Solving $\mathbf{P}_{\textbf{Max-Min}}$

Before solving the problem, notice that its objective function in (2.15) can be rewritten as

$$\begin{aligned} & \min_{j \in \mathcal{J}} \quad \sum_{k \in \mathcal{K}} \ln \left(1 + \frac{|h_{k,j}|^2 f_{k,j} p_{k,j}}{\sigma_n^2 + \sum_{i=1}^{j-1} |h_{k,i}|^2 f_{k,i} p_{k,i}} \right) \\ = & \min_{j \in \mathcal{J}} \quad \left[\sum_{k \in \mathcal{K}} \ln \left(\sigma_n^2 + \sum_{i=1}^{j} |h_{k,i}|^2 f_{k,i} p_{k,i} \right) - \right. \\ & \left. \ln \left(\sigma_n^2 + \sum_{i=1}^{j-1} |h_{k,i}|^2 f_{k,i} p_{k,i} \right) \right]. \end{aligned} \tag{2.25}$$

Both expressions inside the minimum function, $\ln\left(\sigma_n^2 + \sum_{i=1}^{j} |h_{k,i}|^2 f_{k,i} p_{k,i}\right)$ and $\ln\left(\sigma_n^2 + \sum_{i=1}^{j-1} |h_{k,i}|^2 f_{k,i} p_{k,i}\right)$ are concave functions, which implies that their difference is non-concave. The summation of non-concave functions is also non-concave, and, by function composition rules (Boyd & Vandenberghe, 2004), the minimum of a non-concave function is non-concave as well.

Similarly to $\mathbf{P}_{\textbf{Max-SR}}$, the first step in solving $\mathbf{P}_{\textbf{Max-Min}}$ is relaxing the integer constraint on the entries of $\mathbf{F}$ and adding the same penalty function to its objective, leading to problem $\mathbf{P}'_{\textbf{Max-Min}}$, given below

$$
\begin{aligned}
& \mathbf{P}'_{\textbf{Max-Min}}: \\
\max_{\mathbf{P},\mathbf{F}} \quad & \min_{j \in \mathcal{J}} \left[\sum_{k \in \mathcal{K}} \ln\left(\sigma_n^2 + \sum_{i=1}^{j} |h_{k,i}|^2 f_{k,i} p_{k,i}\right) - \right. \\
& \left. \ln\left(\sigma_n^2 + \sum_{i=1}^{j-1} |h_{k,i}|^2 f_{k,i} p_{k,i}\right) \right] + \gamma\,(\mathbf{F}) \qquad (2.26) \\
\textbf{s.t.} \quad & (2.11), (2.12), (2.13), (2.21).
\end{aligned}
$$

After the relaxation, we have the non-concave term from (2.25) and the convex penalty function in the objective. The challenges involved in solving $\mathbf{P}'_{\textbf{Max-Min}}$ are

- Just as in $\mathbf{P}'_{\textbf{Max-SR}}$, the presence of multi-linear terms of the form $f_{k,j} p_{k,j}$ in (2.26) and (2.13).
- Even if $\mathbf{F}$ and $\mathbf{P}$ are updated cyclically, the objective function in (2.20) is non-concave.

To address these issues, we follow the procedure used to solve $\mathbf{P}'_{\textbf{Max-SR}}$, with a few extra steps. Firstly, notice that the feasible sets of $\mathbf{P}'_{\textbf{Max-SR}}$ and $\mathbf{P}'_{\textbf{Max-Min}}$ are the same, and therefore Lemma 1 also holds. We introduce a concave lower bound to (2.26) in the Lemma below.

Lemma 3. *Let* $\theta_j(\mathbf{F}) = \sum_{k\in\mathcal{K}} \ln\left(\sigma_n^2 + \sum_{i=1}^{j-1} |h_{k,i}|^2 f_{k,i} p_{k,i}\right)$. *The function*

$$\begin{aligned}
&\min_{j\in\mathcal{J}} \left[\sum_{k\in\mathcal{K}} \ln\left(\sigma_n^2 + \sum_{i=1}^{j} |h_{k,i}|^2 f_{k,i} p_{k,i}\right) - \right. \\
&\left. \theta_j(\mathbf{F}') - tr\left(\nabla\theta_j(\mathbf{F}')^T(\mathbf{F}-\mathbf{F}')\right)\right] + \\
&\gamma(\mathbf{F}') + tr\left[\nabla\gamma(\mathbf{F}')^T(\mathbf{F}-\mathbf{F}')\right], \qquad (2.27)
\end{aligned}$$

where $\nabla\theta_j(\mathbf{F}') \in \mathbb{R}^{K\times J}$ *is a matrix such that*

$$\begin{aligned}
\left[\nabla\theta_j(\mathbf{F}')\right]_{k,n} &= \left.\frac{\partial\theta_j(\mathbf{F})}{\partial f_{k,n}}\right|_{\mathbf{F}=\mathbf{F}'} \\
&= \begin{cases} \frac{|h_{k,n}|^2 p_{k,n}}{\sigma_n^2 + \sum_{i=1}^{j-1} |h_{k,i}|^2 f'_{k,i} p_{k,i}} & , \forall\, n < j \\ 0 & , \textit{otherwise} \end{cases},
\end{aligned}$$

is a lower bound concave approximation of (2.26) for fixed $\mathbf{P}$ *in the neighborhood of* $\mathbf{F}'$ *which satisfies conditions (2.16)-(2.19).*

Proof. Firstly, as $\theta_j(\mathbf{F})$ is a concave function we have that

$$\theta_j(\mathbf{F}) \leq \theta_j(\mathbf{F}') - \mathrm{tr}\left(\nabla\theta_j(\mathbf{F}')^T(\mathbf{F}-\mathbf{F}')\right)$$

Therefore, the argument of the minimum function in (2.27) is less than the argument of the minimum function in (2.26), which implies that (2.17) holds. Furthermore, (2.27) is obtained by approximating the non concave terms in (2.26) by their first order linear approximation in the neighborhood of $\mathbf{F}'$ and (2.27) is continuous, and hence (2.16), (2.18), and (2.19) also hold. Finally, (2.27) consists of the minimum of the summation over a concave function plus an affine

term. So,

$$\sum_{k\in\mathcal{K}} \ln\left(\sigma_n^2 + \sum_{i=1}^{j}|h_{k,i}|^2 f_{k,i}p_{k,i}\right) - \theta_j\left(\mathbf{F}'\right) - \mathrm{tr}\left(\nabla\theta_j\left(\mathbf{F}'\right)^T\left(\mathbf{F}-\mathbf{F}'\right)\right),$$

is concave. By composition rules (Boyd & Vandenberghe, 2004), the minimum of concave functions is also concave, which proves that (2.27) is concave, and coimpletes the proof. ■

Lemma 4. *Let* $\theta_j\left(\mathbf{P}\right) = \sum\limits_{k\in\mathcal{K}} \ln\left(\sigma_n^2 + \sum\limits_{i=1}^{j-1}|h_{k,i}|^2 f_{k,i}p_{k,i}\right)$. *The function*

$$\min_{j\in\mathcal{J}}\left[\sum_{k\in\mathcal{K}} \ln\left(\sigma_n^2 + \sum_{i=1}^{j}|h_{k,i}|^2 f_{k,i}p_{k,i}\right) - \theta_j\left(\mathbf{P}'\right) - tr\left(\nabla\theta_j\left(\mathbf{P}'\right)^T\left(\mathbf{P}-\mathbf{P}'\right)\right)\right] + \gamma\left(\mathbf{P}'\right) + tr\left[\nabla\gamma\left(\mathbf{P}'\right)^T\left(\mathbf{P}-\mathbf{P}'\right)\right], \tag{2.28}$$

where $\nabla\theta_j\left(\mathbf{P}'\right) \in \mathbb{R}^{K\times J}$ *is a matrix such that*

$$\left[\nabla\theta_j\left(\mathbf{P}'\right)\right]_{k,n} = \left.\frac{\partial\theta_j\left(\mathbf{P}\right)}{\partial p_{k,n}}\right|_{\mathbf{P}=\mathbf{P}'} = \begin{cases} \frac{|h_{k,n}|^2 f_{k,n}}{\sigma_n^2 + \sum\limits_{i=1}^{j-1}|h_{k,i}|^2 f'_{k,i}p_{k,i}} & , \forall\, n < j \\ 0 & , \textit{otherwise} \end{cases},$$

is a lower bound concave approximation of (2.26) for fixed $\mathbf{F}$ *in the neighborhood of* $\mathbf{P}'$ *which satisfies conditions (2.16)-(2.19).*

Proof. See the proof of Lemma 3. ■

With the results from Lemmas 1, 3 and 4 we can establish the convergence to a local optimum of an algorithm to solve $\mathbf{P}'_{\textbf{Max-Min}}$.

Theorem 3. *By updating* $\mathbf{F}$ *and* $\mathbf{P}$ *cyclically with the solutions to* $\mathbf{P}^{(\mathbf{F})}_{\textit{Max-Min}}$ *and* $\mathbf{P}^{(\mathbf{P})}_{\textit{Max-Min}}$ *presented below, we can obtain a locally optimal solution to the relaxed problem* $\mathbf{P}'_{\textit{Max-Min}}$.

$$\boldsymbol{P}^{(\mathbf{P})}_{\textit{Max-Min}}: \quad \max_{\mathbf{P}} \quad (2.28) \quad \textbf{\textit{s.t.}} \quad (2.13),$$

where $\mathbf{P}'$ *is the value of* $\mathbf{P}$ *after the previous update.*

$$\mathbf{P}^{(\mathbf{F})}_{\textit{Max-Min}}: \quad \max_{\mathbf{F}} \quad (2.27) \quad \textbf{\textit{s.t.}} \quad (2.11), (2.12), (2.13), (2.21),$$

where $\mathbf{F}'$ *is the value of* $\mathbf{F}$ *after the previous update.*

Proof. From Lemma 1, the domains of $\mathbf{P}^{(\mathbf{F})}_{\textbf{Max-SR}}$ and $\mathbf{P}^{(\mathbf{P})}_{\textbf{Max-SR}}$ are convex. Also, from Lemmas 3 and 4, we have that (2.27) and (2.28) are concave lower bound approximations to (2.20) satisfying the conditions in (2.16)-(2.19). Therefore, from the result in (Razaviyayn *et al.*, 2013), the solution obtained by iteratively updating $\mathbf{F}$ and $\mathbf{P}$ cyclically is a local optimum of $\mathbf{P}'_{\textbf{Max-SR}}$. ■

The complete algorithm to solve the Min-Max problem, $\mathbf{P}_{\textbf{Max-Min}}$, is described in Algorithm 2.2. The algorithm uses $\mathbf{P}^{(\mathbf{F})}_{\textbf{Max-SR}}$ and $\mathbf{P}^{(\mathbf{P})}_{\textbf{Max-SR}}$ as subroutines.

2.5 Numerical Results

In this section the performance of the algorithms proposed in Section 2.4 is presented. Additionally, we compare our results with the three algorithms proposed in (Dabiri & Saeedi, 2018): the fixed user order (FUO), opportunistic allocation (OA) and proportional fair (PF) algorithms. In these three algorithms, the users are sorted according to a different criteria, and the resources are allocated sequentially by picking the best available resource for the user in the sorted order. The FUO algorithm performs the allocation in a random order, while the OA algorithm sorts the users according to their overall channel qualities, prior to the channel allocation. The PF algorithm takes into account the L past channel qualities when sorting the allocation order in order to improve fairness. In our evaluation we consider $L = 10$ and $\alpha = 0.9$.

Algorithm 2.2 Fairness Maximization

Variable Definition :

1. $\mathbf{F}^{(t)}$ is the subcarrier allocation matrix at the t-th iteration.
2. $\mathbf{P}^{(t)}$ is the power allocation matrix at the t-th iteration.

Initialization :

1. Set the initial values for the power allocation matrix $\mathbf{P}^{(0)}$ randomly.
2. Set the initial values for the subcarrier allocation matrix $\mathbf{F}^{(0)}$ randomly.
3. Set the convergence tolerance for the subcarrier allocation ϵ_F.
4. Set the convergence tolerance for the power allocation ϵ_P.
5. $t \leftarrow 0$

Output :

1. Optimized power allocation $\mathbf{P}^*$.
2. Optimized subcarrier allocation $\mathbf{F}^*$.

while $\left\|\mathbf{F}^{(t)} - \mathbf{F}^{(t-1)}\right\| > \epsilon_F$ *and* $\left\|\mathbf{P}^{(t)} - \mathbf{P}^{(t-1)}\right\| > \epsilon_P$ **do**
  $t \leftarrow t + 1$;
  $\mathbf{F^{(t)}} \leftarrow \arg \mathbf{P}^{(\mathbf{F})}_{\textbf{Max-Min}} \left(\mathbf{F}^{(t-1)}, \mathbf{P}^{(t-1)}\right)$; (see Theorem 3)
  $\mathbf{P^{(t)}} \leftarrow \arg \mathbf{P}^{(\mathbf{P})}_{\textbf{Max-Min}} \left(\mathbf{F}^{(t-1)}, \mathbf{P}^{(t-1)}\right)$; (see Theorem 3)
end while
$\mathbf{P}^* \leftarrow \mathbf{P}^{(t)}$;
$\mathbf{F}^* \leftarrow \mathbf{F}^{(t)}$;

We consider a scenario where one BS is serving 6 users over 4 subcarriers, with $N = 2$ and $d_f = 3$, in a circular cell of radius $R = 300$ m and the users are uniformly distributed inside the cell. It is worth mentioning that an increase in N would result in higher diversity, as each user would transmit its signal on more subcarriers. However, as the value of d_f is tied to N (i.e. $d_f = \binom{K-1}{N-1}$), d_f would also increase, resulting in an exponential increase in the decoding complexity. We consider a path loss exponent $\alpha = 4$. We consider a noise power density of -174 dBm/Hz and a bandwidth of 180 kHz. Also, we consider a normalized slow fading Rayleigh channel, such that the channel remains constant for the duration of each transmitted symbol. Furthermore, we simulate the algorithms' performance for a maximum transmit power per user varying between 3 dBm and 10 dBm. We evaluate the performances according to two metrics: the sum-rate and the Jain's fairness index (Lan, Kao, Chiang & Sabharwal, 2010). The former, is a measure of the overall achievable throughput of the network and the latter is a

measure of the fairness of the resource allocation between the users based on their individual achievable throughputs. Let $\mathbf{c} \in \mathbb{R}^J$ be a vector, such that, its i-th coordinate, c_i, corresponds to the throughput of the i-th user. The Jain's fairness index for a given rate vector, $\mathbf{c} = [c_1, \cdots, r_J]^T$, is

$$J(\mathbf{c}) = \frac{\left(\sum_{j=1}^{J} c_j\right)^2}{J \sum_{j=1}^{J} c_j^2}. \tag{2.29}$$

This index varies from $\frac{1}{J}$, meaning no fairness, to 1, meaning perfect fairness. Furthermore, we consider a normalized Rayleigh fading channel, and the performances are averaged over several channel realizations.

To implement the proposed algorithms, we used the convex optimization modeling language CVXPY (Diamond & Boyd, 2016; Agrawal, Verschueren, Diamond & Boyd, 2018), with the open-source ECOS solver (Domahidi, Chu & Boyd, 2013), due to its support of exponential cones (Serrano, 2015). The comparison of the sum-rate of the five algorithms is shown in Figure 2.3. The sum-rate of the Max-SR algorithm outperforms the Max-Min, FUO, OA, and PF algorithms for the whole range of transmitted power evaluated. The three algorithms proposed in (Dabiri & Saeedi, 2018) present similar performances with the proportional fairness being slightly worse than the other two. Finally, the Max-Min algorithm is greatly outperformed by the other ones. This result is expected since the Max-Min gives up on maximizing the sum-rate in favor of improving the fairness.

Figure 2.4 shows the Jain's fairness index achieved by each algorithm. The Max-Min algorithm greatly outperforms the alternatives for the whole range of transmitted powers. It is worth noting that the Jain's fairness index is bottlenecked by the rate of the user with the worst channel. Therefore, an increase in the maximum transmit power results in a higher throughput for the worst user, consequently, increasing the overall fairness. Furthermore, with increasing maximum transmit power, the fairness of the Max-Min algorithm approaches one. The other algorithms

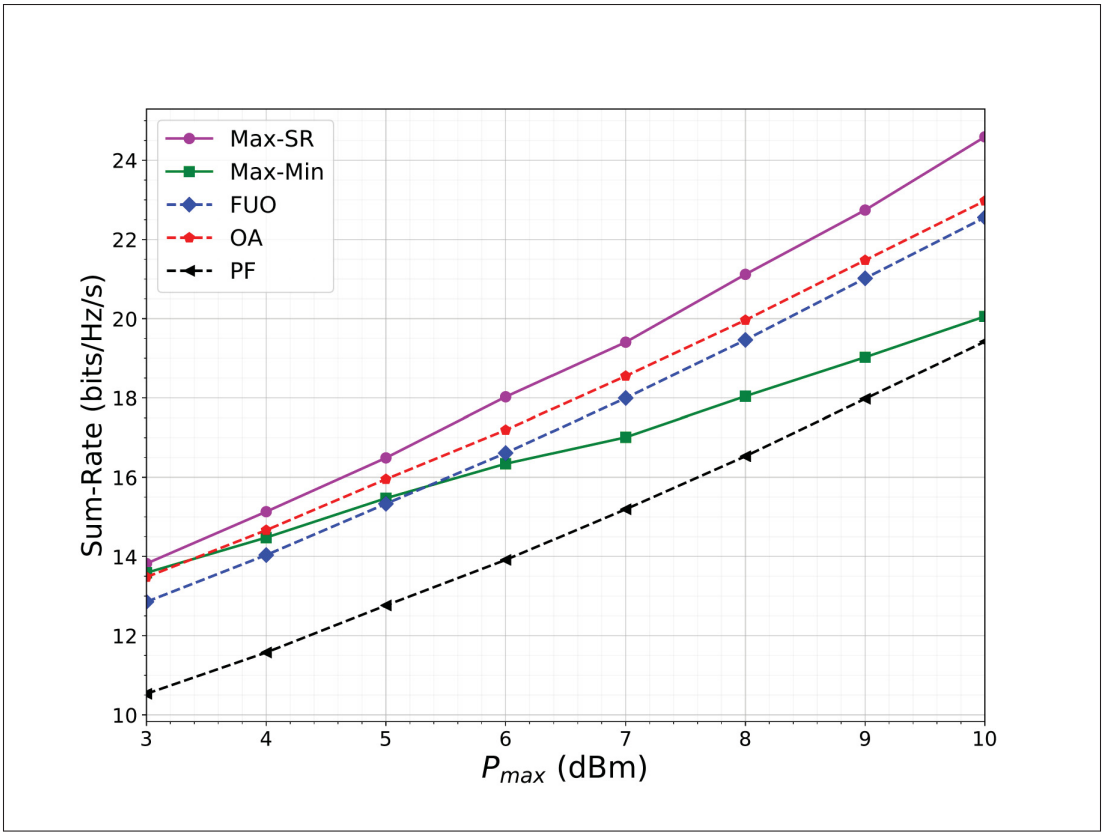

Figure 2.3 Sum-rate comparison for $J = 6$, $K = 4$, $d_f = 3$ and $N = 2$

achieve similar fairness performance, with the PF algorithm achieving slightly better fairness than the others.

In order to evaluate the link level performance of the Max-SR and Max-Min allocation, another simulation, evaluating the BER of both allocation algorithms, is presented. In the simulation, each user transmits a multidimensional symbol with $M = 4$ using a quadrature amplitude modulation (QAM) mother constellation (Nikopour & Baligh, 2013). We assume that the users' channel gains are ordered, such that, $\|\mathbf{H}_1\|_F \leq \|\mathbf{H}_2\|_F \leq \cdots \leq \|\mathbf{H}_J\|_F$, i.e., the first user has the worst channel gain, while the last user has the best one. Figure 2.5, shows a comparison between the BER of the 6 users using Max-SR and Max-Min allocation. As expected, with Max-SR allocation, the error probabilities are small, but there is a large gap between the best and the worst user. On the other hand, Max-Min allocation results in overall larger error probabilities

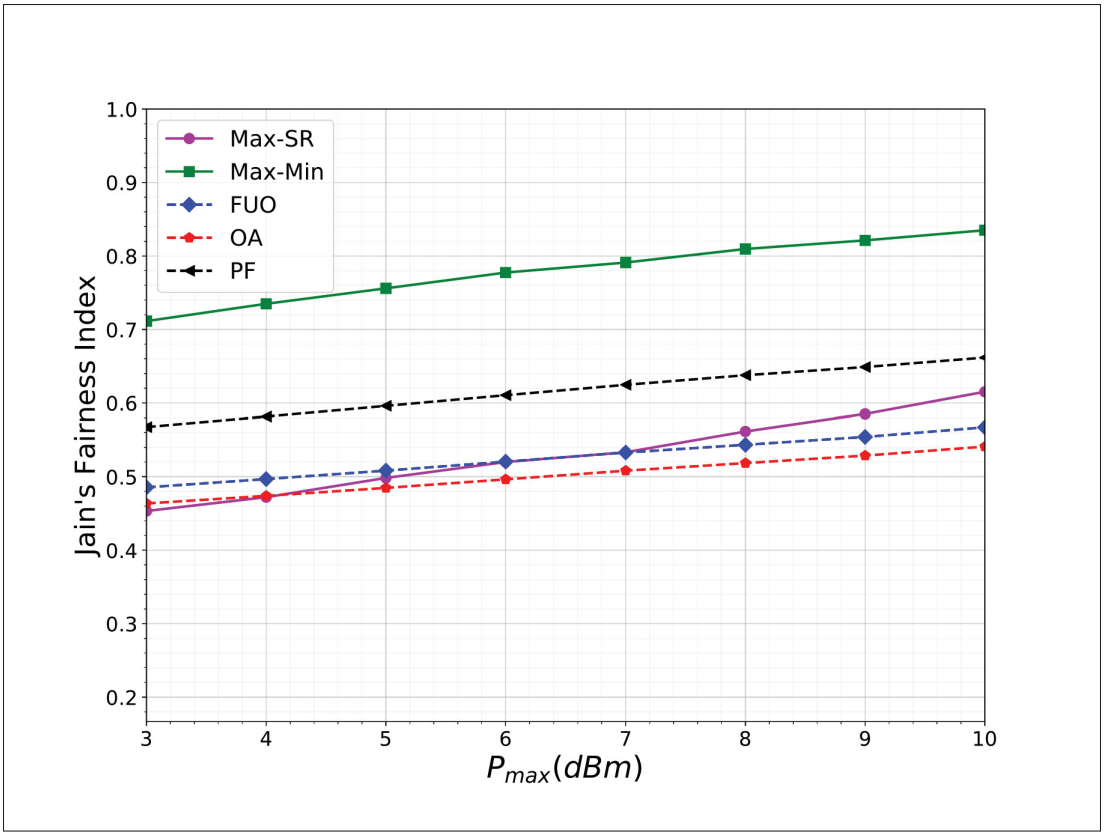

Figure 2.4 Jain's fairness index comparison for $J = 6$, $K = 4$, $d_f = 3$ and $N = 2$

when compared to the Max-SR, but the performance gap between users with different channel quality is smaller.

2.5.1 Performance with Outdated CSI

In this section, we investigate the effect on the performance of the algorithms, under an outdated CSI regime. In the results shown so far, we considered that for every new channel realization the users would send a pilot sequence to the BS, who would run the optimization routine and send the allocations back to the users. This approach requires a large overhead as it requires pilots and allocations to be sent constantly between the users and the BS. Hence, we consider a system where the pilots are sent periodically with period T, and the users reuse the same allocation during the period, as illustrated in Figure 2.6.

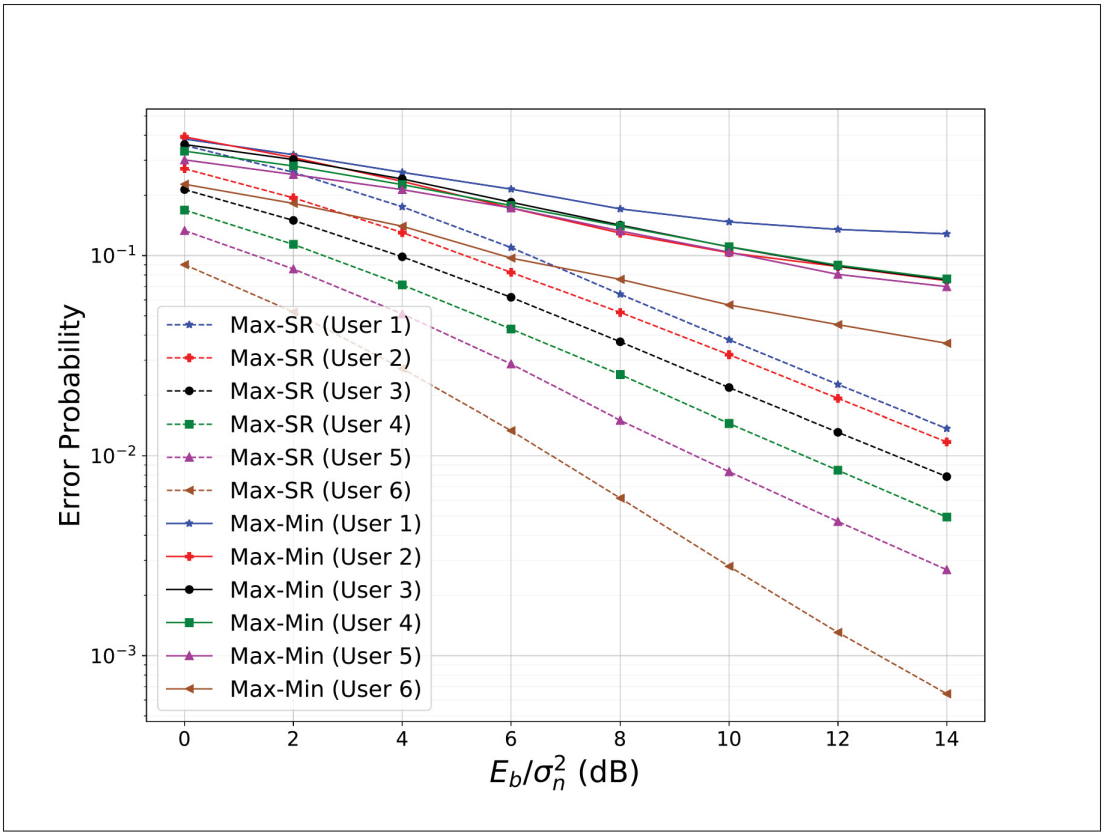

Figure 2.5 BER comparison for $J = 6$, $K = 4$, $d_f = 3$ and $N = 2$

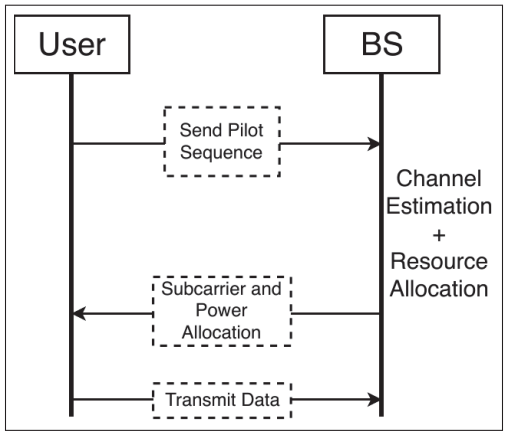

Figure 2.6 Resource allocation procedure

In this experiment, we model the temporal relationship between two successive channel realizations as an i.i.d first-order Gauss-Markov process (Patzold, 2012), for each $k \in \mathcal{K}$ and

$j \in \mathcal{J}$, given by

$$h_{k,j}^{(n+1)} = \rho h_{k,j}^{(n+1)} + w_{k,j}, \tag{2.30}$$

where $h_{k,j}^{(n)} \sim \mathcal{CN}(0,1)$ and $w_{k,j}^{(t)} \sim \mathcal{CN}(0, 1-\rho^2)$ is the innovation component. Moreover The correlation between successive fading components is given by

$$\rho = J_0\left(2\pi f_{\max} T_s\right), \tag{2.31}$$

where $f_{\max}$ is the maximum Doppler frequency, T_s is the time between channel updates, and J_0 is the Bessel function. Figure 2.7 shows the performance deterioration for $T \in [1, 50]$, $P_{\max} = 10$ dBm, $T_S = 0.01$ s, and four values of $f_{\max}$ resulting in $\rho^2 \in \{0.95, 0.62, 0.22, 0.01\}$.

Tables 2.1 and 2.2 summarizes the effects of outdated CSI in the performance of Max-SR and Max-Min algorithms respectively. From the table results we conclude that the Max-SR algorithm is more robust to outdated CSI as for the worst case ($T = 50$ and $\rho^2 = 0.01$), it still achieves 85% of the sum-rate with $T = 1$, while the Max-Min only achieves 75% of the original fairness. Moreover, as in the proposed model the same allocation is reused for subsequent transmissions, and the less correlated the current CSI is with the one used to obtain the allocation (i.e. longer periods between updates), the more it resembles a random allocation, resulting in a performance decrease. For instance, the Max-Min algorithm maximizes the fairness of the system, hence, its fairness index decreases with longer periods. On the other hand, we observe in Figure 2.7 that its sum-rate increases with longer periods, thus, we conclude that the Max-Min algorithm increases fairness at the expense of the sum-rate. The same does not happen in the Max-SR algorithm as the fairness remains roughly the same under the effect of outdated CSI.

2.5.2 Convergence Analysis and Algorithm Complexity

In this section, the convergence rate of the proposed algorithms and their complexity is investigated.

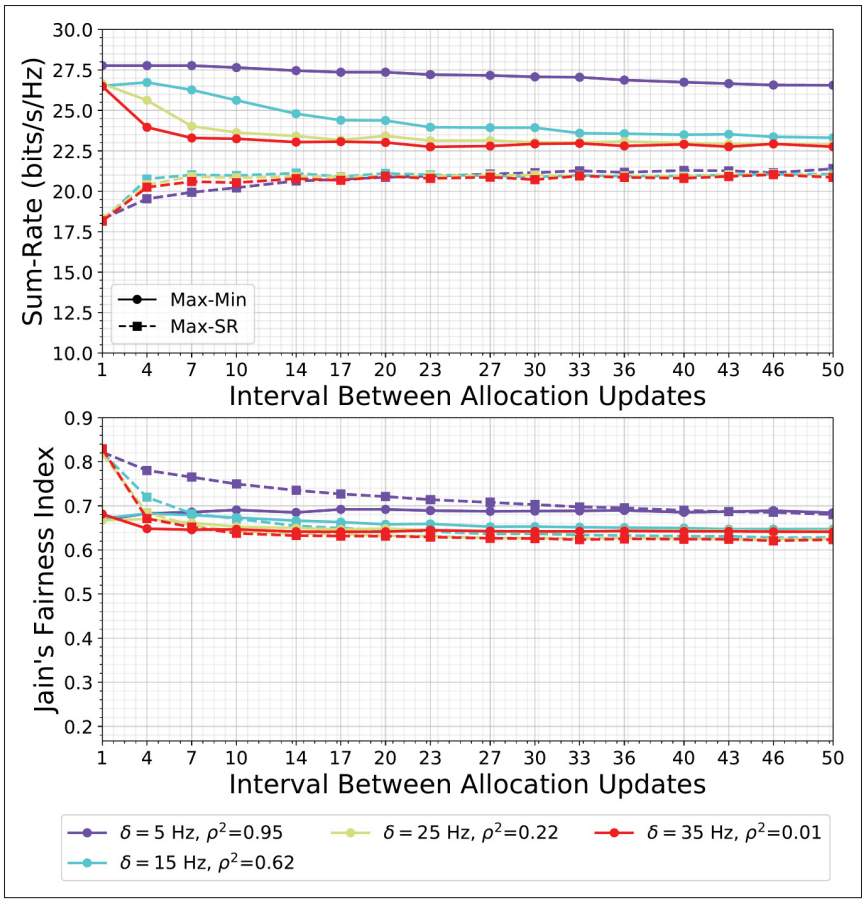

Figure 2.7 Performance of the Max-SR (solid line) and Max-Min (dashed line) allocations for $T \in [1, 50]$ and different values of $f_{\max}$

Table 2.1 Performance Deterioration with Outdated CSI (Max-SR)

	Fairness	**Sum-Rate**
$\rho^2 = 0.95$	102.38%	98.81%
$\rho^2 = 0.62$	96.45%	87.88%
$\rho^2 = 0.22$	96.47%	85.85%
$\rho^2 = 0.01$	94.11%	85.89%

The stopping criteria for the procedure is based on the difference between successive updates of the optimization variables $\mathbf{F}$ and $\mathbf{P}$. When this difference falls below a threshold, ϵ_F and ϵ_P,

Table 2.2 Performance Deterioration with Outdated CSI (Max-Min)

	Fairness	**Sum-Rate**
$\rho^2 = 0.95$	83.58%	119.73%
$\rho^2 = 0.62$	77.22%	114.51%
$\rho^2 = 0.22$	76.66%	112.38%
$\rho^2 = 0.01$	74.99%	115.34%

respectively, the algorithm has converged. In order to illustrate the convergence, Algorithms 2.1 and 2.2 are simulated with $P_{\max}^{(j)} = 10$ dBm $\forall\ j \in \mathcal{J}$, with the same channel gains and users location, but with three randomly chosen initial conditions $(\mathbf{F}^{(0)}, \mathbf{P}^{(0)})$.

Figure 2.8 shows the convergence of Algorithm 2.1. Each iteration in Figure 2.8 consists of a full cycle of updates.

In Figure 2.9, the convergence of Algorithm 2.2 is shown. The algorithm converges in five steps or less for all three initial conditions. Furthermore,

Algorithm 2.1 consistently converges to a higher sum-rate than Algorithm 2.2, while Algorithm 2.2 converges to a higher fairness index as expected.

2.5.2.1 Algorithm Complexity

Each update of the Max-SR algorithm involves solving a convex optimization problem, namely $\mathbf{P}_{\textbf{Max-SR}}^{(\mathbf{F})}$ for the subcarrier allocation update and $\mathbf{P}_{\textbf{Max-SR}}^{(\mathbf{P})}$ for the power allocation update. We consider that both update steps are solved using a primal-dual interior point algorithm (Nocedal & Wright, 2006) with a logarithmic barrier function.

Definition 2.1 (ϵ-optimal solution)**.** *Let*

$$\max_{\mathbf{x}} \quad f(\mathbf{x}) \quad \textit{s.t.} \quad \mathbf{x} \in \mathcal{X},$$

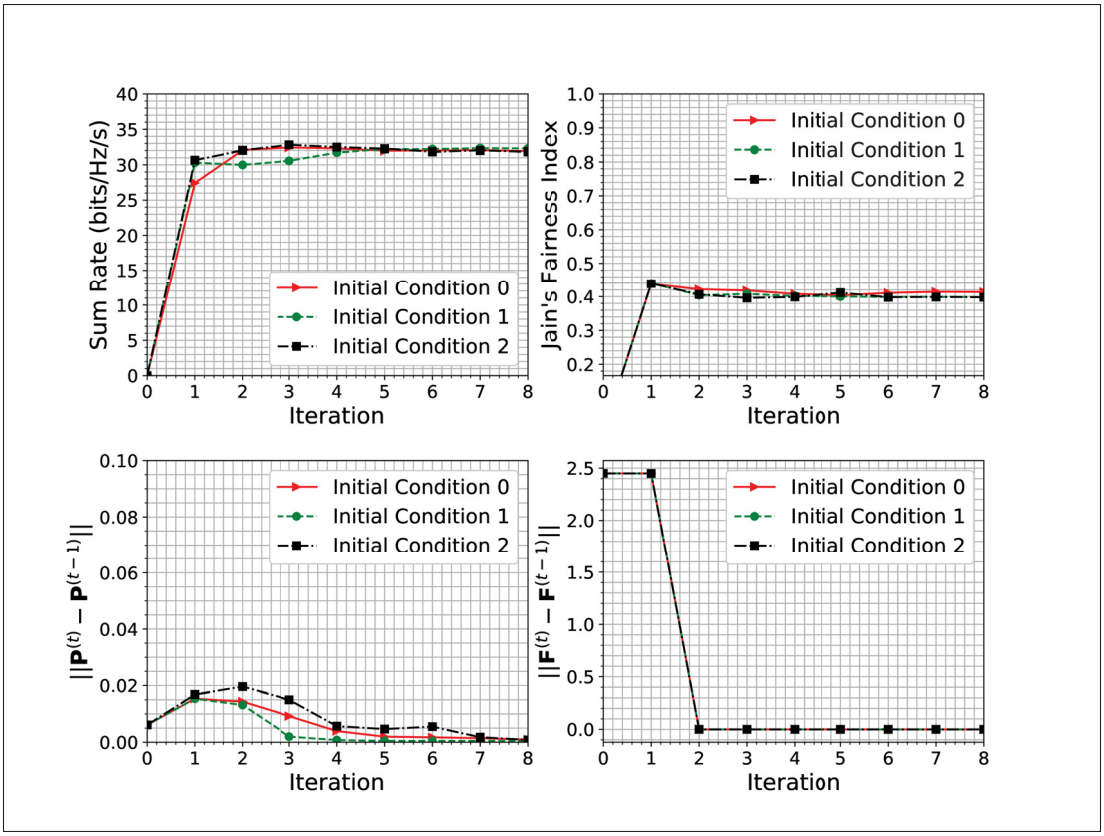

Figure 2.8 Convergence of the $\mathbf{P}_{\textbf{Max-SR}}$, with maximum transmit power of 10 dBm, algorithm for three different initial conditions

where $f(\mathbf{x})$ is a concave function and $\mathcal{X}$ is a convex set be an optimization problem such that $\mathbf{x}^*$ is the unique maximizer to the problem. The vector $\mathbf{x}' \in \mathcal{X}$ is an ϵ-optimal solution to the problem if

$$f(\mathbf{x}^*) - f(\mathbf{x}') \leq \epsilon. \tag{2.32}$$

As derived in (Nesterov, Y. and Nemirovskii, A., 1994), the number of steps required to obtain an ϵ-optimal solution to a convex optimization problem using the interior point algorithm with logarithmic barrier function is $O\left(\sqrt{n}\log_2\left(\frac{1}{\epsilon}\right)\right)$, where n is the number of inequality constraints. The problems solved in the update steps $\mathbf{P}^{(\mathbf{F})}_{\textbf{Max-SR}}$ and $\mathbf{P}^{(\mathbf{P})}_{\textbf{Max-SR}}$ have $2J + K + KJ$ and J inequality constraints, respectively. Therefore, the complexity of each subcarrier allocation update is $O\left(\sqrt{2J + K + KJ}\log_2\left(\frac{1}{\epsilon}\right)\right)$ and the complexity of each power allocation update is $O\left(\sqrt{J}\log_2\left(\frac{1}{\epsilon}\right)\right)$. In order to establish the total number of iterations required for the convergence

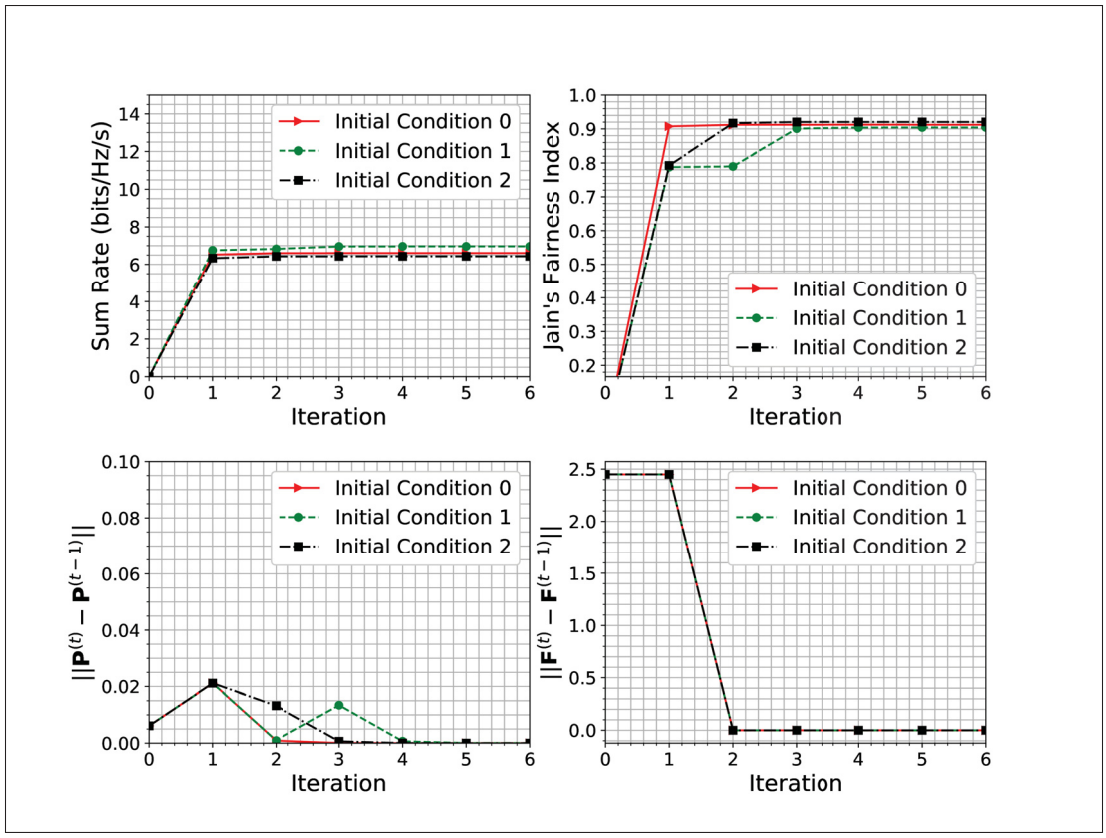

Figure 2.9 Convergence of the $\mathbf{P}_{\text{Max-Min}}$ algorithm, with maximum transmit power of 10 dBm, for three different initial conditions

of the algorithm, we use the result from Theorem 3.1 in (Hong, Wang, Razaviyayn & Luo, 2017). Let

$$\max_{\mathbf{x}} \quad f(\mathbf{x}) \quad \textbf{s.t.} \quad \mathbf{x} \in \mathcal{X},$$

where $f(\mathbf{x})$ might be non-concave and non-smooth, be a generic non-convex optimization problem, and $\mathbf{x}^* \in \mathcal{X}^*$, where $\mathcal{X}^*$ is the set of the problem's stationary points. Then, the optimality gap after the t-th cyclic update of the BLSM algorithm is given by

$$\Delta_t = f(\mathbf{x}^*) - f\left(\mathbf{x}^{(t)}\right) \leq \frac{c}{t}, \tag{2.33}$$

where c is a constant. Therefore, to obtain an ϵ-optimal solution, $\mathcal{O}\left(\frac{1}{\epsilon}\right)$ update steps are necessary. The same results apply to the Max-Min algorithm as the same number of constraints

Table 2.3 Complexity of the Max-SR and Max-Min algorithms

Procedure	Number of Steps
Subcarrier Allocation Update	$O\left(\sqrt{2J+K+KJ}\log_2\left(\frac{1}{\epsilon}\right)\right)$
Power Allocation Update	$O\left(\sqrt{J}\log_2\left(\frac{1}{\epsilon}\right)\right)$
Total Number of Updates	$O\left(\frac{1}{\epsilon}\right)$

are involved to solve the power allocation and subcarrier allocation update problems. Both algorithms complexity are summarized on Table 2.3.

2.6 Conclusions

In this paper, two joint channel and power allocation algorithms are proposed: the Max-SR and the Max-Min algorithms. The former aims for sum-rate maximization, while the latter aims for maximizing fairness. The BSUM framework is employed to obtain algorithms converging to locally optimal points of the relaxed problems. We compare the performance of the Max-SR and the Max-Min algorithms with the ones proposed in (Dabiri & Saeedi, 2018). The results show that the Max-SR algorithm has better performance on the sum-rate sense, while the Max-Min has better performance on the fairness sense. Moreover, a numerical analysis of the convergence of the algorithms is presented. Finally, we derive the worst-case time complexity of both algorithms.

The results show that the Max-SR consistently achieve a better sum-rate, while the Max-Min achieves better fairness.

Furthermore, there is a tradeoff between the fairness and the sum-rate. For future works, we intend to investigate new algorithms that can achieve a compromise between sum-rate and fairness.

CHAPTER 3

ANALYSIS OF CONTENTION-BASED SCMA IN MMTC NETWORKS

Joao V.C. Evangelista[1] , Zeeshan Sattar[1] , Georges Kaddoum[1]

[1] Department of Electrical Engineering, École de Technologie Supérieure,
1100 Notre-Dame Ouest, Montréal, Québec, Canada H3C 1K3

Article published in the IEEE Latincom proceedings, November, 2019.

3.1 Abstract

Massive Machine Type Communication (mMTC) is one of the three new applications of fifth-generation (5G) networks. Users in mMTC applications have different patterns of transmission and requirements than traditional LTE applications; they are massively deployed and transmit small packets of data sporadically. Grant-based access scheme is inefficient to satisfy the mMTC requirements; therefore, grant-free contention-based access (CBA) is appointed as a promising solution to this problem. In this paper, we analyze the performance of contention-based sparse code multiple access (SCMA) concerning the probability of success of transmission and the area spectral efficiency. We derive closed-form expressions for both performance metrics and validate them with numerical simulations. Furthermore, we compare the results with an OFDMA contention-based approach.

3.2 Introduction

The time-line of communication systems is marked heavily by challenging requirements followed by innovative solutions. Every generation of communication systems takes birth in a pool of more stringent performance requirements and use cases than their predecessor. Similarly, the idea of fifth generation (5G) of cellular networks blossomed with the promise of covering new use cases which are not present in LTE networks. The standardization committee for 5G networks identified three new applications, namely enhanced Mobile Broadband (eMBB), massive Machine Type

Communications (mMTC), and Ultra-Reliable Low Latency Communications (URLLC), for the next generation of wireless networks (3GPP, 2017b).

In mMTC applications, the network consists of a dense deployment of user equipment (UE) with low-power and low-cost devices, which transmit small packets sporadically; therefore, we need a random multiple access scheme that is suited for sporadic transmissions of small packets, enables massive connectivity and avoids retransmission, in order to save energy. Radio access in LTE networks follows a grant-based approach with two stages (Hasan, Hossain & Niyato, 2013): the contention-based random access procedure, where the UE transmits a request in a shared channel, and the contention-free stage, where the base station (BS) allocates a dedicated channel to the UE upon successful completion of the first stage. This grant-based approach is inefficient in the mMTC scenario as it incurs in overhead and additional delay, which become more significant when the UE transmits small payloads sporadically.

Grant-free contention-based access (CBA), where the UE transmits its payload directly into the random access shared channel, eliminates the overhead and reduces the delay incurred in the grant-based procedure, is proposed as an alternative in (Zhou, Nikaein, Knopp & Bonnet, 2012). However, as the payload is transmitted in the shared channel, a downside of this approach is that collisions might occur resulting in retransmissions. In order to mitigate this issue, the work in (Singh *et al.*, 2018) proposes multiple transmissions of the same packet to reduce collisions and achieve the target reliability within a latency window.

In (Au *et al.*, 2014), the authors propose a grant-free CBA scheme employing sparse code multiple access (SCMA) (Nikopour & Baligh, 2013). SCMA allows for an overload in the network allowing more connections with the same number of resources. They present a simulation comparing the packet drop rate and the number of supported users for a given outage requirement of a contention-based SCMA network with a contention-based orthogonal frequency division multiple access (OFDMA). The results show that SCMA enables a three-fold increase of the number of supported users in comparison to OFDMA.

3.2.1 Related Work

Most of the research efforts in SCMA has been dedicated to the design of SCMA codebooks (Taherzadeh *et al.*, 2014), and link-level performance metrics, such as the bit-error rate (BER) and symbol-error rate (SER) performance of SCMA (Yu, Fan, Lei & Mathiopoulos, 2017; Cai, Fan & Mathiopoulos, 2017; Lim, Kim & Park, 2017). In (Yang, Lei, Ding, Fan & Karagiannidis, 2017), the sum-rate performance of SCMA in a single hexagonal cell with randomly deployed users is investigated. More recently, authors in (Liu *et al.*, 2017) and (Liu, Sheng, Liu, Wang & Li, 2018) proposed scalable stochastic geometric models to analyze the performance of SCMA in large networks. In (Liu *et al.*, 2017) a comparison between a hybrid device-to-device (D2D) network, employing OFDMA and SCMA is proposed. In (Liu *et al.*, 2018), bounds on the area spectral efficiency (ASE) and the transmission success probability of a large SCMA network are investigated.

3.2.2 Contributions

Our main contribution in this paper, is the modeling and analysis of contention-based SCMA access in a large network. We obtain closed-form expressions for the probability of success and the ASE. To the best of our knowledge, this is the first work where these performance metrics are obtained in closed-form for a large contention-based SCMA network. Additionally, we compare contention-based SCMA's performance with its OFDMA counterpart.

This paper is organized as follows. In Section 3.3, the system model and its assumptions are presented. In Section 3.4, expressions for the probability of success and ASE for contention-based SCMA and OFDMA are derived. Section 3.5 shows a numerical simulation of the performance metrics, where we compare numerical and analytical results. Finally, in Section 3.6, the conclusions are summarized.

3.3 System Model

In LTE networks, the physical random access channel (PRACH) is used to establish a connection between an eNodeB and a user. This procedure involves an exchange of four messages (Laya, Alonso & Alonso-Zarate, 2014) (PRACH preamble, random access response, connection request, and contention resolution) before the user can transmit its payload. This setup is extremely inefficient for the transmission of small packets of data and users with tight delay constraints. In grant-free CBA, the data payload is transmitted together with the PRACH preamble, reducing the data exchange overhead, and potentially reducing access latency. However, this scheme faces challenges when serving a massive number of users. As the number of orthogonal network resources is finite, the likelihood of collisions increases with the number of users served. A promising solution to address the scaling issues of grant-free CBA is to employ SCMA (Au *et al.*, 2014). In this section, we develop analytical models to characterize and compare the performances of OFDMA-based and SCMA-based grant-free CBA.

3.3.1 Network Geometry

We consider a contention-based access network, consisting of randomly deployed BSs and UEs. We model the location of the BSs using a two-dimensional homogeneous Poisson point process (HPPP) $\Phi_B = \{B_1, B_2, \cdots\} \subset \mathbb{R}^2$, with intensity λ_B. Similarly, the locations of the UEs are modeled by another HPPP $\Phi_U = \{U_1, U_2, \cdots\} \subset \mathbb{R}^2$, with intensity λ_U. We assume that each UE is transmitting data to its closest BS and at each time-slot each UE transmits with probability ζ. The distance between U_i and B_j is denoted by $r_{i,j}$, and the distance to the closest BS to U_i is given by $\bar{r}_i = \min r_{i,j} \; \forall \; B_j \in \Phi_B$. The distribution of $\bar{r}_i$ is given as follows (Haenggi, 2013)

$$f_{\bar{r}_i}(r) = 2\lambda_B \pi r e^{-\lambda_B \pi r^2}. \tag{3.1}$$

Without loss of generality, we evaluate the performance of a typical link between a typical UE U_0 and its closest BS B_0. Due to Slivnyak's theorem (Baddeley, Bárány & Schneider, 2007), the performance of the network can be generalized by the performance of a typical link. Fig. 3.1

shows a realization of the point process following this model with $\lambda_U = 10^{-3}$, $\lambda_B = 10^{-4}$. The lines connect the UE to its serving BS.

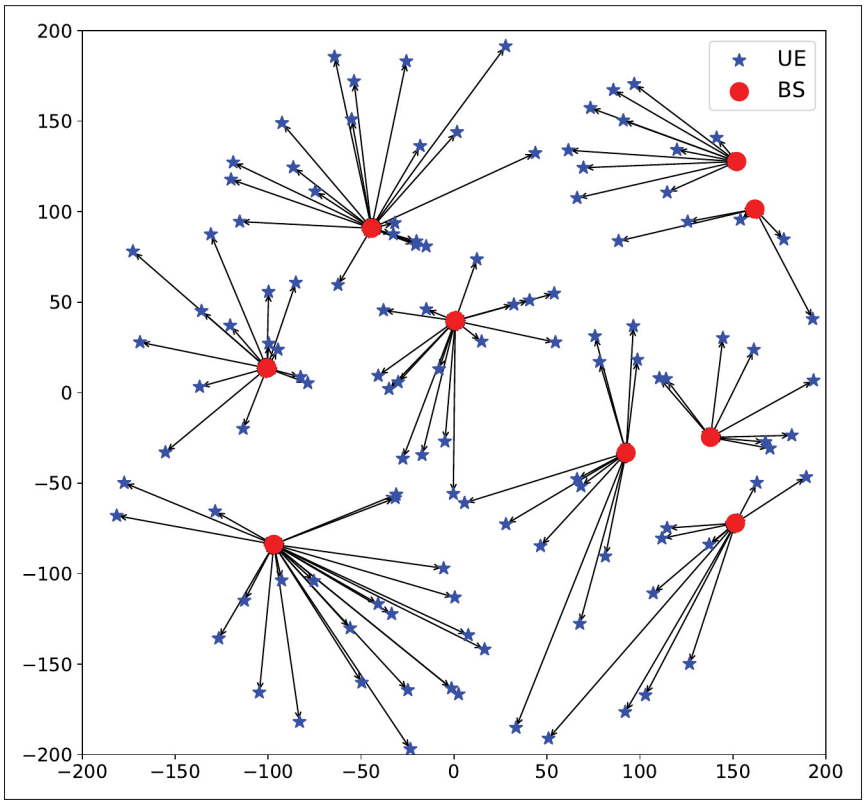

Figure 3.1 Realization of the position of BSs and UEs in a 200 m radius with $\lambda_U = 10^{-3}$, $\lambda_B S = 10^{-4}$. The lines connect the UE to its serving BS

3.3.2 Channel Model

The channel gain between U_i and B_j is given by $g_{i,j} = \left\|h_{i,j}\right\|^2 l(r_{i,j})$, where $h_{i,j}$ is the small scale fading coefficient, $\|x\|$ denotes the absolute value of x, and $l(\cdot)$ is the path loss gain. We assume that each $h_{i,j}$ is an independent identically distributed (i.i.d) complex normal random variable with mean zero and unit variance so $\left\|h_{i,j}\right\|^2 \sim \exp(1)$. Moreover, we assume a singular path loss model, such that $l(r_{i,j}) = r_{i,j}^{-\alpha}$, where α is the path loss exponent. We assume that the network is interference limited, i.e. the noise power is negligible in comparison to the interference (Haenggi, 2013).

3.3.3 Multiple Access

Since our aim is to show the advantages of contention-based SCMA, we compare its performance with an equivalent contention-based OFDMA scheme. From this point on, the subscript/superscript O is used to denote quantities related to the OFDMA method, while S is used to denote quantities related to the SCMA scheme.

In the grant-free contention-based OFDMA network, we assume that there are L orthogonal preambles and K orthogonal subcarriers available for the transmission. At each transmission slot, an UE has new data to transmit with probability ζ. When an UE is transmitting, it randomly selects one preamble and one orthogonal subcarrier to transmit its message with power P. Different UEs interfere with each other if they select the same preamble and the same subcarrier in the same time slot. Therefore, the set of interfering UEs is obtained by thinning the original point process Φ_U, leading to $\widetilde{\Phi}_U^O$ with intensity (Haenggi, 2013)

$$\tilde{\lambda}_U^O = \frac{1}{L}\frac{1}{K}\zeta\lambda_U. \tag{3.2}$$

Furthermore, the received signal at B_0 is the sum between the desired signal coming from U_0 and the interfering signals from users transmitting with the same preamble and subcarrier. Therefore,

$$y_{B_0}^O = \sqrt{P\bar{r}_0^{-\alpha}}h_{0,0}x_0 + \sum_{U_i\in\widetilde{\Phi}_B^O}\sqrt{Pr_{i,0}^{-\alpha}}h_{i,0}x_i, \tag{3.3}$$

where x_i is the symbol transmitted by user i and $E[|x_i|^2] = 1$, and its respective signal-to-interference ratio (SIR) is given by

$$\mathrm{SIR}_O = \frac{P\left\|h_{0,0}\right\|^2 \bar{r}_0^{-\alpha}}{\sum\limits_{U_i\in\widetilde{\Phi}_U^O} P\left\|h_{i,0}\right\|^2 r_{i,0}^{-\alpha}}. \tag{3.4}$$

On the other hand, in the SCMA transmission, J data layers are multiplexed into K subcarriers. Each layer has a codebook containing M codewords of size K, such that each coordinate of a

codeword is mapped into a subcarrier. The SCMA encoder maps a stream of $\log_2(M)$ bits into one of the M codewords from its codebook. Each K dimensional codeword has N non-zero coordinates, such that $N \ll K$ (Nikopour & Baligh, 2013). In this work, we assume that each user is scheduled to transmit its information in one layer. Figure 3.2 illustrates a possible mapping between J layers into K subcarriers, such that each layer is mapped to two subcarriers. The number of data layers J is equal to the number of ways to group N subcarriers out of K, thus, $J = \binom{K}{N}$. Moreover, the optimal decoding of SCMA multidimensional symbols can be achieved with a maximum a priori (MAP) decoder.In this paper, we consider an ideal MAP joint detector, such that codewords from different codebooks are orthogonal (Liu *et al.*, 2017, 2018), hence, users transmitting on different layers do not interfere with each other.

In the SCMA scenario, two users interfere if they transmit on the same time-slot using the same preamble, and data layer. Similarly to the OFDMA scenario, we can obtain the point process of interferers by thinning the original user point process Φ_U and obtaining $\widetilde{\Phi}_U^S$ with intensity

$$\tilde{\lambda}_U^S = \frac{1}{L}\frac{1}{J}\zeta\lambda_U. \tag{3.5}$$

Additionally, the received signal at B_0 is given by

$$y_{B_0}^S = \sum_{n=1}^{N}\sqrt{\frac{P}{N}\bar{r}_0^{-\alpha}}h_{0,0}^n x_0 + \sum_{U_i\in\widetilde{\Phi}_U^S}\sum_{n=1}^{N}\sqrt{\frac{P}{N}r_{i,0}^{-\alpha}}h_{i,0}^n x_i, \tag{3.6}$$

where we assume the power is split equally between the N subcarriers and $h_{i,j}^n$ is the small scale fading coefficient between UE i and BS j on subcarrier n. Hence, the SIR employing SCMA access is given by

$$\mathrm{SIR}_S = \frac{\sum_{n=1}^{N}\frac{P}{N}\left\|h_{0,0}^n\right\|^2\bar{r}_0^{-\alpha}}{\sum_{U_i\in\widetilde{\Phi}_U^S}\sum_{n=1}^{N}\frac{P}{N}\left\|h_{i,0}^n\right\|^2 r_{i,0}^{-\alpha}}. \tag{3.7}$$

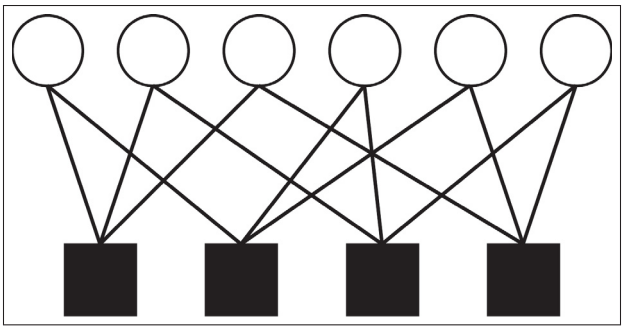

Figure 3.2 Example of a mapping between SCMA layers (empty circles) and subcarriers (filled squares), with parameters $J = 6$, $K = 4$ and $N = 2$

3.4 Analytical Results

The probability of successfully transmitting a symbol (i.e. the SIR at the receiver is large enough to recover the original information) and the ASE (i.e. the upper-bound on the number of bits that can be transmitted over a time-frequency block in an area of the network) are important metrics to evaluate the performance of a network. Having analytical expressions for this quantities is of great help when designing and planning a network. In this section, we obtain analytical expressions for the probability of success in the transmission of a symbol employing contention-based OFDMA (i.e. p_O) and SCMA (i.e. p_S) multiple access. In both scenarios a transmission is successfully decoded if the SIR is higher than a threshold τ, therefore

$$p_i = \mathbb{P}\left\{\text{SIR}_i \geq \tau\right\} \; \forall \, i \in \{O, S\}. \tag{3.8}$$

Furthermore, we also analyze the ASE in both scenarios, which is given by

$$\text{ASE}_i = \lambda_U p_i \log_2(1 + \tau) \, \forall \, i \in \{O, S\}. \tag{3.9}$$

3.4.1 OFDMA Performance Analysis

As the ASE depends on the success probability, we start by obtaining an expression for p_O.

Theorem 4. *The probability of successfully transmitting an OFDMA symbol is given by*

$$\mathbb{P}\left\{\mathrm{SIR}_O \geq \tau\right\} = \frac{\alpha\lambda_B}{2\tilde{\lambda}_U^O \tau^{\frac{2}{\alpha}}\Gamma(1-2/\alpha)\Gamma(2/\alpha)+\alpha\lambda_B}. \tag{3.10}$$

Proof. First, let I_O be the sum of the signals interfering with user U_0 at BS B_0. Then, I_O is written as

$$I_O = \sum_{U_i \in \widetilde{\Phi}_B^O} P\left\|h_{i,0}\right\|^2 r_{i,0}^{-\alpha}.$$

We proceed the derivation by obtaining the probability of success given $\bar{r}_0$ and I_O as follows

$$\begin{aligned}
\mathbb{P}\left\{\mathrm{SIR}_O \geq \tau | \bar{r}_0, I_O\right\} &= \mathbb{P}\left\{\frac{P\left\|h_{0,0}\right\|^2 \bar{r}_0^{-\alpha}}{I_O} \geq \tau\right\} \\
&= \mathbb{P}\left\{\left\|h_{0,0}\right\|^2 \geq \frac{\tau \bar{r}_0^{\alpha} I_O}{P}\right\} \\
&\overset{(a)}{=} \exp\left(-\frac{\tau I_O \bar{r}_0^{\alpha}}{P}\right),
\end{aligned} \tag{3.11}$$

where (a) comes form the fact that $\left\|h_{0,0}\right\|^2$ is exponentially distributed, as mentioned in Section 3.3.2. Let $E_x[\cdot]$ be the expected value over a random variable x. Now, to obtain $\mathbb{P}\left\{\mathrm{SIR}_O \geq \tau | \bar{r}_0\right\}$

we average (3.11) over I_O as shown below

$$\begin{aligned}
&\mathrm{E}_{I_O}\left[\exp\left(-\frac{\tau I_O \bar{r}_0^{\alpha}}{P}\right)\right] \\
&= \mathrm{E}_{\widetilde{\Phi}_U^O}\left[\mathrm{E}_{\|h_{i,0}\|^2}\left[\exp\left(-\frac{\tau \bar{r}_0^{\alpha} \sum\limits_{U_i \in \widetilde{\Phi}_U^O} P\left\|h_{i,0}\right\|^2 r_{i,0}^{-\alpha}}{P}\right)\right]\right] \\
&= \mathrm{E}_{\widetilde{\Phi}_U^O}\left[\prod_{U_i \in \widetilde{\Phi}_U^O} \mathrm{E}_{\|h_{i,0}\|^2}\left[\exp\left(-\tau \bar{r}_0^{\alpha}\left\|h_{i,0}\right\|^2 r_{i,0}^{-\alpha}\right)\right]\right] \\
&\overset{(b)}{=} \mathrm{E}_{\widetilde{\Phi}_U^O}\left[\prod_{U_i \in \widetilde{\Phi}_U^O} \frac{1}{1+\tau \bar{r}_0^{\alpha} r_{i,0}^{-\alpha}}\right] \\
&\overset{(c)}{=} \exp\left(-2\pi \tilde{\lambda}_U^O \int_0^{\infty}\left(1-\frac{1}{1+\tau \bar{r}_0^{\alpha} r_{i,0}^{-\alpha}}\right) r_{i,0} \mathrm{d}r_{i,0}\right) \\
&\overset{(d)}{=} \exp\left(-\frac{2\tilde{\lambda}_U^O \tau^{\frac{2}{\alpha}} \Gamma(1-2/\alpha)\Gamma(2/\alpha)}{\alpha} \bar{r}_0^2\right),
\end{aligned} \tag{3.12}$$

where (b) comes from the Laplace transform of $\left\|h_{i,0}\right\|^2$ evaluated at $\tau \bar{r}_0^{\alpha} r_{i,0}^{-\alpha}$, while (c) is obtained as the probability generating functional of a HPPP (Haenggi, 2013), and, (d) is obtained by solving the integral (see (Gradshteyn & Ryzhik, 2007)). Finally, by averaging (3.12) over $\bar{r}_0$ we obtain

$$\begin{aligned}
p_O = \int \exp&\left(-\frac{2\tilde{\lambda}_U^O \tau^{\frac{2}{\alpha}} \Gamma(1-2/\alpha)\Gamma(2/\alpha)}{\alpha} \bar{r}_0^2 - \lambda_B \pi \bar{r}_0^2\right) \\
&\times 2\pi \lambda_B \bar{r}_0 d\bar{r}_0.
\end{aligned} \tag{3.13}$$

The solution to the integral in (3.13) is (3.10), concluding the proof. ■

Next, by substituting (3.10) into (3.9), the ASE for the OFDMA network is obtained as follows

$$\mathrm{ASE}_O = \frac{\alpha \frac{\lambda_B}{\tilde{\lambda}_U^i}}{2\tau^{\frac{2}{\alpha}}\Gamma(1-2/\alpha)\Gamma(2/\alpha) + \alpha\frac{\lambda_B}{\tilde{\lambda}_U^i}} \log_2(1+\tau). \tag{3.14}$$

3.4.2 SCMA Performance Analysis

Similarly to Section 3.4.1, we start by deriving the probability of success in a contention-based SCMA network. Firstly, we consider the case where each codeword has N non-zero coordinates, for which we derive a non closed-form result.

Theorem 5. *The probability of successfully transmitting a SCMA symbol is given by*

$$p_S = \int_0^\infty e^{-\rho\bar{r}_0^2}\left(1 + \sum_{i=1}^{N-1}\frac{1}{i!}\sum_{l=1}^{i}\theta_l^i \bar{r}_0^{2l}\right) 2\pi\lambda_B \bar{r}_0 e^{-\lambda_B\pi\bar{r}_0^2} d\bar{r}_0, \tag{3.15}$$

where

$$\rho = \frac{\tilde{\lambda}_U^S}{\Gamma(N)}\pi\tau^{2/\alpha}\Gamma(1-2/\alpha)\Gamma(N+2/\alpha), \tag{3.16}$$

and

$$\theta_l^i = \left(\frac{2\tilde{\lambda}_U^S\pi\tau^{2/\alpha}\Gamma(N+2/\alpha)}{\Gamma(N)\alpha}\right)^l \sum_{M\in\mathcal{M}_l^{(i)}} \frac{C_M}{l!}\prod_{j=1}^{l}\Gamma(m_j - 2/\alpha), \tag{3.17}$$

where $\mathcal{M}_l^i \subseteq \mathbb{N}^l$ is the set of all vectors such that its elements $\left\|m_j\right\|_1 = i$, and,

$$C_M = \frac{i!}{\prod_{j=1}^{l} m_j!}.$$

Proof. We follow a similar procedure used to prove Theorem 4. First, let I_S be the sum of signals interfering with user U_0 at BS B_0. Then, I_S is given by

$$I_S = \sum_{U_i \in \tilde{\Phi}_U^S} \sum_{n=1}^{N} \frac{P}{N} \left\| h_{i,0}^n \right\|^2 r_{i,0}^{-\alpha}. \tag{3.18}$$

The probability of success given $\bar{r}_0$ and I_S is given by

$$\mathbb{P}\left\{\text{SIR}_S \geq \tau | \bar{r}_0, I_S\right\} = \mathbb{P}\left\{ \sum_{n=1}^{N} \left\| h_{0,0}^n \right\|^2 \geq \frac{\tau \bar{r}_0^{-\alpha} I_S}{P/N} \right\}. \tag{3.19}$$

As defined in Section 3.3.2, each $\left\| h_{0,0}^n \right\|^2$ is an i.i.d exponential random variable with scale parameter equal to one. Therefore, we have that $\sum_{n=1}^{N} \left\| h_{0,0}^n \right\|^2 \sim \Gamma(N,1)$ follows a Gamma distribution. Using the sum representation of the upper incomplete Gamma function we have that the complementary cumulative distribution function (CCDF) in (3.19) is given by

$$\begin{aligned} &\mathbb{P}\left\{ \sum_{n=1}^{N} \left\| h_{0,0}^n \right\|^2 \geq \frac{\tau \bar{r}_0^{\alpha} I_S}{P/N} \middle| \bar{r}_0, I_S \right\} \\ &= \sum_{i=0}^{N-1} \frac{\left[\tau \bar{r}_0^{\alpha}\right]^i}{i!} I_S \exp\left(-\tau \bar{r}_0^{\alpha} r_{i,0}^{-\alpha}\right). \end{aligned} \tag{3.20}$$

Using Theorem 2 in (Schilcher *et al.*, 2016), the average of (3.20) over I_S is given as follows

$$\begin{aligned} &\mathbb{P}\left\{SIR_S \geq \tau | \bar{r}_0\right\} \\ &= \exp\left(-2\pi \tilde{\lambda}_U^S \int_0^{\infty} \left[1 - \left(1 + \tau \bar{r}_0^{\alpha} r_{i,0}^{-\alpha}\right)^N\right] dr_{i,0}\right) \\ &\times \left[1 + \sum_{i=0}^{N-1} \frac{1}{i!} \sum_{l=1}^{i} \sum_{M \in \mathcal{M}_l^{(i)}} \frac{C_M}{l!} \prod_{j=1}^{l} \tilde{\lambda}_U^S \frac{\Gamma(N+m_j)}{\Gamma(N)} \right. \\ &\left. \times \left(2\pi \int_0^{\infty} \frac{\left(\tau \bar{r}_0^{\alpha} r_{i,0}^{-\alpha}\right)^{m_j}}{\left(1 + \tau \bar{r}_0^{\alpha} r_{i,0}^{-\alpha}\right)^{N+m_j}} dr_{i,0}\right)\right] \end{aligned} \tag{3.21}$$

Now let ρ be

$$\rho = \int_0^\infty \left[1 - \left(1 + \tau \bar{r}_0^\alpha r_{i,0}^{-\alpha}\right)^N\right] dr_{i,0}, \tag{3.22}$$

and, θ_l^i be

$$\begin{aligned}\theta_l^i = \quad & 2\pi \int_0^\infty \frac{\left(\tau \bar{r}_0^\alpha r_{i,0}^{-\alpha}\right)^{m_j}}{\left(1 + \tau \bar{r}_0^\alpha r_{i,0}^{-\alpha}\right)^{N+m_j}} dr_{i,0} \\ & \times \sum_{M \in \mathcal{M}_l^{(i)}} \frac{C_M}{l!} \prod_{j=1}^{l} \tilde{\lambda}_U^S \frac{\Gamma(N + m_j)}{\Gamma(N)}.\end{aligned} \tag{3.23}$$

Hence, (3.21) can be rewritten as

$$\mathbb{P}\left\{SIR_S \geq \tau | \bar{r}_0\right\} = e^{-2\pi \tilde{\lambda}_U^S \rho} \left(1 + \sum_{i=0}^{N-1} \frac{1}{i!} \sum_{l=1}^{i} \theta_l^i\right) \tag{3.24}$$

The solutions to the integrals in (3.22) and (3.23) are given by (3.16) and (3.17), respectively. By averaging (3.24) over $\bar{r}_0$ we obtain (3.15), thus, concluding the proof. ■

The expression for p_S obtained in (3.15) is given in terms of an expectation over the distance from U_0 to its closes BS. If we fix the number of sucarriers per layer to $N = 2$ it is possible to obtain a closed-form expression for p_S as shown below.

Corollary 1. *The probability of successful SCMA transmission with $N = 2$ is*

$$p_S = \mathbb{P}\left\{SIR_S \geq \tau\right\} = \frac{\pi \lambda_B \left(\theta_1^1 \pi \lambda_B + \rho\right)}{\left(\pi \lambda_B + \rho\right)^2} \tag{3.25}$$

Proof. If we fix $N = 2$, then (3.15) is equal to

$$\mathbb{P}\left\{SIR_S \geq \tau\right\} = \int_0^\infty e^{-\rho \bar{r}_0^2} (1 + \theta_1^1 \bar{r}_0^2) 2\pi \lambda_B \bar{r}_0 e^{-\lambda_B \pi \bar{r}_0^2} d\bar{r}_0.$$

By solving the integration above we obtain (3.25), therefore, concluding the proof. ■

Table 3.1 Simulation's parameters

Parameter	Value
λ_B	10^{-4} m
λ_U	$[10^{-3}, 10^{-1}]$ m
L	8 preambles
K	16 subcarriers
N	2 subcarriers per user
ζ	0.7
α	4
P	1 W

Then, the ASE for SCMA transmission with $N = 2$ is given by

$$\mathrm{ASE}_S = \tilde{\lambda}_U^S \frac{\pi\lambda_B \left(\theta_1^1 \pi\lambda_B + \rho\right)}{\left(\pi\lambda_B + \rho\right)^2} \log_2(1+\tau). \tag{3.26}$$

3.5 Numerical Simulation

In order to validate the results from Section 3.4, we evaluate the probability of success and the ASE of the OFDMA and the SCMA methods, through a Monte Carlo simulation. The simulation's parameters are shown in Table 3.1.

To make a fair comparison, the same number of subcarriers is available for transmission and each user transmits with the same power in both scenarios. At each realization the user's and the BS's point process are generated inside a circle with 1 Km radius. Afterwards, the user process is thinned according to (3.2) and (3.5) for the OFDMA and for the SCMA networks, respectively. Finally, the SIR of each user at its closest BS is evaluated, according to the system model in Section 3.3, and the transmission is considered successful if its SIR is greater than τ.

As shown in Fig. 3.3 the probability of a successful transmission employing SCMA multiple access is greater than using OFDMA for the whole investigated range of the user process intensity. Additionally, it decays slower with the increase in the user intensity. As SCMA always has an

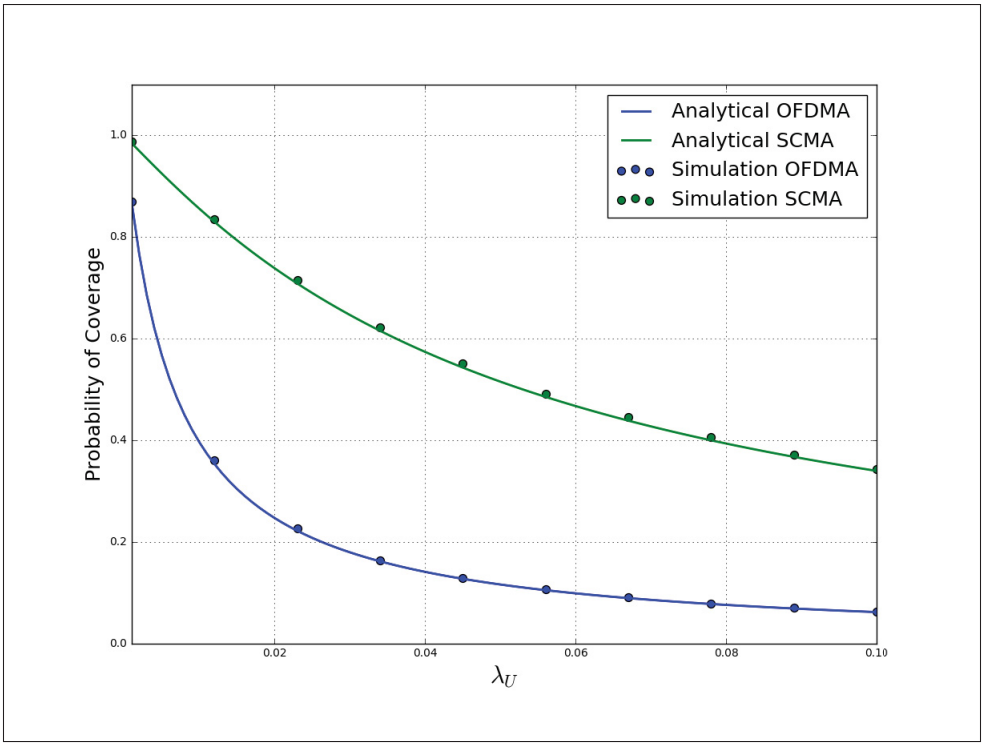

Figure 3.3 Comparison between the probability of success for an OFDMA and a SCMA network

overloading factor greater than 1, we have that J is always greater than K. Therefore, if we compare (3.2) and (3.5), the intensity of the interferer process for SCMA access will always be smaller than OFDMA's (i.e. $\tilde{\lambda}_U^S < \tilde{\lambda}_U^O$). Due to its higher probability of succes, we conclude that the contention-based SCMA network requires less retransmissions of lost packets, which result in power savings, as each transmission is more likely to be successful in comparison to OFDMA. Furthermore, the probability of success in SCMA transmission decays slower, with the increase of user density, than its OFDMA counterpart. Consequently, as the ASE is proportional to the probability of success, SCMA's ASE grows with the user intensity for the whole range investigated in this work, while the ASE of OFDMA saturates, as shown in Fig. 3.4. Hence, the ASE performance of the SCMA network scales better with an increase of the user density, which makes it a promising alternative to orthogonal access in grant-free contention-based mMTC networks.

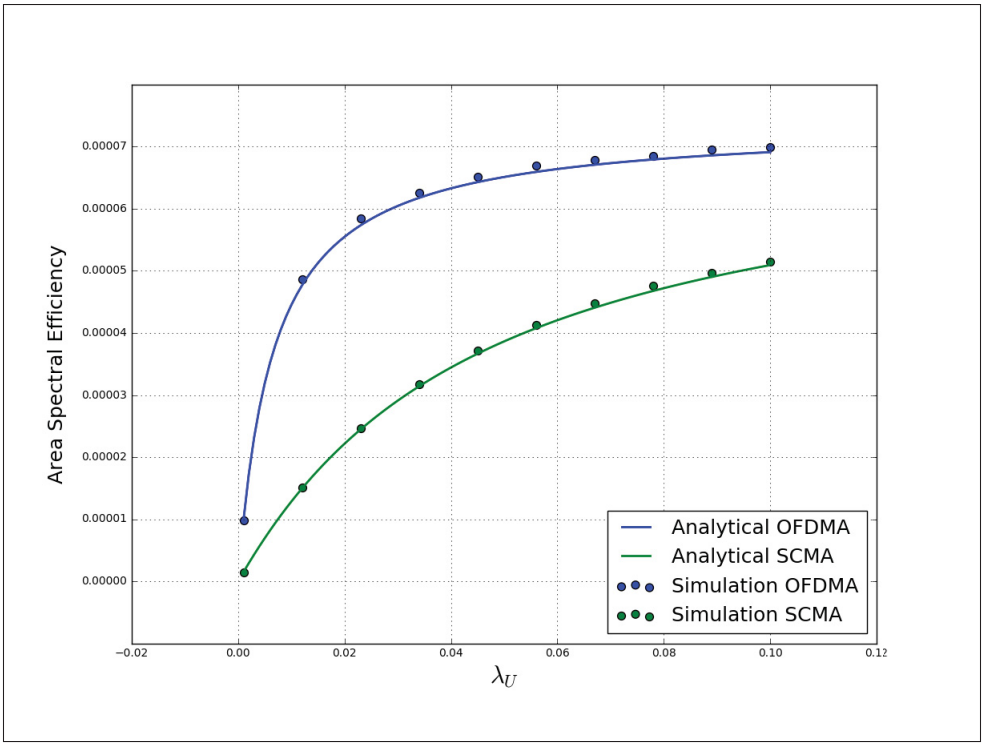

Figure 3.4 Comparison between the ASE for OFDMA and SCMA contention-based networks

3.6 Conclusion

CBA is a promising alternative to enable 5G mMTC networks, where power-limited UEs transmit small packets sporadically, as it can reduce the latency, eliminate the overhead incurred in requesting a dedicated channel, and provides massive connectivity by allowing multiple users to share the same resources. In this paper, we analyze two different CBA approaches, the first employing OFDMA while the second employs SCMA. The probability of success and the ASE of both approaches are analyzed, and closed-form expressions are derived. From the results, contention-based SCMA shows a higher probability of success and ASE than its OFDMA counterpart. Moreover, SCMA's probability of success decreases slowly with the increase in the density of UEs in comparison with OFDMA. Also, OFDMA's ASE saturates after a small increase in the UE density, while SCMA's ASE keeps growing. Therefore, it is possible to

conclude that SCMA is a key-enabler for mMTC applications as its performance scales better for high user densities.

CHAPTER 4

RELIABILITY AND USER-PLANE LATENCY ANALYSIS OF MMWAVE MASSIVE MIMO FOR GRANT-FREE URLLC APPLICATIONS

Joao V.C. Evangelista[1] , Georges Kaddoum[1]

[1] Department of Electrical Engineering, École de Technologie Supérieure,
1100 Notre-Dame Ouest, Montréal, Québec, Canada H3C 1K3

Article submited to the IEEE Transactions on Communications, July, 2021.

4.1 Abstract

5G cellular networks are designed to support a new range of applications not supported by previous standards. Among these, ultra-reliable low-latency communication (URLLC) applications are arguably the most challenging. URLLC service requires the user equipment (UE) to be able to transmit its data under strict latency constraints with high reliability. To address these requirements, new technologies, such as mini-slots, semi-persistent scheduling and grant-free access were introduced in 5G standards. In this work, we formulate a spatiotemporal mathematical model to evaluate the user-plane latency and reliability performance of millimetre wave (mmWave) massive multiple-input multiple-output (MIMO) URLLC with reactive and K-repetition hybrid automatic repeat request (HARQ) protocols. We derive closed-form approximate expressions for the latent access failure probability and validate them using numerical simulations. The results show that, under certain conditions, mmWave massive MIMO can reduce the failure probability by a factor of 32. Moreover, we identify that beyond a certain number of antennas there is no significant improvement in reliability. Finally, we conclude that mmWave massive MIMO alone is not enough to provide the performance guarantees required by the most stringent URLLC applications.

4.2 Introduction

The 3rd generation partnership project (3GPP) has identified three distinct use cases for 5G new radio (NR) and beyond cellular networks based on their different connectivity requirements: enhanced mobile broadband (eMBB) massive machine-type communication (mMTC) and ultra reliable low-latency communication (URLLC) (ITU, 2015). Since the inception of the idea of 5G NR, it has been argued that its main revolution is a change of paradigm from a smartphone-centric network to a network capable of satisfying the requirements of diverse services, such as machine-to-machine and vehicle-to-vehicle communications (Bjornson, Larsson & Lozano, 2021). The URLLC scenario targets applications that require high reliability and low latency, such as augmented reality (AR) virtual reality (VR) vehicle-to-everything (V2X) critical internet of things (cIoT) industrial automation and healthcare. According to the use cases defined in (3GPP, 2020), the main key performance indicator (KPI) to be satisfied in URLLC applications is the latent access failure probability, which incorporates the reliability and latency requirements needed in such applications. The requirements for URLLC applications vary from $1 - 10^{-5}$ transmission reliability to transmit 32 bytes of data with a user-plane latency of less than 1 ms to a $1 - 10^{-5}$ reliability to transmit 300 bytes with a user-plane latency of between 3 and 10 ms, depending on the application (3GPP, 2020).

Long term evolution (LTE) and prior networks were not designed with such constraints in mind. Scheduling in long-term evolution (LTE) follows a grant-based approach, where the user equipment (UE) must request resources in a 4-step random access (RA) procedure before transmitting data (Vilgelm *et al.*, 2018). In the best-case scenario, it takes at least 10 ms for a UE to start transmitting its payload.

Therefore, new mechanisms were introduced into the 5G NR specification to support the latency requirements of URLLC applications. Firstly, a flexible numerology was proposed, introducing the concept of a mini-slot that last as little as 0.125 ms (3GPP, 2018b), in contrast to the 1 ms minimum slot duration on LTE, enabling fine-grained scheduling of network resources (Zaidi *et al.*, 2018). Secondly, the introduction of semi-persistent scheduling (SPS) of grants (3GPP,

2018a; Karadag, Gul, Sadi & Coleri Ergen, 2019), where some of the network's resource blocks are periodically reserved for URLLC applications, thereby avoiding the grant request procedure. Despite the efforts, not all URLLC applications have a periodic traffic pattern and are therefore unable to benefit greatly from SPS. Additionally, some services require low latency and reliable transmission to transmit small sporadic packets. With that in mind, both the standards committee (3GPP, 2017a) and researchers have put a lot of effort to investigate grant-free transmission, where the UE transmit their payload directly in the RA channel. This culminated with the introduction of the 2-step RA procedure introduced in Release 16 (3GPP, 2017a). The 2-step RA procedure follows a grant-free approach, where instead of waiting for a dedicated channel to be assigned by the network, it transmits its data directly into the RA channel and waits for feedback from the network (Kim *et al.*, 2021).

Moreover, massive multiple input multiple output (MIMO) is a fundamental part of 5G NR (Lu, Li, Swindlehurst, Ashikhmin & Zhang, 2014; Larsson, Edfors, Tufvesson & Marzetta, 2014; Björnson, Hoydis & Sanguinetti, 2018). It provides performance gains by improving diversity against fading and, along with advanced signal processing techniques, can provide directivity to transmission/reception, mitigating interference between spatially uncorrelated UE (Marzetta, Larsson, Yang & Ngo, 2016). The performance enhancements provided by MIMO are essential to ensure the reliability and the low latency required by URLLC applications. In conjunction with massive MIMO comes millimeter wave (mmWave) transmission. Due to its small wavelength, mmWave antennas can be packed into massive arrays, making it a key enabler of massive MIMO systems which attracted a significant interest on the topic (Rappaport *et al.*, 2013; Rangan, Rappaport & Erkip, 2014; Andrews *et al.*, 2017; Sattar, Evangelista, Kaddoum & Batani, 2017, 2019a,b). However, mmWave propagation comes with its own challenges due to the severe propagation loss experienced by electromagnetic signals in this frequency range.

In this paper, we develop a spatiotemporal analytical model to evaluate the performance of mmWave massive MIMO communication systems for URLLC applications. We use tools from stochastic geometry and probability theory to evaluate and compare system performance metrics

by deriving closed-form approximate expressions for its latent access failure probability under different hybrid automatic repeat request (HARQ) protocols.

4.2.1 Related Work

In (Gao & Dai, 2019), the authors propose a queueing model to compare the throughput performance of packet-based (grant-free) and connection-based (grant-based) random access. They conclude that packet-based systems with sensing can achieve greater throughput than connection-based one for small packet transmissions. In (Liu, Deng, Zhou, Elkashlan & Nallanathan, 2021; Evangelista, Sattar, Kaddoum, Selim & Sarraf, 2021), the optimization of grant-free access networks is investigated. The former considers the dynamic optimization of HARQ and scheduling parameters with non-orthogonal multiple access (NOMA) while the former considers the distributed link adaptation problem. Both papers formulate the respective optimization tasks as multiagent reinforcement learning (MARL) problems. The probability of success and the area spectral efficiency of a grant-free sparse code multiple access (SCMA) system is evaluated in (Lai, Lei, Deng, Wen & Chen, 2021; Evangelista, Sattar & Kaddoum, 2019a), in an mMTC context, using stochastic geometry. However, none of the works consider the temporal aspects of the system, which are crucial to analyze the latency and reliability of URLLC service. In (Ding, Qu, Jiang & Jiang, 2019), the probability of success of grant-free RA with massive MIMO in the sub-6 GHz band is investigated, and analytical expressions are derived for conjugate and zero-forcing beamforming. Despite its contribution, the authors do not evaluate the system's temporal behavior, which is fundamental to characterize URLLC service's performance. Moreover, due to its distinct propagation characteristics, this model is unsuitable for mmWave frequency bands.

The authors in (Gharbieh *et al.*, 2018) evaluate the scalability of scheduled uplink (grant-based) and random access (grant-free) transmissions in massive internet of things (IoT) networks, although they frame the problem through a revolutionary spatiotemporal framework, fusing stochastic geometry and queueing theory. They conclude that grant-free transmission offers lower latency, however, it does not scale well to a massive number of devices. In our work, we

show that using massive MIMO base station (BS) is a viable solution to address the scalability issues of grant-free transmission without sacrificing its latency, rendering it particularly suitable for URLLC applications. In (Jiang, Deng, Kang & Nallanathan, 2018a), the authors use a similar spatiotemporal model to characterize the performance of different RA schemes with respect to the probability of a successful preamble transmission in a grant-based massive IoT system. They conclude that a backoff scheme performs close to optimally in diverse traffic conditions. In (Jacobsen *et al.*, 2017), the authors perform system-level simulations of a grant-free URLLC network under different HARQ configurations, and compare it to a baseline grant-based system. They conclude that grant-free systems provide significantly lower latency at the $1 - 10^{-5}$ reliability level. The same scenario is evaluated in (Liu *et al.*, 2020), however, the authors characterize system performance analytically, using a stochastic geometry-based spatiotemporal model. This paper identifies the suitability of each HARQ scheme for different network loads and received power levels.

Stochastic geometry has become the de facto tool for analyzing large networks (Lu, Salehi, Haenggi, Hossain *et al.*, 2021; Hmamouche, Benjillali, Saoudi, Yanikomeroglu & Renzo, 2021; Jiang, Deng, Nallanathan, Kang & Quek, 2018b), and has been successfully used to investigate the performance of MIMO systems for a while now (Tanbourgi, Dhillon & Jondral, 2015; Nguyen, Jeong, Quek, Tay & Shin, 2013; Adhikary, Dhillon & Caire, 2015; Lee, Morales-Jimenez, Lozano & Heath, 2014). In (Afify, ElSawy, Al-Naffouri & Alouini, 2016), a unified stochastic geometric mathematical model for MIMO cellular networks with retransmission is proposed. In (Ding, Fan & Poor, 2017), a stochastic geometry-based analytical model for the performance of downlink mmWave NOMA systems is developed. The authors propose two random beamforming methods that are able to reduce system overhead while providing performance gains for BS with a large number of antennas.

We seek to answer the following main questions that are to the best of our knowledge missing from the current literature:

- How do we formulate a tractable spatiotemporal model to investigate the reliability and latency of URLLC applications powered by BS equipped with massive antenna arrays operating on mmWave frequencies?
- What closed-form analytical expressions can we derive for the latent access failure probability in this scenario?
- What are the performance gains obtained from increasing the number of antennas at the BS, and what are the limitations?

4.2.2 Contributions

This paper makes three major contributions:

- We formulate a mathematical model to evaluate the performance of mmWave massive MIMO on uplink grant-free URLLC networks with HARQ. This model uses stochastic geometry to capture the spatial configuration of the UE and the BS, a mmWave channel model, and probability theory to obtain the temporal characteristics necessary to evaluate the performance of URLLC applications.
- We derive closed-form approximate expressions for the latent access failure probability using reactive and K-repetition HARQ schemes. To the best of our knowledge, no previous works has presented closed-form analytic expressions for this key performance measure of URLLC applications in a mmWave massive MIMO communication system.
- We analyze the system performance for an extensive range of scenarios, identifying the gains and limitations provided by using the mmWave spectrum together with a massive number of antennas at the BS, and identify the scenarios that benefit the most from these two technologies.

4.2.3 Notation and Organization

Italic Roman and Greek letters denote deterministic and random variables, while bold letters denote deterministic and random vectors. The capital Greek letter Φ denotes a point process and $x \in \Phi$ represents a point belonging to said process. The notation $\Phi(A)$, where $A \in \mathbb{R}^d$, is

the counting process associated with Φ (Haenggi, 2012). Notice that we overload the meaning of Φ so that it can signify a point process, a counting measure or a set depending on the context. $\binom{n}{k} = \frac{n!}{k!(n-k)!}$ is the binomial coefficient of n choose k.

The uniform, complex normal and binomial distributions are represented by $Uniform(a, b)$, $\mathcal{CN}(\mu, \sigma^2)$ and $Binomial(p)$, respectively. The vector $\mathbf{x}^H$ is the Hermitian transpose of vector $\mathbf{x}$. The function $\mathbb{P}(\cdot)$ denotes the probability of the event within parentheses. The notation $\mathbf{1}\{\cdot\}$ denotes the indicator function, which is equal to one whenever the event within curly braces is true and zero otherwise.

This work is divided into five sections and an appendix. In Section 4.2, we introduce the contents of the manuscript and contextualize within the relevant literature. In Section 4.3, we present a mathematical model to characterize the performance of the grant-free mmWave massive MIMO system in URLLC applications. In Section 4.4, we derive the latent access failure probability of the proposed system using reactive and K-repetition HARQ protocols. In Section 4.5, we show the results of the system simulation. We use these results to validate the analytical derivations, investigate the system's performance for an extensive range of parameters and finish it by interpreting the results in the context of URLLC applications. In Section 4.6, we summarize our findings and present our conclusions. Finally, in the appendix, we show the detailed proofs of the lemmas and theorems required by the derivations in the paper.

4.3 System Model

In most cellular applications, uplink transmissions use a dedicated resource (frequency, time or a MIMO spatial layer) previously assigned by the network to transmit their data payload. Thus, when an UE receives new data, it must send a request for the network to schedule a resource. With dedicated resources, each UE can utilize the wireless channel to its full capacity, thus maintaining good quality of service (QoS) TIn 5G NR networks, the schedule request consists of four steps, illustrated in Figure 4.1:

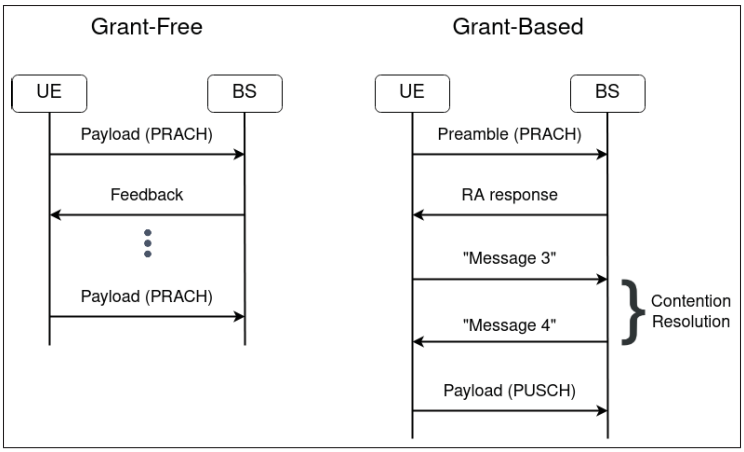

Figure 4.1 Comparison of the transmission procedure in grant-free and grant-based systems

- The UE randomly selects one of the available preambles and transmits it on the physical random access channel (PRACH)
- The BS transmits a random access request (RAR) acknowledging receipt of the preamble and time-alignment commands.
- The UE and BS exchange contention resolution messages (messages 3 and 4) that are used to identify possible collisions arising from two different devices transmitting the same preamble.
- If the grant request is successful, the UE transmits its payload on the physical uplink shared channel (PUSCH).

This grant-based scheme is efficient for applications that need to use the channel multiple times to transmit large amounts of data (e.g., video streaming) or data that's being continuously generated (e.g., voice). However, in some URLLC applications, UE sporadically generate data that need to be transmitted reliably and with low latency, such as cIoT and sensors for industrial automation. In such scenarios, the time spent on the schedule request renders grant-based schemes inefficient. A more suitable alternative is to transmit the data directly on the PRACH and thereby avoidall the overhead involved in requesting a grant, as illustrated in Fig. 4.1. Nonetheless, with grant-free transmission comes the possibility of collisions whenever two UE randomly select the same preambles. Therefore, HARQ is used to ensure the reliability

and robustness of grant-free transmission. HARQ consists of using feedback information from the BS so the UE can retransmit packets that were not successfully received. Despite this, it can be quite challenging to scale grant-free networks because wireless resources are finite and expensive. To this end, massive MIMO and beamforming can be applied to reduce the interference of spatially uncorrelated UE and thereby increasing the reliability of the system.

In this section, we discuss the spatial model of the network, the mmWave channel model, the BS receiver beamforming procedure and the different HARQ schemes used.

4.3.1 Physical Layer Model

Stochastic geometry and the theory of random point processes has proven to be able to accurately model the spatial distribution of modern cellular network deployments (Lu & Di Renzo, 2015). Therefore, we consider a cell of radius R consisting of a BS, equipped with K antennas, located at the origin. We model the spatial location of the single-antenna UE according to a homogeneous Poisson point process (HPPP) (Haenggi, 2012), denoted by Φ_U with intensity λ_U. Furthermore, the distance between the i-th UE, $x_i \in \Phi_U$, and the BS is given by $\|x_i\|$. Both the distance from the UE to the BS and its normalized angle from the BS are uniformly distributed random variables (Haenggi, 2012), $\|x_i\| \sim Uniform(0, R)$ and $\theta_i \sim Uniform(-1, 1)$, respectively.

Due to path loss attenuation, the signal received from UE located further from the BS is "drowned" by the signal from closer users transmitting with the same power, also known as the near-far problem. Uplink power control is fundamental to deal with this issue. We consider that the UE utilize path loss inversion power control (ElSawy & Hossain, 2014), with received power threshold ρ, where each user controls its transmit power such that the average received power at its associated BS is ρ, by selecting their transmit powers as $p_i = \rho \|x_i\|^{\alpha}$, where α is the path loss exponent. We assume that there are N_S subcarriers reserved for grant-free URLLC transmissions and N_P orthogonal preambles. Thus, at each transmission time interval (TTI) the active UE select a subcarrier and preamble randomly from the N_S available subcarriers and N_P available preambles. Moreover, we assume that at $t = 0$, one packet arrives to the transmitting

queue of each UE. Therefore, the HPPP of active users Φ_A on a specific subcarrier is obtained by thinning Φ_U (Haenggi, 2012) and its effective intensity at $t = 0$ is given by

$$\lambda_A = \frac{\lambda_U}{N_S}. \tag{4.1}$$

Massive MIMO technology and mmWave frequencies are intrinsically connected. Even though one does not imply the other, they complement each other really well. The former requires large antenna arrays, and the size of such arrays is proportional to the targeted wavelength. Moreover, mmWave antennas must be really small to operate in such large frequencies, therefore, a larger number of them are necessary to gather enough energy. In this work, we consider that the BS is equipped with a massive uniform linear array (ULA) containing $K \gg 1$ antennas operating at mmWave frequencies, while the UE possess a single antenna. The channel vector between user i and the BS is given by

$$\mathbf{h}_i = \sqrt{K}\left[\underbrace{\frac{g_{i,0}\mathbf{a}(\theta_i^0)}{\sqrt{\|x_i\|^{\alpha_{LOS}}}}}_{\text{LOS component}} + \underbrace{\frac{\sum_{j=1}^{J} g_{i,j}\mathbf{a}(\theta_i^j)}{\sqrt{\|x_i\|^{\alpha_{NLOS}}}}}_{\text{NLOS components}}\right], \tag{4.2}$$

where $g_{i,j} \sim \mathcal{CN}(0,1)$ is the complex gain on the j-th path and θ_i^j is the normalized direction of the j-th path. We assume that the complex gains of different paths are independent. α_{LOS} and α_{NLOS} denote the path loss exponent of the line-of-sight (LOS) and non-line-of-sight (NLOS) paths, respectively. The vector

$$\mathbf{a}(\theta) = \frac{1}{\sqrt{K}}\begin{bmatrix} 1 & e^{-j\pi\theta} & \dots & e^{-j\pi(K-1)\theta} \end{bmatrix}^T \tag{4.3}$$

denotes the phase of the signal received by each antenna. Due to high penetration losses suffered by mmWave signals, the LOS path has a dominant effect on channel gain, being 20 dB larger than the NLOS in some cases (Ding *et al.*, 2017; Lee *et al.*, 2014). Hence, we can safely approximate

$\mathbf{h}_i$ as

$$\mathbf{h}_i \approx \sqrt{K}\frac{g_i \mathbf{a}(\theta_i)}{\sqrt{\|x_i\|^{\alpha}}} \tag{4.4}$$

for mathematical tractability. Additionally, to avoid cluttering the notation, we drop the subscripts denoting different paths and distinguishing LOS and NLOS variables.

Due to the dominant effect of the LOS link, the channel model also needs to consider a blockage model to determine the probability that the LOS path between the UE the BS is obstructed. To model the effects of blockage, we adopt the model proposed in (Thornburg *et al.*, 2016). This model is obtained by assuming that the obstructing building and structures form an HPPP with random width, length and orientation. So, let LOS be the set of LOS UE; then, the probability that user x_i has a LOS link is given by

$$\mathbb{P}\left(x_i \in LOS\right) = \exp\left(-\beta \left\|x_i\right\|\right), \tag{4.5}$$

where β is directly proportional to the density, and the average width and length of obstructing structures. This model nicely captures the exponentially vanishing probability of having a LOS link the further you move away from the BS, and can be easily fitted to real urban scenarios.

Signal Model

At each TTI, the active users transmit an information signal s_i such that $|s_i| = 1$. Therefore, the vector of the signal received at the BS is given by

$$\mathbf{y} = \sum_{x_i \in \Phi_A} \mathbf{1}\left\{x_i \in LOS\right\} \sqrt{\rho}\mathbf{h}_i s_i + \mathbf{n}, \tag{4.6}$$

where $\mathbf{n} \sim \mathcal{CN}\left(0, \sigma_2 \mathbf{I}\right)$ is a circularly symmetric complex Gaussian random variable representing additive white Gaussian noise (AWGN) To successfully recover the data transmitted by a given user, the BS must be able to accurately estimate its channel response.

Definition 4.1 (Preamble Collision)**.** *Preamble collision event, denoted by C, happens when two or more devices transmit the same preamble on the same subcarrier.*

We assume that the BS is able to perfectly estimate the UE channel response $\mathbf{h}_i$ whenever there is no preamble collision. Then, the BS performs conjugate beamforming to separate the intended user's signal from those of the other interfering UE by multiplying the received signal by the Hermitian transpose of the intended user channel response. Therefore the recovered signal of the intended user, the j-th user, is

$$\begin{aligned} y_j &= \mathbf{1}\left\{x_j \in LOS\right\}\mathbf{1}\left\{\bar{C}\right\}\sqrt{\rho}\mathbf{h}_j^H\mathbf{h}_j s_j + \\ &\quad \sum_{x_i\in\Phi_A\setminus\{x_j\}} \mathbf{1}\left\{x_i \in LOS\right\}\sqrt{\rho}\mathbf{h}_j^H\mathbf{h}_i s_i + \tilde{n}_j, \end{aligned} \tag{4.7}$$

where $\bar{C}$ is the event when user j does not experience preamble collision and $\tilde{n}_j \sim \mathcal{CN}\left(0,\sigma^2\right)$ is a linear combination of the noise vector, which is a Gaussian distributed random variable. Therefore, the signal-to-interference-plus-noise-ratio (SINR) experienced by user j is given by

$$\begin{aligned} \text{SINR} &= \frac{\mathbf{1}\left\{x_j \in LOS \cap \bar{C}\right\}\rho\left|\mathbf{h}_j^H\mathbf{h}_j\right|^2}{\sum\limits_{x_i\in\Phi_A\setminus\{x_j\}}\mathbf{1}\left\{x_i \in LOS\right\}\rho\left|\mathbf{h}_j^H\mathbf{h}_i\right|^2+\sigma^2} \\ &= \frac{\mathbf{1}\left\{TX_j\right\}\rho\left|g_j\right|^2\left|\mathbf{a}\left(\theta_j\right)^H\mathbf{a}\left(\theta_i\right)\right|^2}{I+\sigma^2}, \end{aligned} \tag{4.8}$$

where $TX_j = \{x_j \in LOS \cap \bar{C}\}$ is the probability that user j has a LOS link and does not suffer from preamble collision, and $I = \sum\limits_{x_i\in\Phi_A\setminus\{x_j\}}\mathbf{1}\left\{x_i \in LOS\right\}\rho\left|g_i\right|^2\left|\mathbf{a}\left(\theta_j\right)^H\mathbf{a}\left(\theta_i\right)\right|^2$ is the interference from the other UE. Moreover, the beamforming gain, $\left|\mathbf{a}\left(\theta_j\right)^H\mathbf{a}\left(\theta_i\right)\right|^2$, can be expressed as (Lee, Sung & Seo, 2015)

$$\left|\mathbf{a}\left(\theta_j\right)^H\mathbf{a}\left(\theta_i\right)\right|^2 = F_K\left(\frac{\pi}{2}\left(\theta_i-\theta_j\right)\right) = \frac{1}{K}\left|\frac{\sin\left(\frac{K\pi}{2}\left(\theta_i-\theta_j\right)\right)}{\sin\left(\frac{\pi}{2}\left(\theta_i-\theta_j\right)\right)}\right|^2, \tag{4.9}$$

where $F_K(x)$ is the Fejer kernel (Marsden, Hoffman *et al.*, 1993), with $F_K(0) = K$. A useful

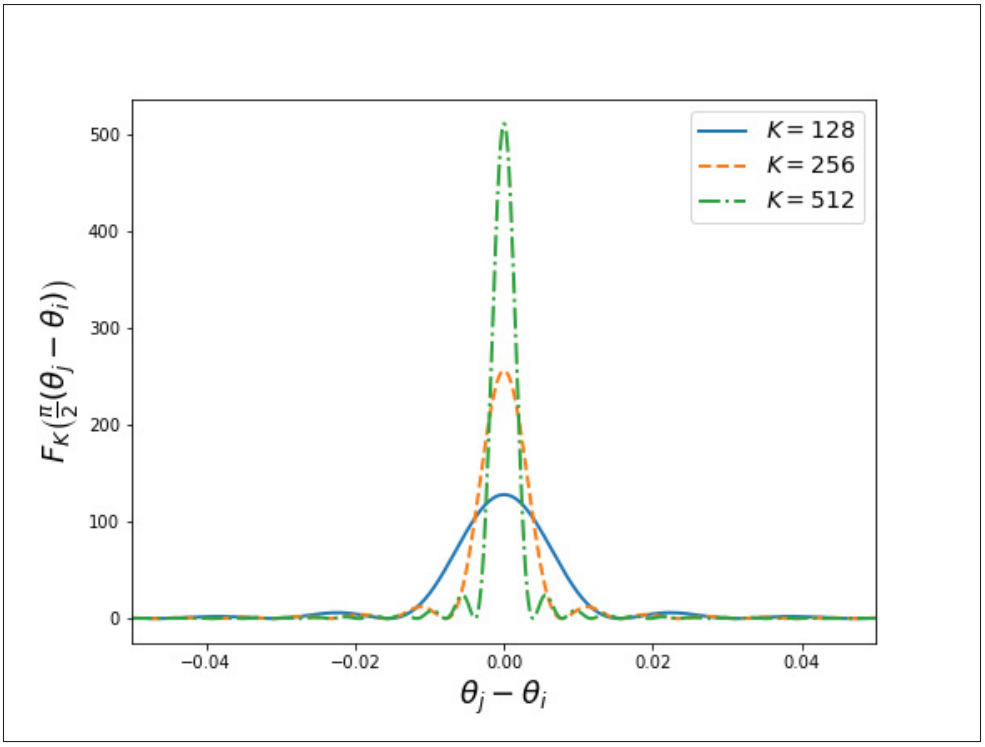

Figure 4.2 Fejer kernel value for normalized angles of arrival varying from −0.05 to 0.05

property of the Fejer kernel is that (Marsden *et al.*, 1993)

$$\lim_{K\to\infty} \int_{\delta\leq|x|\leq\pi} F_K(x)dx = 0, \tag{4.10}$$

meaning that for an asymptotically large value of K, the interference for the signals not aligned with beam angle θ_j goes to zero. Fig. 4.2 illustrates this property by plotting the Fejer kernel for increasing values of K.

4.3.2 HARQ Schemes

HARQ protocols determine how transmitters and receivers exchange information about successful packet reception, by transmitting an acknowledgement (ACK) signal, and how UE retransmit in the event of failure, which is signaled by the transmission of a negative acknowledgement (NACK) signal. They are especially important to ensure reliability in grant-free transmission.

The HARQ protocol used also impacts the overall latency of the system. Hence, in this paper, we investigate the performance of the massive MIMO URLLC network under two distinct HARQ protocols.

With respect to transmissions latency, the HARQ protocols investigated have a few aspects in common. First, the UE spends T_A TTI to process a newly arrived packet. As soon as the packet is processed, it spends T_{TX} TTI transmitting it. Upon receipt of the packet, the BS spends T_{DP} TTI to process it and T_F TTI to send feedback and for it to reach the UE. Once the UE receives the feedback signal, it takes T_{UP} TTI to process it. We consider that the transmit and feedback time already take into account the propagation delay between the transmitter and receiver. Without loss of generality, we assume that $T_A = T_{TX} = T_{DP} = T_{UP} = 1$ TTI. Another concept shared between different HARQ protocols is the round-trip time (RTT) which consists of the time it takes from the start of a transmission by the UE to the end of processing of the feedback signal, either ACK or NACK, the UE received from the BS.

4.3.2.1 Reactive Scheme

The reactive HARQ protocol is the more straight-forward one of the two considered in this paper. The UE attempts to transmit one packet and waits for feedback from the BS. Once the feedback is processed, it either attempts to retransmit the same packet if it got a NACK signal or sits idle until a new packet arrives. This protocol is illustrated in Fig. 4.3, which shows the processing times and signal exchange between the UE and the BS. Under the assumptions considered in this paper, the reactive RTT T_{RTT}^{reac} is given by

$$T_{RTT}^{reac} = 4 \text{ TTIs}. \tag{4.11}$$

From (4.11), the user-plane latency of the m-th HARQ round-trip is

$$T^{reac}(m) = T_A + 4m \text{ TTIs}. \tag{4.12}$$

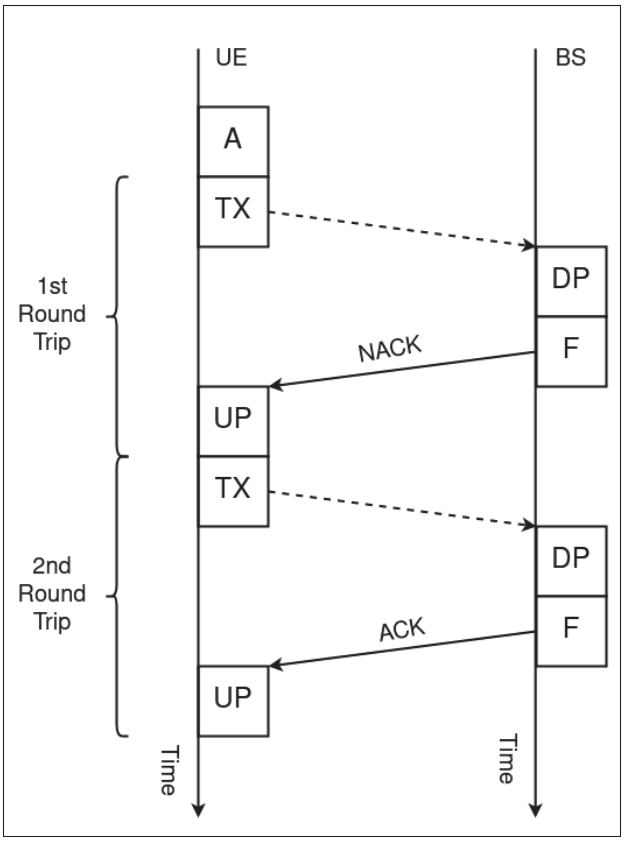

Figure 4.3 An illustration of a couple of reactive HARQ protocol round trips

4.3.2.2 K-Repetition Scheme

To increase the reliability and robustness of each transmission attempt, the K-repetition HARQ protocol repeats the same packet K_{rep} times on each attempt. Therefore, the only way a transmission attempt fails is if each of the K_{rep} transmissions fail, which translates into an increased reliability of the overall system. However, feedback on the transmission attempt is sent only after the last repetition is processed by the BS. So, there is a tradeoff between enhancing the reliability of each transmission and increasing the latency of a transmition attempt. Fig. 4.4 shows two K-repetition round-trip transmissions, where the first transmission fails and the second is successful. The RTT of the K-repetition HARQ protocol is

$$T_{RTT}^{K_{rep}} = K_{rep} + 3 \text{ TTIs}. \tag{4.13}$$

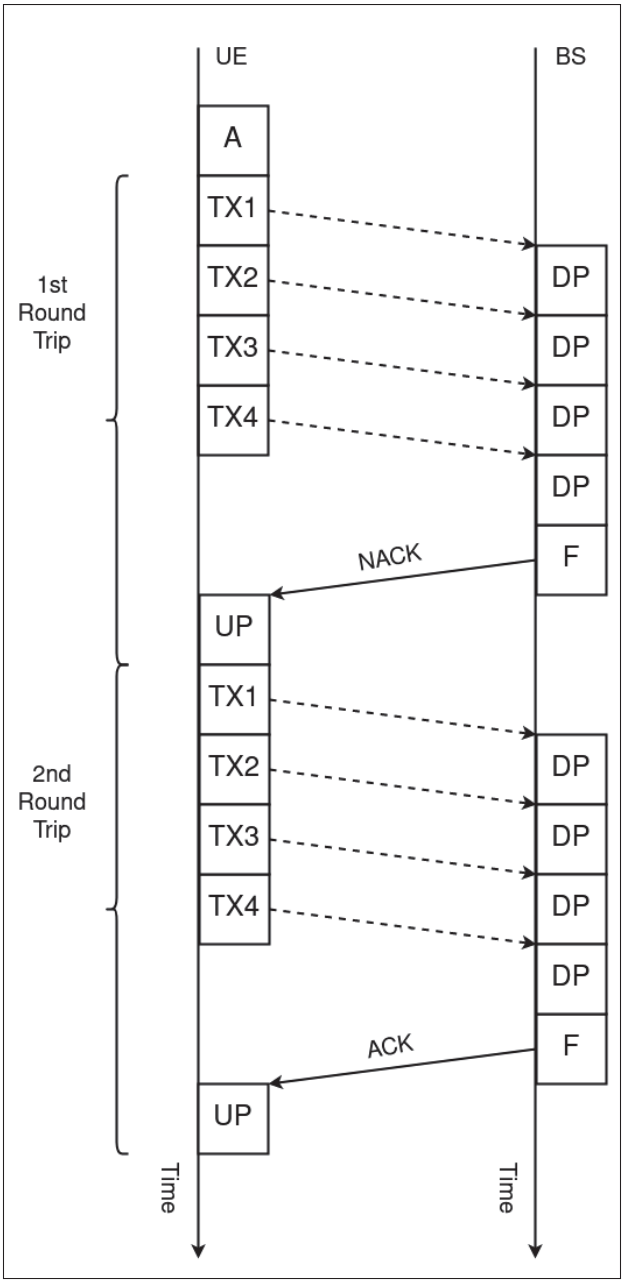

Figure 4.4 An illustration of a couple of K-repetition HARQ protocol round trips

Therefore, the total latency of m K-repetition transmissions is given by

$$T^{K_{rep}}(m) = T_A + mT_{RTT}^{K_{rep}} = 1 + m(K_{rep} + 3) \text{ TTIs.} \tag{4.14}$$

4.4 System Analysis

The main requirement of URLLC applications is to reliably keep the user-plane latency below an application-dependent latency constraint. We begin this section by unambiguously defining what we mean by reliably and user-plane latency.

Definition 4.2 (User-Plane Latency)**.** *User-plane latency is the time spent between the arrival of a packet to the UE's queue and the successful processing of an ACK signal received from the BS.*

Definition 4.3 (Latent Access Failure Probability Requirement)**.** *Latent access failure probability $\mathcal{P}_F(T \leq \tau)$, where T is the user-plane latency and τ is the latency constraint, is the probability that the UE data cannot be successfully decoded.*

Therefore, the QoS requirement of URLLC applications can be stated as

$$\mathcal{P}_F(T \leq \tau) \leq \epsilon, \tag{4.15}$$

where τ is the latency constraint and ϵ is the minimum reliability, and both are application-dependent. Thus, to satisfy the QoS requirement, the probability that an UE cannot transmit its data before τ must be bounded by ϵ. Typically, τ varies between 1 and 10 ms and ϵ varies between 10^{-5} and 10^{-6} depending on the URLLC application.

Let M be the maximum number of retransmissions under the latency constraint τ. Moreover, notice that some of the UE will transmit successfully earlier than others, and if the UE's transmission queue stays idle, the interference levels in distinct retransmissions are different. Therefore, the latent access failure probability is a function of the fraction of active users at the m-th retransmission ($\mathcal{A}_m$), the probability that the m-th retransmission is successful ($\mathcal{P}_m($ and the maximum number of retransmissions (M), as given by (Liu *et al.*, 2020)

$$\mathcal{P}_F(T \leq \tau) = \begin{cases} 1, & \text{, if } M = 0 \\ 1 - \sum\limits_{m=1}^{M} \mathcal{A}_m \mathcal{P}_m & \text{, if } M \geq 1, \end{cases} \tag{4.16}$$

where $\mathcal{A}_m$ is

$$\mathcal{A}_m = \begin{cases} 1, & \text{, if } m = 1 \\ 1 - \sum_{i=1}^{m-1} \mathcal{A}_i \mathcal{P}_i & \text{, if } m \geq 2. \end{cases} \tag{4.17}$$

Given the expressions for $\mathcal{P}_m$, the latent access failure probability is obtained by recursively computing (4.17) and (4.16).

In the rest of this section, we derive closed-form expressions for $\mathcal{P}_m$ under the reactive and K-repetition HARQ protocols, denoted by $\mathcal{P}_m^{reac}$ and $\mathcal{P}_m^{Krep}$, respectively. To do so, we use stochastic geometric analysis to obtain the probability of success of a randomly chosen user x_0, herein the typical user. From Slivnyak's theorem (Baccelli & Błaszczyszyn, 2009), the performance of the typical user in an HPPP is representative of the average user's performance.

4.4.1 Reactive HARQ

The maximum number of HARQ transmissions following the reactive HARQ protocol with the delay constraint τ is given by

$$M^{reac} = \left\lceil \frac{\tau - 1}{T_{RTT}^{reac}} \right\rceil = \left\lceil \frac{\tau - 1}{4} \right\rceil. \tag{4.18}$$

The first step in deriving an expression for the latent access failure probability is to obtain the probability that the m-th reactive retransmission is successful ($\mathcal{P}_m^{reac}$).

Let $\Phi_I = \{x_i | x_i \in \Phi_A \setminus \{x_0\} \cap x_i \in LOS_m\}$ be the set of users interfering with the typical user's transmission on the m-th RTT. Notice that due to the exponentially decreasing probability of a LOS link with the increase in distance, Φ_I is a non-HPPP with density $\lambda_I(x) = \lambda_A \exp(-\beta \|x\|)$. The mean measure of Φ_I, the average number of points in a given area, is obtained as

$$\begin{aligned} \Lambda(b(0,r)) &= E[\Phi_I(b(0,r))] = \int_{\mathbb{R}^2} \lambda_I(x) dx \\ &= 2\pi\lambda_A \int_0^r \exp(-\beta r) \, r dr d\theta = \frac{2\pi\lambda_A}{\beta^2} [1 - \exp(-\beta r)(1 + \beta r)], \end{aligned} \tag{4.19}$$

where $b(0,r)$ is a 2-dimensional ball with radius r that is centered at the origin. Now, let N_m be a random variable denoting the number of users that interfere with the typical user on the m-th retransmission. From (4.19), the probability that there are n interferers in the cell with radius R is derived as

$$\mathbb{P}\left(N_m = n\right) = \frac{\left[\mathcal{A}_m^{reac}\Lambda\left(b(0,R)\right)\right]^n}{n!}\exp\left(-\mathcal{A}_m^{reac}\Lambda\left(b(0,R)\right)\right). \tag{4.20}$$

Lemma 5. *If $K \gg 1$, the probability that the m-th reactive HARQ retransmission of the typical user conditioned on the events that the typical user does not experience preamble collision, has a LOS link and is affected by n interferers can be approximated as*

$$\begin{aligned}&\mathbb{P}\left(\mathrm{SINR}_m \geq \gamma \,\middle|\, \bar{C}, x_0 \in LOS_m, N_m = n\right)\\ \approx\ &\sum_{n'=0}^{n}\binom{n}{n'}\left(\frac{2}{K}\right)^{n'}\left(1-\frac{2}{K}\right)^{n-n'}\exp\left(-\frac{\gamma}{\rho K}\right)\left[\frac{\tanh^{-1}\left(\sqrt{\frac{\gamma}{1+\gamma}}\right)}{\sqrt{\gamma\left(1+\gamma\right)}}\right]^{n'},\end{aligned} \tag{4.21}$$

where n' is the number of interferers within the primary lobe of the beam directed at the typical user.

Proof. See Appendix II, Section 1. ■

After deriving the expressions for the probability of having N_m users interfere with retransmission m in (4.20) and the conditional probability of success obtained in Lemma 5, the success probability can be obtained as follows:

Theorem 6. *The probability that the m-th reactive HARQ retransmission is successfully decoded is*

$$\begin{aligned}\mathcal{P}_m^{reac} = \sum_{n=0}^{\infty}\ &\mathbb{P}(N_m = n)\mathbb{P}\left(\bar{C}\,|N_m = n\right)\\ &\mathbb{P}(x_0 \in LOS_m)\mathbb{P}(\mathrm{SINR}_m \geq \gamma \,|\bar{C}, x_0 \in LOS_m, N_m = n),\end{aligned} \tag{4.22}$$

where $\mathbb{P}(N_m = n)$ is the probability that there are n interferers in the cell and is given by (4.20). The probability of no preamble collision is given by

$$\mathbb{P}\left(\bar{C}\middle| N_m = n\right) = \left(1 - \frac{1}{Ns}\right)^n. \tag{4.23}$$

And finally, the probability that the typical user has a LOS link to the BS is

$$\mathbb{P}\left(x_i \in LOS_m\right) = \frac{1}{R}\int_0^R \exp\left(-\beta \left\|x_i\right\|\right) d\left\|x_i\right\| = \frac{1}{\beta R}\left[1 - \exp\left(-\beta R\right)\right]. \tag{4.24}$$

Proof. The proof is straight forward if the conditional probability obtained in Lemma 5 is averaged out. ■

From the results of Theorem 6, the latent access failure probability can be easily obtained by recursively computing

$$\mathcal{P}_F(T \le \tau) = \begin{cases} 1, & \text{, if } M^{reac} = 0 \\ 1 - \sum\limits_{m=1}^{M^{reac}} \mathcal{A}_m^{reac}\mathcal{P}_m^{reac} & \text{, if } M^{reac} \ge 1. \end{cases} \tag{4.25}$$

4.4.2 K-Repetition HARQ

In the K-repetition HARQ system, the RTT lasts from when the UE transmits the first repetition until it receives the ACK/NACK feedback signal. Thus, under delay constraint τ, the maximum number of retransmissions is

$$M^{K_{rep}} = \left\lceil \frac{\tau - 1}{T_{RTT}^{K_{rep}}} \right\rceil = \left\lceil \frac{\tau - 1}{K_{rep} + 3} \right\rceil. \tag{4.26}$$

Under the K-repetition HARQ, the same data is repeated K_{rep} times for every transmission attempt, and after the BS receives all the repetitions, it sends either an ACK or a NACK signal depending whether any of the repetitions sent in the transmission could be successfully decoded.

Additionally, the UE selects a new random subcarrier and preamble for the transmission of each distinct repetition. To obtain a closed-form expression for the latent access failure probability, we follow the same steps as were taken for the reactive HARQ derivation.

Lemma 6. *If $K \gg 1$, the probability that the m-th K-repetition HARQ retransmission of the typical user, conditioned on the event that the typical user does not experience preamble collision, has a LOS link and is affected by n interferers can be approximated as*

$$\begin{aligned}
&\mathbb{P}\left(\bigcup_{l=1}^{K_{rep}} \mathrm{SINR}_{m,l} \geq \gamma \,\middle|\, \bar{C}, x_0 \in LOS_m, N_m = n\right) \\
&\approx \sum_{l=1}^{K_{rep}} \binom{K_{rep}}{l} (-1)^{l+1} \sum_{n'=0}^{n} \binom{n}{n'} \left(\frac{2}{K}\right)^{n'} \left(1 - \frac{2}{K}\right)^{n-n'} \\
&\qquad \exp\left(-\frac{l\gamma}{\rho K}\right) \left[\frac{\tanh^{-1}\left(\sqrt{\frac{\gamma}{1+\gamma}}\right)}{\sqrt{\gamma\,(1+\gamma)}}\right]^{ln'}, \qquad (4.27)
\end{aligned}$$

where the double subscript m, l indicates the l-th repetition of the m-th HARQ retransmission attempt.

Proof. See Appendix II, Section 2. ■

With the result from Lemma 6, the probability that the m-th retransmission attempt is successful can be obtained by averaging (4.27) over the conditional random variables.

Theorem 7. *The probability that the m-th K-repetition HARQ retransmission is successfully decoded is given by*

$$\begin{aligned}
\mathcal{P}_m^{K_{rep}} = \sum_{n=0}^{\infty} \; & \mathbb{P}(N_m = n)\mathbb{P}\left(\bar{C} \,|N_m = n\right) \\
& \mathbb{P}(x_0 \in LOS)\mathbb{P}\left(\bigcup_{l=1}^{K_{rep}} \mathrm{SINR}_{m,l} \geq \gamma \,\middle|\, \bar{C}, x_0 \in LOS_m, N_m = n\right), \qquad (4.28)
\end{aligned}$$

where the closed-form expression for $\mathbb{P}\left(\bigcup_{l=1}^{K_{rep}} \text{SINR}_{m,l} \geq \gamma \,\middle|\, \bar{C}, x_0 \in LOS_m, N_m = n\right)$ *is derived on Lemma 6.*

Given the analytical expression for the probability that the m-th K-repetition HARQ retransmission is successfully received by the BS in Theorem 7 and the fact that the probability that a randomly selected UE is active can be computed from (4.17), the latent access failure probability is derived as

$$\mathcal{P}_F(T \leq \tau) = \begin{cases} 1, & \text{, if } M^{K_{rep}} = 0 \\ 1 - \sum_{m=1}^{M^{K_{rep}}} \mathcal{A}_m^{K_{rep}} \mathcal{P}_m^{K_{rep}} & \text{, if } M^{K_{rep}} \geq 1. \end{cases} \tag{4.29}$$

4.5 Numerical Results and Discussion

In this section, we report the results of Monte-Carlo simulations of the system model described in Section 4.3. We use the simulation results to: a) validate the closed-form analytical approximations derived in Section 4.4 b) characterize the performance of the two HARQ protocols in the mmWave massive MIMO scenario and c) discuss the insights provided by the analytical results.

At the beginning of each simulation instance, the users' locations are generated according to an HPPP inside a cell with radius $R = 0.5$ km. At every TTI:

- The channel gain between the UE and the BS located at the origin is generated as an exponential random variable with unit mean.
- All active UE are determined to have either a LOS or NLOS link according to the probability in (4.24), with $\beta = 1$.
- All active UE select a random subcarrier from one of the $N_S = 48$ subcarriers available.
- All active UE select a random preamble from one of the $N_P = 64$ preambles available.
- The BS checks all UE with LOS links on every subcarrier for preamble collision.

- The BS computes the dot product between the signal received and the conjugate beam for all the UE whose preambles have not collided. If the resulting SINR is greater than $\gamma = -2$ dB, the transmission is successful, otherwise it fails.
- The BS sends an ACK feedback signal to the UE whose transmission was successful and a NACK feedback signal to those whose transmission attempt failed. As the main goal of this work is to characterize grant-free uplink performance, we assume that the feedback sent through the downlink channel is error free.
- All UE move to a new location.

In accordance with 3GPP standards (3GPP, 2021a,b), we consider a TTI mini-slot having a duration of 0.125 ms and a subcarrier spacing of 60 kHz, which is a configuration compatible with 5G NR frequency range 2 (FR2) operation, located in the mmWave spectrum. We consider a noise figure of -174 dBm/Hz, a path loss exponent of $\alpha = 4$ and a received power threshold of $\rho = -130dBm$.

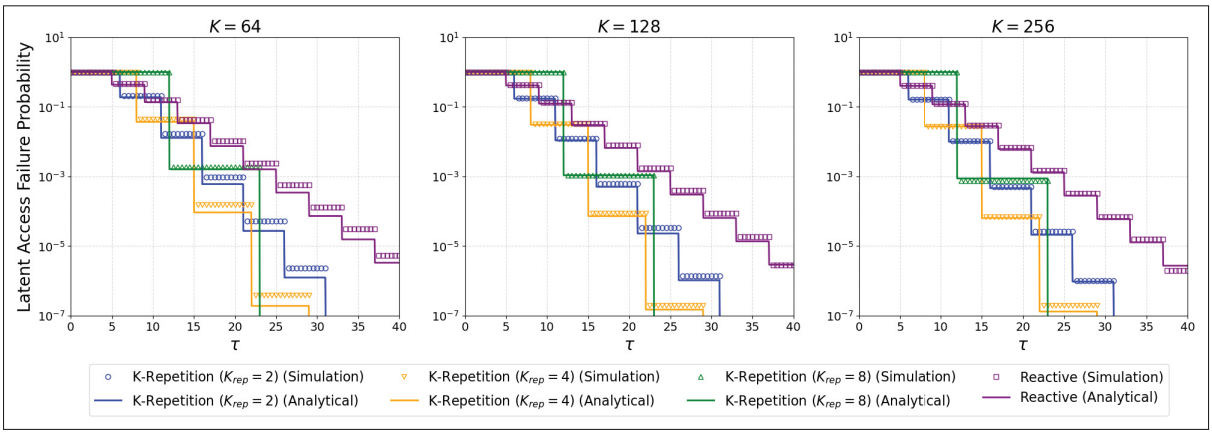

Figure 4.5 CCDF of the latent access failure probability for $\lambda_U = 1000$ UE/km^2 for the reactive and K-repetition HARQ protocols with $K_{rep} = 2, 4, 8$. The plots in the figure show the results for $K = 64$, $K = 128$ and $K = 256$ antennas

Figs. 4.5 and 4.6 show the complementary cumulative distribution function (CCDF) of the latent access probability for a user density of $\lambda_U = 1000$ UE/km^2 and $\lambda_U = 5000$ UE/km^2, respectively. The three plots in each figure display the performance for 64, 128 and 256 antennas, from left to right. The behavior of the performance curves, where the latent access failure

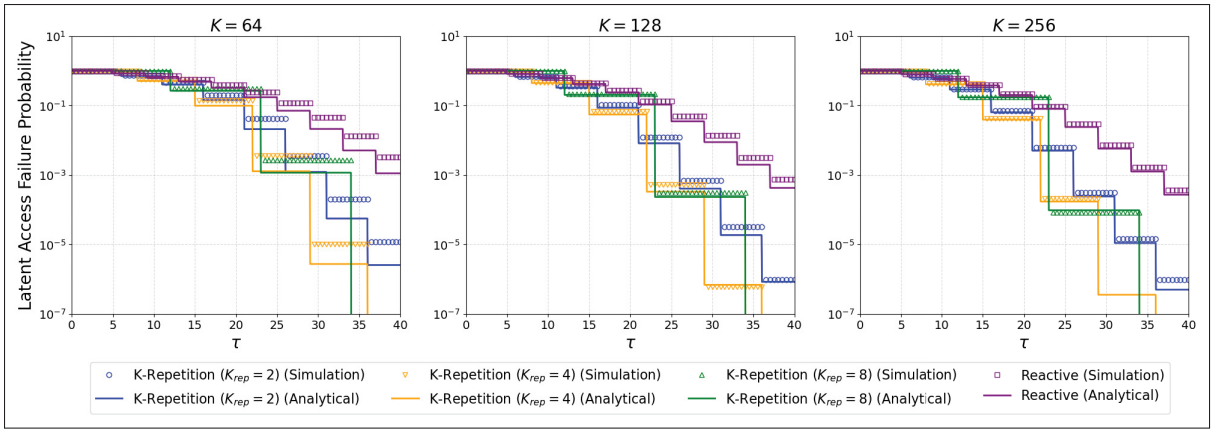

Figure 4.6 CCDF of the latent access failure probability for $\lambda_U = 5000$ UE/km^2 for the reactive and K-repetition HARQ protocols with $K_{rep} = 2, 4, 8$. The plots in the figure show the results for $K = 64$, $K = 128$ and $K = 256$ antennas

probability remains constant for a period of time and then drops on the following TTI, is due to the transmission propagation time on the uplink and the feedback, and the processing times. Fig. 4.5 depicts the performance with a moderate UE density scenario and shows that the reactive HARQ protocol is the best option for strict delay constraints, with $\tau \leq 6$ TTI (0.725 ms), as there is no time for any of the K-repetition configurations to finish their first round-trip. When the first and second round-trips for $K_{rep} = 2$ are completed, it has the best performance in $6 \leq \tau \leq 8$ TTI and $11 \leq \tau \leq 12$ TTI intervals. From this point on, the best performance is dominated by $K_{rep} = 4$ and $K_{rep} = 8$, with the best configuration being the one that has more completed round-trips in under τ TTI. A similar trend occurs with a higher user density as shown in Fig. 4.6.

Tables 4.1 and 4.2 show the reduction in the latent access failure probability upon increasing the number of antennas from 64 to 256. There is little improvement for a delay constraint of 1 ms in either scenario. In applications with a moderate UE density and a delay constraint of 2 ms or more, we notice an average improvement of around 2 across both HARQ protocols investigated, while in applications with a higher user density, the failure probability is reduced by as much as 32 times for $K_{rep} = 8$ repetitions and a delay constraint greater or equal to 3 ms. Nonetheless, notice from Figs. 4.5 and 4.6 that increasing the number of antennas from 128

Table 4.1 Latent access failure probability reduction in increasing from 64 to 256 antennas when $\lambda_U = 1000$ UE/km^2

HARQ	$T \leq 1$ **ms**	$T \leq 2$ **ms**	$T \leq 3$ **ms**
$K_{rep} = 2$	1.25	1.59	1.982
$K_{rep} = 4$	1	2.18	1.98
$K_{rep} = 8$	1	2.49	-
Reactive	1.12	1.42	1.64

Table 4.2 Latent access failure probability reduction in increasing from 64 to 256 antennas when $\lambda_U = 5000$ UE/km^2

HARQ	$T \leq 2$ **ms**	$T \leq 3$ **ms**	$T \leq 4$ **ms**
$K_{rep} = 2$	1.54	6.81	13.69
$K_{rep} = 4$	3.25	17.13	-
$K_{rep} = 8$	1.75	32.51	32.51
Reactive	1.40	2.60	6.18

to 256 does not change the latency performance significantly. Additionally, the increase in the number of antennas has a larger impact on performance for the higher user density scenario shown in Fig. 4.6 than for the moderate density one in Fig. 4.5. Later in this section, we discuss why this happens and how to possibly address it.

As the approximation used to derive the results in Section 4.4 relies on $K \gg 1$, there is a gap between the analytical and simulation results when $K = 64$ as, in this regime, the value of $F_K(x)$, and consequently the interference, outside the main lobe are no longer negligible in comparison to the gain on the main lobe.

Figs. 4.7 and 4.8 show how system reliability, i.e., in the probability of transmission failure under the latency constraint τ, scales with an increase in user density for a latency constraint of $\tau = 1$ ms and $\tau = 3$ ms, respectively. In both figures the user density ranges from 100 to 5000 UE/km^2. Fig. 4.7 shows that that the combination of mmWave and massive MIMO is not enough to satisfy the QoS requirement of URLLC applications with the stricter delay constraint

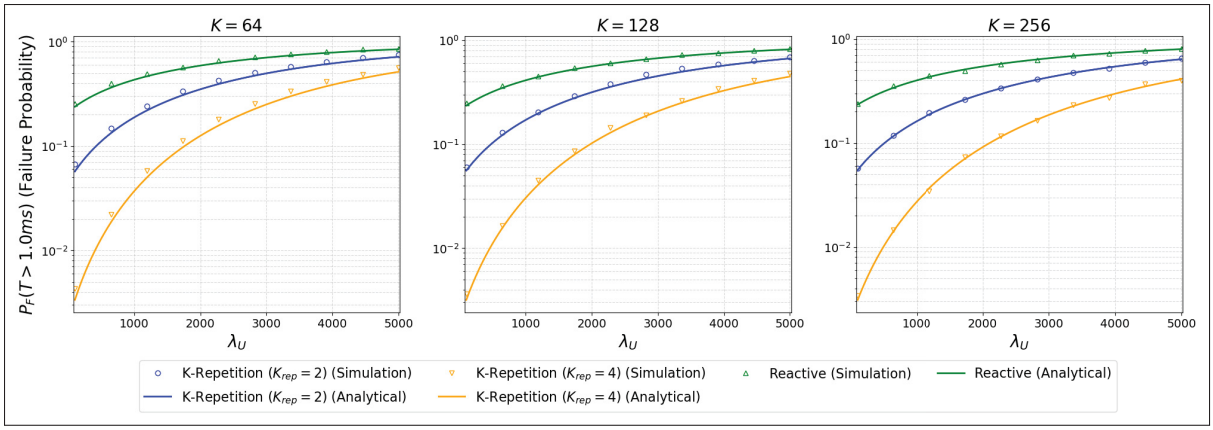

Figure 4.7 The probability that an UE fails to transmit its packet under $\tau = 1$ ms for an user density ranging from 100 UE/km^2. The plots show the results for $K = 64$, $K = 128$ and $K = 256$ antennas, respectively

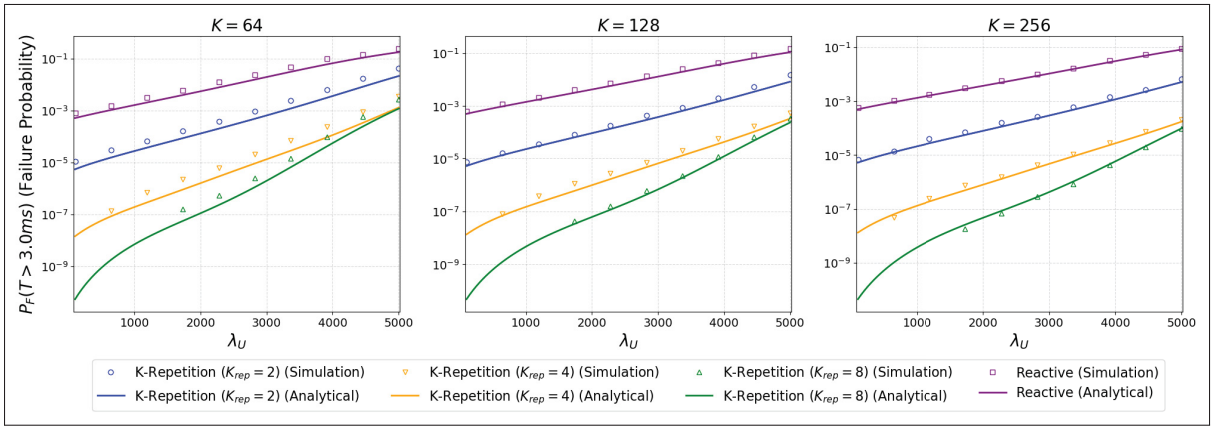

Figure 4.8 The probability that an UE fails to transmit its packet under $\tau = 3$ ms for an user density ranging from 100 UE/km^2. The plots show the results for $K = 64$, $K = 128$ and $K = 256$ antennas, respectively

(failure probability below 10^{-6}). Also, in this latency range, the benefit from increasing the number of BS antennas is rather small. For applications with less stringent delay constraints, shown in Fig. 4.8, the K-repetition HARQ protocol with $K_{rep} = 4$ and $K_{rep} = 8$ is able to support the URLLC QoS requirements. Table 4.3 depicts the highest UE density that can be supported by each HARQ and MIMO configuration. When $K_{rep} = 4$, increasing the number of BS antennas from 64 to 128 increases the supported user density by 11% and increasing the

number from 128 to 256 increases it by only 7.5%. For $K_{rep} = 8$, those values are 14% and 5%, respectively. It is worth noting that as long as the QoS constraints are satisfied, it is desirable to use the HARQ configuration with the least number of repetitions as possible in order to save UE power.

Table 4.3 User density supported (failure probability below 10^{-6}) by each configuration

HARQ	$K = 64$ **antennas**	$K = 128$ **antennas**	$K = 256$ **antennas**
$K_{rep} = 2$	-	-	-
$K_{rep} = 4$	1800 UE/km^2	2000 UE/km^2	2150 UE/km^2
$K_{rep} = 8$	2800 UE/km^2	3200 UE/km^2	3350 UE/km^2
Reactive	-	-	-

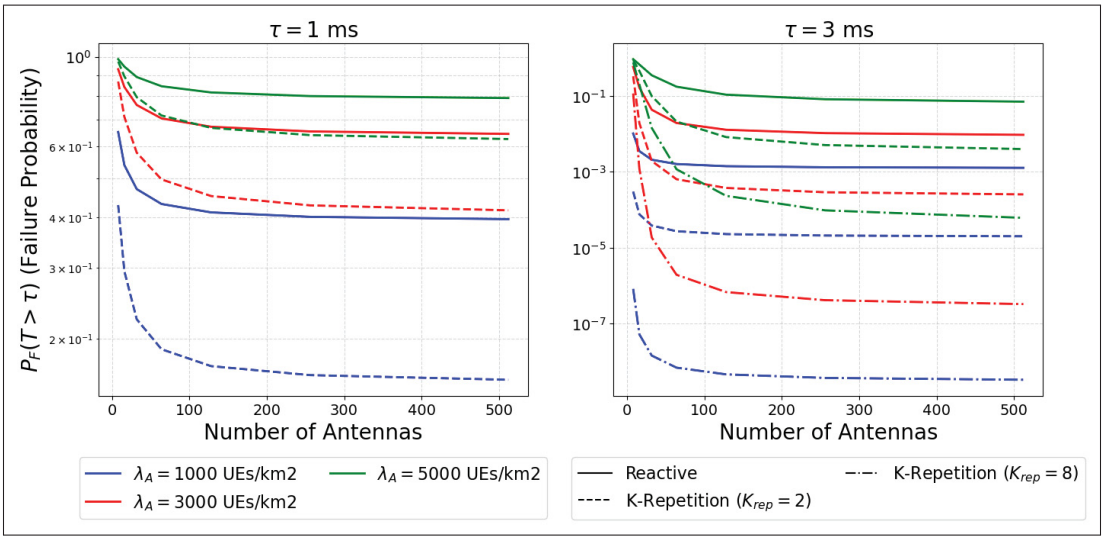

Figure 4.9 The impact of the number of antennas on the latent access failure probability. The leftmost plot shows results for delay constraint $\tau = 1$ ms, while the rightmost for $\tau = 3$ ms

In Fig. 4.9, we show the impact of increasing the number of antennas on the failure probability for a delay constraint of $\tau = 1$ ms on the left and $\tau = 3$ ms on the right. From this figure, we can conclude that increasing the number of antennas beyond 100 for the configuration under consideration ($R = 0.5$ km and $\beta = 1$) has a decreasing impact on latency performance. Moreover, the K-repetition HARQ protocol benefits more from an increased number of antennas

than the reactive HARQ protocol does. Also, the plot on the right shows that the latency performance of applications with a moderate latency constraint (τ = 3 ms) and higher user densities ($\lambda_U \geq 3000$ UE/km^2) is greatly improved by changing from traditional MIMO to massive MIMO. This is explained by the capability of producing narrower receiver beams on systems with a higher number of antennas. Nevertheless, as of a certain point, the probability of having a LOS link becomes the dominant bottleneck in reducing the latent access failure probability. As the LOS link probability is unaffected by the number of antennas, another measure must be taken to further reduce the latency. In the system model formulated in this paper, one way to achieve this would be to increase the BS deployment density, effectively decreasing the radius of the cells.

4.6 Conclusions

In this work, we formulated a model to analyze the latency and reliability of mmWave massive MIMO URLLC applications using reactive and K-repetition HARQ protocols. We used stochastic geometric spatiotemporal tools to derive closed-form approximations of the system's latent access failure probability. We validated the analytical results using Monte-Carlo simulations, identifying the limitations of our analytical results. Also, we investigated how the system's performance is impacted by the application's latency constraint, the density of UE served by the system, and the number of antennas in the BS. We concluded that:

- Other than for extremely strict delay constraints (τ = 0.625 ms), the K-repetition HARQ protocol is a better choice.
- Increasing the number of BS antennas from 64 to 256 BS antennas can reduce the latent access failure probability by a factor of 32 for the cell configuration analyzed in the manuscript.
- Massive MIMO's interference reduction capability significantly improves the reliability of systems with high user density and moderately improves the performance of systems with low user density.

- The increase in reliability from increasing the number of BS antennas beyond 100 is greatly reduced in the configuration investigated in Section 4.5, as the probability of having a LOS link between the UE and the BS becomes the main bottleneck.
- Under the configurations investigated in this manuscript, the system can support a UE density as high as 3350 UE/km^2 for a URLLC application with latency and reliability constraints of 3 ms and 10^{-6}, respectively.

Overall, we can conclude that it is possible to increase the reliability of URLLC applications by using mmWave massive MIMO, and when this technique is combined with selecting reasonable configuration parameters, these two techniques together can improve reliability under a strict latency constraint ($\tau = 1$ ms) and can satisfy URLLC QoS requirements under a less strict latency constraint ($\tau = 3$ ms).

CHAPTER 5

INTELLIGENT LINK ADAPTATION IN GRANT-FREE ACCESS CELLULAR NETWORKS: A DISTRIBUTED DEEP REINFORCEMENT LEARNING APPROACH

Joao V.C. Evangelista[1] , Zeeshan Sattar[1] , Georges Kaddoum[1] , Bassant Selim[2] , Aydin Sarraf[2]

[1] Department of Electrical Engineering, École de Technologie Supérieure,
1100 Notre-Dame Ouest, Montréal, Québec, Canada H3C 1K3
[2] Global Artificial Intelligence Accelerator, Ericsson Canada,
8275 Trans Canada Route, Saint-Laurent, Quebec, Canada H4S 0B6

Article submitted to the IEEE Transactions on Wireless Communications, July, 2021.

5.1 Abstract

With the continuous growth of machine-type devices (MTDs), it is expected that massive machine-type communication (mMTC) will be the dominant form of traffic in future wireless networks. Applications based on this technology, have fundamentally different traffic characteristics from human-to-human (H2H) communication, which involves a relatively small number of devices transmitting large packets consistently. Conversely, in mMTC applications, a very large number of MTDs transmit small packets sporadically. Therefore, conventional grant-based access schemes commonly adopted for H2H service, are not suitable for mMTC, as they incur in a large overhead associated with the channel request procedure. We propose three grant-free distributed optimization architectures that are able to significantly minimize the average power consumption of the network. The problem of physical layer (PHY) and medium access control (MAC) optimization in grant-free random access transmission is modeled as a partially observable stochastic game (POSG) aimed at minimizing the average transmit power under a per-device delay constraint. The results show that the proposed architectures are able to achieve significantly less average latency than a baseline, while spending less power. Moreover, the proposed architectures are more robust than the baseline, as they present less variance in the performance for different system realizations.

5.2 Introduction

The rapid growth of the Internet of Things (IoT) autonomous vehicles, smart grids, and other technologies propelled machine-to-machine (M2M) communications into one of the dominant applications in cellular networks (Machina Research, 2015). Machine communication have fundamentally different traffic patterns compared to human-to-human (H2H) ones. In H2H, a few users consume and produce large quantities of data, whereas in M2M applications a large number of devices generate small amounts of data with diverse quality of service (QoS) requirements (Machina Research, 2015). Given this difference, the grant-based transmission approach adopted by current cellular standards is inefficient in the massive machine-type communication (mMTC) scenario (Gao & Dai, 2019).

A considerable amount of the devices using the mMTC service are battery powered, whereas in currently deployed wireless systems, a lot of the energy consumed by communicating devices is used for establishing and maintaining connections. As identified in (Au *et al.*, 2014), when transmitting small packets, the grant request procedure can result in a significant overhead. While the semi-persistent connection, as adopted by the narrowband internet of things (NB-IoT) standard, might reduce the signaling overhead, it can only do so efficiently in the case of periodic traffic arrival (Hoymann *et al.*, 2016). The specifications of 5G new radio (NR) introduced the two-step random access procedure (in the rest of this work referred to as grant-free access) (3GPP, 2018a), which allows the users of the network to transmit their data directly on the random access channel (RACH) as opposed to the traditional four-step channel request approach used in long term evolution (LTE) (in the rest of this work referred to as grant-based access). This flexibility with regards to the random access mechanism gives us the opportunity to rethink the design of future networks to service M2M communications.

A grant-free access mechanism can enable devices to transmit data in an arrive and-go manner in the next available slot. Unlike the current grant-based access mechanism in the LTE uplink, devices using grant-free transmission need not wait for a specific uplink grant from the base station. Such a scheme is more desirable for the two broad IoT use cases in 5G, namely mMTC

and ultra-reliable low-latency communications (URLLC), as it enables reduced transmission latency, smaller signaling overhead due to the simplification of the scheduling procedure, and improved energy efficiency (battery life) of the IoT devices with a reduction in signaling and ON time. Grant-free and semi-grant-free transmission are considered for low latency IoT transmission in (3GPP, 2017).

Notwithstanding, in grant-free access, as the transmissions are not scheduled on orthogonal time-frequency resources, there is a high probability that different devices will randomly choose the same resource blocks for uplink transmission, resulting in the superposition of data (collision). The cross-layer optimization of a grant-free network requires consideration of both physical layer (PHY) and medium access control (MAC) layer measurements while taking into account their interaction to obtain the relevant performance metrics (e.g. the average power consumption and delay), making it a very challenging problem. Moreover, grant-free transmission poses new challenges in the design of PHY and MAC protocols. In this context, static policies for adaptive modulation and coding (AMC) power control, and packet retransmission are not able to efficiently satisfy the diverse throughput, latency, and power saving requirements of mMTC. Furthermore, due to a lack of scheduling by a central entity in such networks, a distributed optimization approach with partial state information is a natural choice to optimize the network performance while keeping communication overhead to a minimum. In this light, we argue that modeling the problem as a partially observable stochastic game (POSG) and proposing a solution within the multiagent reinforcement learning (MARL) framework is the best approach to this problem. While the POSG model is able to elegantly capture the evolution of the wireless environments and its interactions with the users in time, the MARL framework enables a distributed decision-making solution, balancing short-term and long-term performance goals.

5.2.1 Related Work

Random access is an essential component of every multiuser wireless communication system, either as a method of establishing a connection between an user and a base station (BS) (in grant-based systems), or to transmit data (in grant-free systems). Recently, the rise in prominence

of mMTC applications has sparked a debate around which of the competing methods should be adopted. A large portion of the research community started advocating for the adoption of a grant-free approach to serve mMTC applications (Liu *et al.*, 2018; Bockelmann *et al.*, 2016). In (Gao & Dai, 2019) an extensive comparison of the performance of grant-free and grant-based systems with and without subcarrier sensing against a variable packet length is presented. The authors concluded that for shorter packet lengths (as expected in mMTC applications) grant-free transmission with sensing results in the best throughput, making a stronger case for grant-free mMTC systems. Moreover, in (Evangelista *et al.*, 2019a; Liu *et al.*, 2020), stochastic geometric models and analytical results for grant-free non-orthogonal multiple access (NOMA) are presented.

In (Abreu *et al.*, 2018), the authors propose an open loop power control scheme with path loss compensation in an uplink grant-free ultra reliable low-latency communication (URLLC) network to minimize the outage probability. They investigate the effects of the path-loss compensation factor and the expected received power on the network outage probability. In (Jacquelin, Vilgelm & Kellerer, 2019), the authors introduce a model to abstract multi-packet reception in grant-free networks. They analyze the dynamics of the network and propose a reinforcement learning (RL) approach to determine the amount of resource blocks to allocate to grant-free transmission in order to maximize the normalized throughput. In (Huang, Wong & Schober, 2019), the effects of pilot selection in a grant-free NOMA system are investigated, and a deep reinforcement learning (DRL) approach is proposed, where each user, without any information exchange, selects its pilots in order to maximize its throughput. Despite their contributions, none of these works address the interactions between the PHY and MAC layers and how to harness their flexibility to improve the overall network performance.

In (Mastronarde & van der Schaar, 2013), a reinforcement learning algorithm is proposed to jointly select an AMC, and dynamic power management (DPM) in order to minimize the transmitted power in a single-user system while satisfying a certain delay constraint. Afterwards, in (Mastronarde, Modares, Wu & Chakareski, 2016) the work in (Mastronarde & van der Schaar, 2013) is extended to consider a multiuser system in an IEEE 802.11 network with

subcarrier sensing multiple access (CSMA). The authors considered three users contending for channel access, and adopted an independent learners approach (Claus & Boutilier, 1998), where each user optimizes its own rewards, ignoring all interactions with other users. Despite its simplicity, the independent learners solution is known to have several issues such as Pareto-selection, nonstationarity, stochasticity, alter-exploration and shadowed equilibria (Matignon, Laurent & Le Fort-Piat, 2012).

Although instructive, none of these works addressed the challenges involved in the distributed cross-layer optimization of the grant-free uplink transmission for mMTC service. Moreover, previous works on this topic have failed to address the issues involved in the massive scale aspect of mMTC applications, despite their contributions. In this manuscript, we propose three distributed solutions based on MARL, ranging from a fully distributed solution to a centralized learning with distributed inference, to minimize the average power consumption of the network while satisfying delay constraints.

5.2.2 Contributions

Although instructive, none of these works addressed the challenges involved in the distributed cross-layer optimization of the grant-free uplink transmission for mMTC service. In this manuscript, we propose three distributed solutions based on MARL, ranging from a fully distributed solution to a centralized learning with distributed inference, to minimize the average power consumption of the network while satisfying delay constraints. The contributions of this paper are summarized as:

- We propose a POSG to model the PHY and MAC dynamics of a grant-free mMTC network and to formulate the cross-layer power minimization problem. This model considers the channel and packet generation dynamics, and accommodates machine-type device (MTD) with diverse QoS requirements and packet arrival intensities.
- We propose a fully distribute independent learners (IL) architecture, based on the proximal policy optimization (PPO) algorithm (Schulman, Levine, Abbeel, Jordan & Moritz, 2015), to eliminate the all the communication overhead involved in the cross-layer optimization.

- We propose a distributed actors with centralized critic (DACC) architecture where the PPO actor and critic are split and each agent trains its own actor while a single critic is trained by a central entity running on an edge computing node. This architecture achieves a reduced overhead while allowing the possibility of cooperative behavior to arise among the MTD, in our second scheme. As the central entity is able to aggregate measurements from every user, the critic's loss function is calculated from a global performance measure.
- We propose centralized learning with decentralized inference (CLDI) architecture to eliminate the exponential increase of the policy search space with more MTD. In this scheme, every MTD uses the same policy, which is trained on an edge computing node. However, each MTD uses the model in a distributed fashion by making decisions based on local data.
- We provide an extensive analysis of the performance of all three architectures when servicing MTD with diverse QoS requirements and packet arrival rates. Moreover, we compare their performance with a reactive hybrid automatic repeat request (HARQ) protocol with power boosting as a baseline. Finally, we include a quantitative analysis of the tradeoffs involving the performance and the overhead of the proposed architectures in scenarios with different device deployment densities.

5.2.3 Notation

Throughout this paper, italic lowercase letters denote real and complex scalar values. Lower case boldface letters denote vectors, while upper case boldface denote matrices. A lowercase letter with one subscript, x_i, represents the i-th element of the vector $\mathbf{x}$, while two subscripts $x_{i,j}$ is used to denote the element on the i-th row and j-th column of matrix $\mathbf{X}$. The operator $E[\cdot]$ denotes the expected value of a random variable. The function $\mathbb{P}(\cdot)$ represents the probability of an event and $\mathbf{x} \sim \mathcal{CN}(\boldsymbol{\mu}, \mathbf{K})$, denotes that $\mathbf{x}$ is a circularly symmetric complex Gaussian random vector, with mean $\boldsymbol{\mu}$ and covariance matrix $\mathbf{K}$. The notation $x \sim U(\mathcal{X})$ denotes that x is drawn uniformly from the set $\mathcal{X}$. The indicator function takes an event as argument and is equal to one if the event happens and zero otherwise, and is represented by $\mathbf{1}(\cdot)$. Sets $\mathbb{R}$ and $\mathbb{C}$ and are the sets of real and complex numbers, respectively. The set $\mathbb{B} = \{0, 1\}$ represents the binary numbers. A

calligraphic uppercase letter, such as $\mathcal{X}$, denotes a set and $|\mathcal{X}|$ is its cardinality. Throughout the paper several variables denote quantities related to a particular user at a given moment in time (e.g. $x_{i,t}$ is related to the i-th user on time slot t). To avoid cluttering the notation we drop the subscript related to the time and use it only when indexing a variable over multiple periods of time is necessary.

5.2.4 Organization

This paper is organized as follows: In Section 5.3 we present the system model, discussing in details the dynamics of the environment introducing the optimization problem we aim to solve. In Section 5.4, we present the three distributed learning architectures proposed in this work. In Section 5.5, the performance of the three proposed architectures is evaluated and the results are discussed. Finally, in Section 5.6, we summarize the conclusions.

5.3 System Model

In this paper, we consider the problem of designing a distributed link adaptation solution for a grant-free access 5G network providing mMTC service. In a grant-free network, there is no guarantee that a transmission attempt is going to be successful. Hence, the usage of a HARQ protocol is essential to guarantee some reliability to the packet transmissions. In the system under analysis, the MTD use a reactive HARQ protocol, where after each transmission attempt the device receives either an acknowledgement (ACK) feedback, in case the transmission attempt was successfully decoded, or a negative-acknowledgement (NACK) feedback, in case the transmission attempt could not be decoded (Mahmood *et al.*, 2019). Notice that we choose the reactive HARQ protocol because the alternative protocols require repeating the same data on every transmission attempt, increasing the transmission power per attempt, which goes against our design objective of minimizing the power expenditure in the network.

We consider a network with N_U MTD and N_B base stations randomly located within a circular area of radius R. The distance between the i-th device and the j-th BS is denoted by $d_{i,j}$.

Moreover, each device is associated to its closest BS. We assume there are N_K orthogonal subcarriers reserved for uplink transmission, and N_P orthogonal preambles. In every transmission time interval (TTI) the active devices randomly select one out of the N_P available orthogonal preambles, and one subcarrier out of the N_K available to transmit its data on. The orthogonal preambles are used by the network to detect user activity and estimate the MTD' channel response. It is worth highlighting that all the variables discussed in this section are associated to a given TTI; However, for notation convenience, we drop the subscript t used to denote a specific TTI. Additionally, if x is a variable at time t we use a prime superscript x' to denote the value of the same variable at $t + 1$.

All devices transmit symbols from a quadrature amplitude modulation (QAM) with order $\beta_i \in \{1, \ldots, M\}$, where M is the maximum modulation order. Furthermore, before the start of every TTI, each device has the option to turn off its radio to save power. The radio state is represented by the variable $x_i \in \{0, 1\}$, whenever $x_i = 1$, the radio is on and consumes P_{ON} watts plus whatever power used for the transmission, and when $x_i = 0$, the radio is off and spends P_{OFF} watts. If the radio is on, the device attempts to transmit its data on that particular TTI, hence, the user must select a transmission power $p_i \in \mathcal{P} = \{\rho_1, \ldots, \rho_{\max}\}$. So, the received signal at the j-th BS on the k-th subcarrier is

$$r_k = \sum_{i=1}^{N_U} x_i \theta_{i,k} \sqrt{p_i} h_{i,j,k} d_{i,j}^{-\alpha/2} u_i + w_k, \tag{5.1}$$

where $\theta_{i,k} \in \{0, 1\}$ indicates whether user i is transmitting on subcarrier k, $w_k \sim \mathcal{CN}(0, N_0)$ is a circularly symmetric complex normal random variable modeling the additive white Gaussian noise (AWGN) and α is the path loss exponent. The variable u_i is a symbol from a QAM constellation with order β_i and $\|u_i\|^2 = 1$. Moreover, $h_{i,j,k}$ represents the small-scale fading experienced by the i-th user's signal to the j-th BS on the k-th subcarrier. We assume that the channel remains constant during the TTI duration. To model the relationship between subsequent channel realizations we consider a first-order Gauss-Markov small-scale flat fading

model (Evangelista, Sattar, Kaddoum & Chaaban, 2019b) where

$$h'_{i,j,k} = \kappa h_{i,j,k} + n_{i,j,k}, \tag{5.2}$$

where the innovation $n_{i,j,k} \sim \mathcal{CN}(0, 1 - \kappa^2)$ is a circularly symmetric complex normal random variable. The correlation between successive fading components is given by (Patzold, 2012)

$$\kappa = J_0 \left(2\pi f_{\max} \Delta_t\right), \tag{5.3}$$

where $f_{\max}$ is the maximum Doppler frequency, Δ_t is the duration of a single TTI and J_0 is the zero-th order Bessel function of the first kind.

In order to guarantee a harmonious access to the channel and avoid congestion, the system under investigation employs a rate-adaptive listen before talk (LBT) mechanism with random backoff on every subcarrier to control the congestion. This approach is well aligned with the specifications of 5G networks operating on the unlicensed spectrum (Dahlman *et al.*, 2018; Kim, Yi & Bahk, 2020; Maldonado, Rosa & Pedersen, 2020; Song *et al.*, 2019). A TTI is divided into two phases: contention and transmission. During the contention phase, the device listens to the channel on a specific subcarrier for a random backoff time $\tau^C < \Delta_t$. If no other user has started transmission during this time, the device starts its transmission for an amount of time $\tau^{TX} = \Delta_t - \tau^C$. The protocol is illustrated in Fig. 5.1, where we show a situation in which 4 devices are transmitting on the same subcarrier. The red shaded areas indicate the random backoff time τ^C drawn by each user. In this figure, as device 2 drew the smallest backoff time, it takes hold of the channel and transmits its data in the remaining time available in the time slot. In this model, a collision occurs if two devices draw the same random backoff time.

We consider a rate-adaptive congestion control protocol, similar to the one proposed in (Mastronarde *et al.*, 2016), where a congestion window (CW) given by $CW_{\min}(\beta_i) = \lfloor A 2^{M-\beta_i} \rfloor$, where $A \in \mathbb{R}$ is a design parameter, is assigned to the device according to its modulation order. The backoff time of the i-th device is uniformly chosen from $[0, CW_{\min}(\beta_i)]$ and is reset at the end of the time slot.

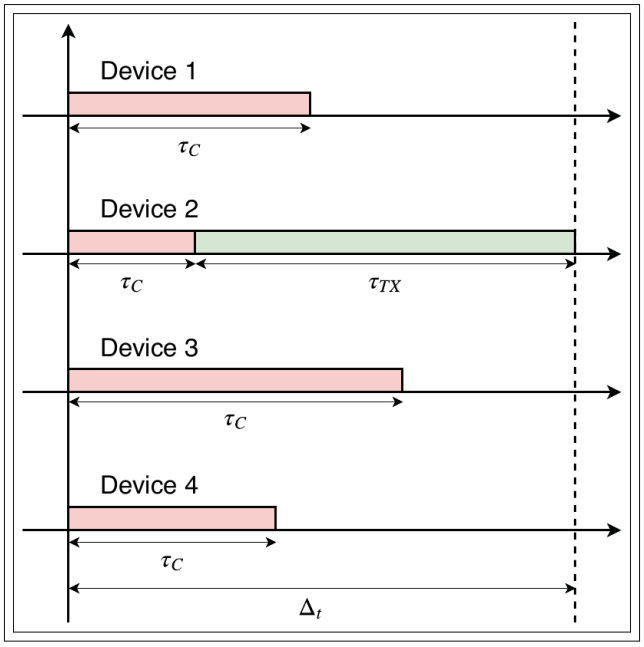

Figure 5.1 Illustration of the considered LBT procedure for 4 devices sharing the same channel. The red shaded area represents the random backoff listening time and the green shaded one denotes the transmission time

Definition 5.1 (Collision)**.** *We consider that a collision occurs whenever two devices being served by the same BS select the same preamble and the same subcarrier, and, draw the same random backoff time* τ^C.

If a collision occurs, the devices' CW are set to $CW_{\max} = A2^M$. Note that the MTD attempts to transmit

$$z_i = \left\lfloor \frac{\beta_i \tau^{TX}}{LT_S} \right\rfloor \tag{5.4}$$

packets in a given TTI, where L is the packet length and T_S is the symbol duration. This approach increases the likelihood that a device that intends to transmit at higher rates obtains channel access, avoiding the anomaly identified in (Heusse, Rousseau, Berger-Sabbatel & Duda, 2003), where low-rate users significantly degrade the performance of the whole network.

Furthermore, we assume that each device has a packet buffer with a capacity of L_B packets. Let b_i be the number of packets in the i-th device's buffer. We assume that the number of arriving packets follow a Poisson distribution $l_i \sim Poisson(\lambda_i)$, where λ_i is th mean packet arrival rate. The number of packets departing (the goodput) the device's buffer is denoted by g_i. The goodput of the i-th MTD is a function of the device's transmit power, its selected subcarrier, its channel to the receiving BS, and the interference power at the receiving BS. Let the interference suffered by the i-th MTD's transmission on the k-th subcarrier be

$$I_{i,k} = \sum_{\substack{n=1 \\ n \neq i}}^{N_U} x_n \theta_{n,k} p_n \left\| h_{n,j,k} \right\|^2 d_{n,j}^{-\alpha} \tag{5.5}$$

The probability that the j-th BS decodes a bit transmitted by the i-th MTD in error (denoted as P_i^e) can be approximated by (Proakis, 2007)

$$P_i^e \approx \begin{cases} \frac{1}{2}\text{erfc}\left\{ \sqrt{\frac{p_i \left\| h_{i,j,k} \right\|^2 d_{i,j}^{-\alpha}}{I_{i,k}+N_0}} \right\} & \text{if } \beta_i = 1 \\ 2\text{erfc}\left\{ \sqrt{\frac{3\log_2(\beta_i) p_i \left\| h_{i,j,k} \right\|^2 d_{i,j}^{-\alpha}}{2(\beta_i - 1)(I_{i,k}+N_0)}} \right\} & \text{if } \beta_i > 1, \end{cases} \tag{5.6}$$

Given the approximate probability of decoding a bit in error given in (5.6), we obtain the probability of losing a packet as

$$P_i^{loss} = 1 - \left(1 - P_i^e\right)^L. \tag{5.7}$$

Moreover, the number of overflown packets, i.e. packets that arrive while the buffer is full and must be dropped, at the i-th device's buffer is given by

$$\xi_i = \max(b_i + l_i - g_i - L_B, 0). \tag{5.8}$$

5.3.1 Problem Formulation

The main goal of this work is to derive a link adaptation algorithm to minimize the average power consumption over time of the network under a constraint on the average delay. Notice that as the MTD transmission attempts are not scheduled by a central network the proposed algorithm must run on each device in a distributed fashion. Also, although the goal is to minimize the average power consumption the algorithm has only local information to make decisions on the link adaptation. This problem can be formulated as a POSG (Neyman & Sorin, 2003). A POSG, models how multiple agents, with distinct and possibly adversarial goals, interact with a stochastic changing environment in discrete time slots. At each time slot, the agents receive a partial, and possibly noisy, observation of the environment and select an action to take in the next slot based on this observation. Each set of actions selected by the agents incurs a cost and the objective of the problem is to find the joint policy that minimizes the cost. In this work, we are concerned with infinite horizon POSGs (Puterman, 2014), as the task we are optimizing cannot be described by finite length episodes. The POSG problem is formally defined by a tuple $(\mathcal{U}, \mathcal{S}, \mathcal{A}, \mathcal{P}_{\mathcal{S}}, c, \mathcal{O})$, where $\mathcal{U}$ is the set of agents, where each MTD out of the N_U total constitutes an agent. $\mathcal{S}$ and $\mathcal{A} = \times_{i \in \mathcal{U}} \mathcal{A}_i$ denote the state space and the joint action space of the system, respectively, where $\mathcal{A}_i$ is the action space of the i-th agent. The state-action transition probability $\mathcal{P}_{\mathcal{S}} : \mathcal{S} \times \mathcal{A} \times \mathcal{S} \rightarrow [0, 1]$ gives the probability $\mathcal{P}(\mathbf{s}'|\mathbf{s}, \mathbf{a})$ of transitioning to a state $\mathbf{s}'$, given the current state $\mathbf{s}$ and the joint selected action $\mathbf{a}$. The set $\mathcal{O} = \{O_i : O_i \subseteq \mathcal{S}\ \forall i \in \mathcal{U}\}$ contains the observation space of each device, which is a subset of the complete state space. Furthermore, $c : \mathcal{S} \times \mathcal{A} \rightarrow \mathbb{R}$ is the cost function associated to the problem. The cost function gives the cost of taking action a while on state s.

Definition 5.2 (Policy)**.** *A policy $\pi(a|o)$, for $a \in \mathcal{A}$ and $o \in O_i$ is a conditional probability distribution that gives the probability that the agent selects the action a given that it observes the local observation o.*

The joint policy of all the agents is denoted by $\boldsymbol{\pi} = [\pi_1, \ldots, \pi_{N_U}]$. Notice that $\boldsymbol{\pi}$ is also a conditional probability function given by

$$\pi(\mathbf{a}|\mathbf{s}) = \prod_{i=1}^{N_U} \pi_i(a_i|o_i) \tag{5.9}$$

The optimality criteria defines the optimization objective of the problem. In the case of an infinite-horizon POSG, we want the average cost over time to be minimized. Therefore, a natural optimality criteria for the joint policy $\boldsymbol{\pi}$ is the expected discounted cost (Oliehoek & Amato, 2016), which is given by

$$C_\pi(\mathbf{s}) = E_{\boldsymbol{\pi}} \left[\sum_{t=0}^{\infty} \gamma^t c(\mathbf{s}_t, \mathbf{a}_t) \middle| \mathbf{s}_0 = \mathbf{s} \right], \tag{5.10}$$

where $0 < \gamma < 1$ is the discount factor. So, the cost function takes into account the effect of the action on the current and future TTI. The discount factor is necessary to keep the summation in (5.10) bounded and can be interpreted as how much weight should the agent's decision give to future costs.

Let $\boldsymbol{\Pi} = \{\boldsymbol{\pi} | \boldsymbol{\pi} : \mathcal{A} \times \mathcal{S} \rightarrow [0, 1]\}$ be the set of all possible joint policies. Then, the solution of a POSG is defined as

$$\boldsymbol{\pi}^* = \arg\min_{\boldsymbol{\pi} \in \boldsymbol{\Pi}} E_{\mathbf{s} \sim \mathbb{P}(\mathbf{s})} \left[C_\pi(\mathbf{s}) | \, \mathbf{s}_0 = \mathbf{s} \right] = \arg\min_{\boldsymbol{\pi} \in \boldsymbol{\Pi}} E_{\mathbf{s} \sim \mathbb{P}(\mathbf{s}), \boldsymbol{\pi}} \left[\sum_{t=0}^{\infty} \gamma^t c(\mathbf{s}_t, \mathbf{a}_t) \middle| \mathbf{s}_0 = \mathbf{s} \right], \tag{5.11}$$

where $\mathbb{P}(\mathbf{s})$ is the probability distribution over the set of states $\mathcal{S}$ while following the joint policy $\boldsymbol{\pi}$, and, $\boldsymbol{\pi}^*$ is the policy that minimizes the expected discounted cost from the set of all possible policies. The problem in (5.11) is known to be undecidable, meaning that given a threshold, it is not possible to tell whether there exists a policy that has an expected discounted cost smaller than the threshold (Madani, Hanks & Condon, 1999); However, as we show in Section 5.4, we can reformulate the problem in (5.11) to a proxy problem, and approximate the policies π_i by a parametric function approximator $\pi_{\mathbf{w}_i}$, where $\mathbf{w}_i$ is the set of parameters for the device's policy. Consequently, the set of all possible joint policies $\boldsymbol{\Pi}$ becomes constrained to the set of all

possible policies that can be approximated by the parametric model. Considering a differentiable parametric model, we can use a data-driven learning approach to optimize the parameters and obtain high-quality sub-optimal solutions to (5.11).

The cellular system model described so far can be conveniently mapped into the POSG problem formulation. The state of the system can be denoted by

$$\mathbf{s} = (\mathbf{h}, \mathbf{b}, \mathbf{l}, \mathbf{g}) \,, \tag{5.12}$$

where $\mathbf{h} = \text{vec}\left(\left[\mathbf{H_1}, \ldots, \mathbf{H_{N_U}}\right]\right)$ and $\mathbf{H}_i = [\left\|h_{i,j,k}\right\|^2 d_{i,j}^{-\alpha}]_{j,k}$ is a $(N_B \times N_S)$ matrix where each entry is the channel gain between the i-th MTD and the j-th BS on the k-th subcarrier. Additionally, **b**, **l**, and **g** are vectors containing the number of packets in the buffer, the number of arriving packets and the goodput of each MTD, respectively. As the devices only have access to their local information the observation vector is given as

$$\mathbf{o}_i = [\text{vec}\left(\mathbf{H}_i\right), x_i, b_i, l_i, g_i] \,. \tag{5.13}$$

Furthermore, we map the optimization variables of the power minimization problems into the joint action vector as

$$\mathbf{a} = (\boldsymbol{\theta}, \boldsymbol{\beta}, \mathbf{p}, \mathbf{x}), \tag{5.14}$$

where $\boldsymbol{\theta} = \left[\boldsymbol{\theta}_1, \ldots, \boldsymbol{\theta}_{N_U}\right]$ and $\boldsymbol{\theta}_i \in \{0, 1\}^{N_S}$ is the subcarrier selection vector of the i-th user, and, $\sum_{k=1}^{N_S} \theta_{i,k} \leq 1$. Also, $\boldsymbol{\beta}$, **p**, **x** correspond to the modulation order, power and radio state selected by each MTD, respectively.

In this work, we want to minimize the power usage subject to a latency constraint. The POSG problem formulation is not compatible with a constrained objective. Hence, we follow the approach in (Altman, 1999) to model contrained Markov decision processes (CMDPs) and augment the objective function with a Lagrangian penalty (Nocedal & Wright, 2006). Furthermore, according to Little's theorem (El-Taha & Stidham Jr., 2012), the average number of packets queued in the buffer is proportional to the average packet delay in queues with stable

buffers (i.e. no overflow). Hence, we design the cost function to discourage large number of packets in the queue, which we refer to as the holding cost, while simultaneously penalizing dropped packets, which we refer to as the overflow cost. Therefore, in the POSG formulation, the cost function is

$$c(\mathbf{s},\mathbf{a}) = \sum_{i=1}^{N_U} \underbrace{x_i(P_{ON}+p_i)+(1-x_i)P_{OFF}}_{\text{power cost}} + \omega_i \left(\underbrace{b_i}_{\text{holding cost}} + \underbrace{\mu\xi_i}_{\text{overflow cost}} \right), \tag{5.15}$$

where ω_i is a Lagrange multiplier. Thus, if the i-th MTD has a delay constraint equal to δ_i, then, $\omega_i \propto \max(0, [b_i + \mu\xi_i] - \delta_i)$ is proportional to how much the delay constraint is being violated. Moreover, μ is the overflow penalty factor. The overflow penalty factor must be chosen such that dropping packets is sub-optimal, while encouraging devices to transmit with low-power. To meet these requirements, we choose a value of μ such that dropping a packet costs as much as the largest possible discounted expected cost incurred by holding a packet in the buffer, which happens if the packet is held in the buffer forever. Therefore

$$\mu = \sum_{t=0}^{\infty} \gamma^{t+1} = \frac{\gamma}{1-\gamma}. \tag{5.16}$$

5.4 Distributed Learning Architectures

Finding the optimal police to the proposed infinite-horizon POSG problem is undecidable. Deep neural networks (DNNs) are universal function approximators and can be trained to learn a mapping from data efficiently through gradient descent and backpropagation (Goodfellow, Bengio & Courville, 2016). Thus, we can use DNN to approximate the policies and use the agents' experience to learn policies that minimize the cost. This deep MARL has been proven to be successful in many complex multiagent tasks (Foerster, Assael, de Freitas & Whiteson, 2016; Foerster *et al.*, 2017; Foerster, Farquhar, Afouras, Nardelli & Whiteson, 2018; Lowe, Wu, Tamar, Harb & Abbeel, 2017; Omidshafiei, Pazis, Amato, How & Vian, 2017). However, many of the problems traditionally investigated in the MARL literature can be trained on computer clusters,

where the computing nodes are connected together through high-speed network interconnections and can easily share information among themselves to mitigate the partial observability of POSG (Claus & Boutilier, 1998). On the other hand, when the computing nodes (in our case MTD and edge computing infrastructure) are connected via wireless links, sending additional information incurs in an expensive overhead. Therefore, it is imperative to propose novel ways to train these DNN to solve the POSG problem, while sharing as little information between the computing nodes as possible. For this reason, we chose an actor-critic policy gradient approach (Sutton & Barto, 2018), as we have more flexibility on distributing the training and inference by placing the actor and the critic on different computing nodes.

In this setting, we propose three different distributed learning architectures: IL, DACC and CLDI. Fig. 5.2 illustrates the main differences between these architectures. Firstly, in the IL architecture, each MTD has its own network for policy selection (the actor) and value estimation (the critic). Secondly, in the DACC, the value estimator and policy selection networks are decoupled. Each MTD has its own policy selection network and an edge agent, which we assume is connected to every BS and has access to the state of every MTD, stores and trains a value estimator network. At each TTI the edge node feedbacks the critic value of the current state to all MTD through a broadcast channel. MTD use the fedback value estimate as the actor-critic's baseline to train their policy selection network. In the CLDI architecture, we follow a similar approach to (Lowe *et al.*, 2017; Foerster *et al.*, 2018), and consider that the edge node trains the weights (only from local observations) of a single policy network that is shared among all agents and sends it periodically through a broadcast channel. Then, MTD are able to select their actions only from local observations. Notice that in the DACC and CLDI architectures, the MTD need to feedback their state information back to the BS. This can be achieved by appending the buffer information to the transmitted packets, or by scheduling periodic state information transmission through a collision free channel. Nevertheless, in this paper, our aim is to evaluate the performance of the proposed architectures, and thus, we assume the state information can be reliably transmitted to the BS. Each approach presents its own advantages and challenges, as detailed in the rest of this section.

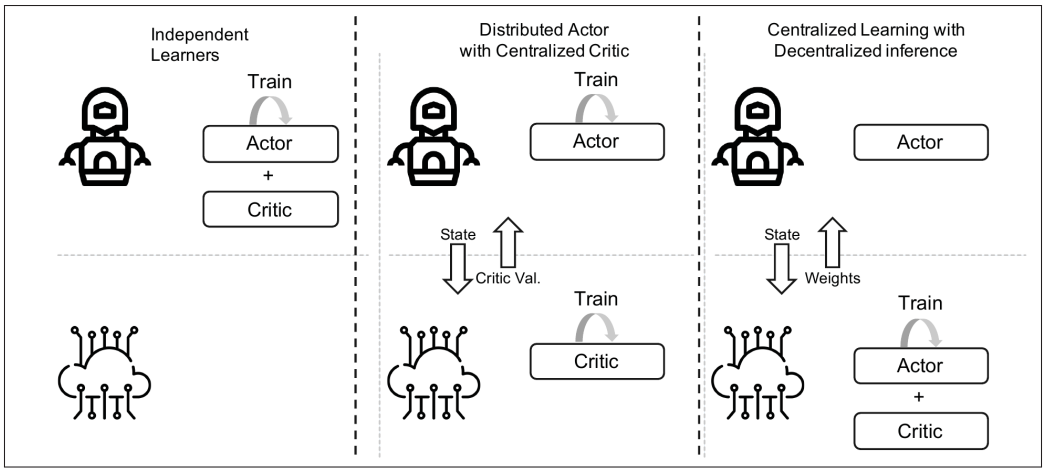

Figure 5.2 The diagram illustrates the differences between the three proposed architectures

In order to provide a fair comparison, in all of the proposed architectures, we consider an actor-critic style PPO algorithm (Schulman, Wolski, Dhariwal, Radford & Klimov, 2005), due to its ease of implementation, the possibility of decoupling the policy and the value estimator, reduced sample complexity compared to trust region policy optimization (TRPO) (Schulman *et al.*, 2015), and first-order updates. We start this section by introducing policy gradient methods and the PPO algorithm, and proceed to describe the three proposed architectures in detail.

5.4.1 Policy Gradient Methods

In contrast to action-value methods, such as Q-learning (Watkins & Dayan, 1992), where the agent learns an action-value function and derives a policy from selecting the actions that maximize its output, policy gradient methods learn a parametrized policy that selects the actions without consulting a value function. Let $\mathbf{w} \in \mathbb{R}^d$ be the policy parameter vector, then the parametrized policy $\pi_{\mathbf{w}}(a|s) = \mathbb{P}(a|s, \mathbf{w})$ denotes the probability of selecting action a, while at state s with policy parameter $\mathbf{w}$.

In order to learn the policy parameter vector, we need to have an objective function of $\mathbf{w}$ to be maximized. Consider a scalar performance function $J(\mathbf{w})$, differentiable with respect to $\mathbf{w}$. Then, the learning procedure consists in maximizing $J(\mathbf{w})$ through gradient ascent updates of

the form (Sutton & Barto, 2018)

$$\mathbf{w}' = \mathbf{w} + \eta \nabla_{\mathbf{w}} \tilde{J}(\mathbf{w}), \tag{5.17}$$

where η is the learning rate, and $\nabla_{\mathbf{w}} \tilde{J}(\mathbf{w})$ is an estimator of the gradient of the performance measure. A common choice of performance measure is

$$J(\mathbf{w}) = \pi_{\mathbf{w}}(a|s) A_{\pi}(s, a), \tag{5.18}$$

where $A_{\pi}(s, a) = Q_{\pi}(s, a) - V_{\pi}(s)$ is the advantage function, which gives the advantage of taking action a while at state s in comparison to the state value function, which gives the value of the average action. The state value function for policy π, $V_{\pi}(s)$, is given by the expected discounted reward of state s while following policy π, defined as

$$V_{\pi}(s) = E_{\pi} \left[\sum_{t=0}^{\infty} - \gamma^t c(s_t, a_t) \middle| s_0 = s \right]. \tag{5.19}$$

Furthermore, the action-value function for policy π, $Q_{\pi}(s, a)$, gives the expected discounted reward of taking action a while in state s and then continuing to follow policy π, which is given as

$$Q_{\pi}(a, s) = E_{\pi} \left[\sum_{t=0}^{\infty} - \gamma^t c(s_t, a_t) \middle| s_0 = s, a_0 = a \right]. \tag{5.20}$$

Notice that both (5.19) and (5.20) can be estimated from experience. This class of algorithms are known as *actor-critic* because we evaluate the difference between the actor estimate ($Q_{\pi}(s, a)$) and the critic estimate ($V_{\pi}(s)$), as presented in (5.18).

Let $\mathcal{E}_{\pi_{\mathbf{w}}}$ be the set of the experience tuples collected while following policy $\pi_{\mathbf{w}}$, where an experience tuple consists of the state, action, and cost. Then, the gradient of the performance measure can be estimated by taking the average gradient over a random finite batch of experience tuples as

$$\nabla_{\mathbf{w}} \tilde{J}(\mathbf{w}) = \hat{E}_{\mathcal{E}_{\pi_{\mathbf{w}}}} \left[\nabla_{\mathbf{w}} \ln \pi_{\mathbf{w}}(a|s) A(s_t, a_t) \right], \tag{5.21}$$

where $\hat{E}_{\mathcal{E}_{\pi_\mathbf{w}}}$ denotes the empirical average over a batch of randomly sampled experience tuples.

5.4.2 Proximal Policy Optimization

The PPO algorithm, originally proposed in (Schulman *et al.*, 2005), consists in maximizing a clipped surrogate objective $J^{\text{clip}}(\mathbf{w})$ instead of the original performance measure $J(\mathbf{w})$, therefore avoiding the destructively large updates experienced in policy gradient methods without clipping as shown in (Schulman *et al.*, 2005). The surrogate objective is defined as

$$J^{\text{clip}}(\mathbf{w}) = \hat{E}_{\mathcal{E}_{\pi_\mathbf{w}}}[\min(\Gamma(\mathbf{w})A(s,a), \text{clip}(\Gamma(\mathbf{w}), 1-\epsilon, 1+\epsilon)A(s,a))], \tag{5.22}$$

where $\Gamma(\mathbf{w}) = \frac{\pi_\mathbf{w}(a|s)}{\pi_{\mathbf{w}_{\text{old}}}(a|s)}$ is the importance weight, ϵ is a hyperparameter that controls the clipping, and $\mathbf{w}_{\text{old}}$ are the policy weights prior to the update. Due to the term $\text{clip}(\Gamma(\mathbf{w})A(s,a), 1-\epsilon, 1+\epsilon)$ in (5.22), the importance weight is clipped between $1-\epsilon$ and $1+\epsilon$, minimizing the incentives for large destabilizing updates. Furthermore, by taking the minimum of the clipped and unclipped functions, the resulting surrogate objective is a lower bound first-order approximation of the unclipped objective around $\mathbf{w}_{\text{old}}$.

Furthermore, the performance measure is augmented to include a value function loss term, corresponding to the critic output, given by

$$J^{\text{VF}}(\mathbf{w}) = \hat{E}_{\mathcal{E}_{\pi_\mathbf{w}}}\left[\left(V_{\pi_\mathbf{w}}(s) - \sum_{k=0}^{|\mathcal{E}|-1}\gamma^k r\right)^2\right]. \tag{5.23}$$

Finally, a final term of entropy bonus $H(\pi_\mathbf{w})$ is added to encourage exploration of the state space (Mnih *et al.*, 2016). The final surrogate objective function to be maximized is given by

$$J^{\text{surr}}(\mathbf{w}) = J^{\text{clip}}(\mathbf{w}) - k_1 J^{\text{VF}}(\mathbf{w}) + k_2 H(\pi_\mathbf{w}), \tag{5.24}$$

where k_1 and k_2 are system hyperparameters. The PPO algorithm is summarized in Algorithm 5.1. We use two DNN, one to approximate the policy $\pi(a|s)$, which takes the state as an input

Algorithm 5.1 PPO algorithm

Initialization :

1. Set learning rate $\alpha \in [0, 1)$
2. Set the update period T
3. Set ϵ, k_1, k_2
4. Initialize $\mathbf{w}_{\text{old}}$ randomly
5. Set $s = s_0 \in \mathcal{S}$
6. Set $t \leftarrow 0$

loop
  $\mathcal{E} \leftarrow$ Initialize with an empty array of size T;
  for $m = 1...T$ **do**
    $a' \sim \pi_{\mathbf{w}_{\text{old}}}(a|s)$;
    $s' \sim \mathbb{P}(s'|s, a)$;
    $c' = c(s, a)$;
    $\mathcal{E}_m \leftarrow (s, a', c', s')$;
  end for
  for $n = 1...N_{\text{epochs}}$ **do**
    Sample minibatch $\tilde{\mathcal{E}}$ from $\mathcal{E}$ such that $|\tilde{\mathcal{E}}| < T$;
    $\nabla_{\mathbf{w}} \tilde{J}(\mathbf{w}) \leftarrow \hat{E}_{\tilde{\mathcal{E}}} \left[\nabla_{\mathbf{w}} \ln \pi_{\mathbf{w}}(a|s) A(s_t, a_t)\right]$;
    $\mathbf{w} \leftarrow \mathbf{w}_{\text{old}} + \alpha \nabla_{\mathbf{w}} \tilde{J}^{\text{surr}}(\mathbf{w})$;
  end for
  $\mathbf{w}_{\text{old}} \leftarrow \mathbf{w}$
end ;

and outputs a probability distribution over $\mathcal{A}$ and the action a is sampled from this distribution. This network is trained to maximize the PPO surrogate performance measure in (5.24). The second DNN approximates $V_\pi(s)$, and is trained to minimize the mean squared error between the output of the network and the average value of the state observed so far. The DNN architecture used by all of the algorithms considered in this paper is described in detail on Appendix III, Section 2.

5.4.3 Independent Learners

In the IL architecture, each device has its own set of weights $\mathbf{w}_i$ and is running its own learning algorithm to update their weights without sharing information about their policies or current and

previous states. As each device has only a local view of the state of the environment, it cannot learn the optimal joint-policy in (5.11). Therefore, each MTD tries to find its local optimal policy as

$$\pi_i^* = \arg\min_{\pi_i \in \Pi_i^{IL}} E_{\mathbf{o}_i \sim \mathbb{P}(\mathbf{o}), \pi_i} \left[\sum_{t=0}^{\infty} \gamma^t c_i(\mathbf{o}_{i,t}, \mathbf{a}_{i,t}) \middle| \mathbf{o}_{i,0} = \mathbf{o}_i \right], \tag{5.25}$$

where $\Pi_i^{IL} = \{\pi | \pi : \mathcal{A}_i \times \mathcal{O}_i \rightarrow [0, 1]\}$ is the set of all possible policies mapping the action-observation space into a probability. Notice that the joint policy search space of the IL POSG is $\mathbf{\Pi}^{IL} = \Pi_1^{IL} \times \Pi_2^{IL} \times \cdots \times \Pi_{N_u}^{IL}$. Additionally, the local cost function is given by

$$c_i(\mathbf{o}_i, \mathbf{a}_i) = x_i(P_{ON} + p_i) + (1 - x_i)P_{OFF} + \omega_i \left(b_i + \mu_i \xi_i\right). \tag{5.26}$$

Consequently, the local cost functions leads to the definition of a local value function

$$V_{\pi_i}^{IL}(o_i) = E_{\pi_i} \left[\sum_{t=0}^{\infty} -\gamma^t c(o_{i,t}, a_{i,t}) \middle| o_{i,0} = o_i \right]. \tag{5.27}$$

Furthermore, the policy function is approximated by a DNN $\pi_{\mathbf{w}_i}$ that is trained on its previous experience using Algorithm 5.1. As both the policy and value DNN are trained on the same MTD, both the actor and the critic networks share the same weights to reduce the memory footprint, but have different output heads, the actor head outputs the probabilities of selecting each action, while the critic head outputs critic values. The diagram in Fig. 5.3 illustrates this architecture.

Effectively, each agent tries to solve the problem defined in (5.25) while ignoring the effects of other agents, treating it as part of the environment. So, the problem reduces to a MDP (Puterman, 2014). The agents change their policies independently of one another, but their actions affect the costs experienced by other agents. Therefore, the agents perceive the environment as non-stationary (Omidshafiei *et al.*, 2017). To the best of our knowledge, there are no known algorithms that give theoretical guarantees of convergence and optimality in the non-stationary MDP setting nor on the solution of the general POSG problem posed in (5.11). However, the IL

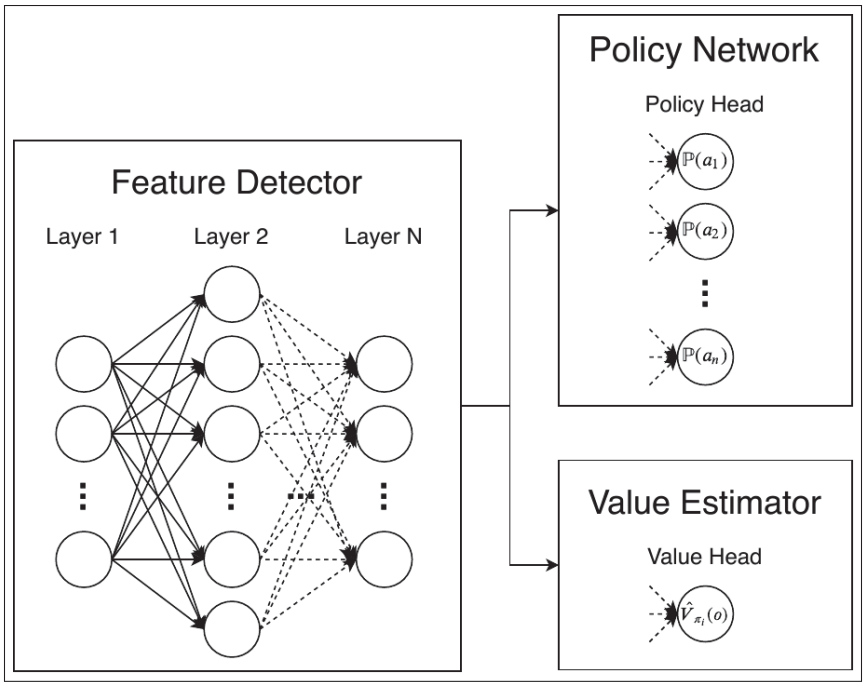

Figure 5.3 Diagram of DNN architecture with shared weights and split actor and critic heads

is considered to be a reasonable heuristic to find sub-optimal solutions to a POSG (Matignon *et al.*, 2012). As shown in Fig 5.2, the main advantage of this approach is that it does not require any form of communications between devices nor between a device and the BS. On the other hand, it requires every device to have its own set of weights and to run its own learning algorithm, which can result in a high power consumption. Also, as each agent faces a non-stationary environment, there are no guarantees of convergence to an optimal solution.

5.4.4 Distributed Actor with Central Critic

The PPO algorithm makes use of two networks: the actor, which models the agent's policy, and the critic, which estimates the value of a state. Originally, the algorithm proposes that both networks can share weights to accelerate convergence and reduce memory costs (Schulman *et al.*, 2005); In the DACC architecture, each agent learns its own policy based on its local cost, similar to the IL architecture, while a single critic is stored and trained on an edge computing

node. The goal of this architecture is to mitigate the effects of the partial observation by having a critic that has access to the data of all the agents (the whole state) to estimate the value of the whole state $\mathbf{s}$, defined in (5.19), and not only the local value based on the local observations as done by the IL architecture. Thus, the DACC POSG problem is given by

$$\pi_i^* = \arg \min_{\pi_i \in \Pi_i^{DACC}} E_{\mathbf{o}_i \sim \mathbb{P}(\mathbf{o}), \pi_i} \left[\sum_{t=0}^{\infty} \gamma^t c_i(\mathbf{o}_{i,t}, \mathbf{a}_{i,t}) \middle| \mathbf{o}_{i,0} = \mathbf{o}_i \right], \tag{5.28}$$

where $\Pi_i^{DACC} = \{\pi | \pi : \mathcal{A}_i \times \mathcal{O}_i \rightarrow [0, 1]\}$ is the set of all possible probability distributions over the action-ovservation space, and the joint policy search space of the DACC POSG is $\mathbf{\Pi}^{DACC} = \Pi_1^{DACC} \times \Pi_2^{DACC} \times \cdots \times \Pi_{N_u}^{DACC}$. While the critic value is computed on local observation data in the IL architecture, as shown in (5.27), the critic value in the DACC architecture is computed over global state information, i.e. $V_{\boldsymbol{\pi}}^{DACC}(\mathbf{s}) = V_{\boldsymbol{\pi}}(\mathbf{s})$.

Both the policy function π_i and the value function estimator $V_{\boldsymbol{\pi}}^{DACC}(\mathbf{s})$ are approximated by DNN. The policy DNN $\pi_{\mathbf{w}_i}$ is trained and stored on each device, while the value function estimator is stored and computed on an edge computing node. Hence, in this architecture, the surrogate objective function in (5.24) is split into two, with one to be minimized by the devices to train the policy network, given by

$$J_a^{\text{surr}}(\mathbf{w}_i) = J^{\text{clip}}(\mathbf{w}_i) + k_2 H(\pi_{\mathbf{w}_i}), \tag{5.29}$$

and the other to be minimized on the edge to train the value function network, given by

$$J_c^{\text{surr}}(\mathbf{w_c}) = J^{\text{VF}}(\mathbf{w_c}). \tag{5.30}$$

Furthermore, as illustrated in Fig. 5.2, each agent keeps its own set of weights $\mathbf{w}_i$ for the actor network, while the weights of the value function estimator $\mathbf{w}_c$ are stored and updated on the edge computing node. Additionally, both the MTD and the edge node must perform backpropagation to update their weights. While each MTD has access to its own local information, the value

estimator trained on the edge can leverage the data collected by all agents, and thus, the edge agent is able to backpropagate on the global state information.

Moreover, as shown in (5.21), the critic value is necessary to compute the PPO gradient. Therefore, this architecture requires the BS to feedback the value of each state, $V_{\boldsymbol{\pi}}(\mathbf{s})$ given in (5.19), after every TTI, such that the agents are able to perform backpropagation and train their policy networks. Moreover, while the channel response can be estimated by the network from the preambles, the buffer occupancy information b_i needs to be sent by the MTD to the edge in every TTI, thus, the edge node is able to compute the value functions and its weight's update.

5.4.5 Centralized Learning with Distributed Inference

As the number of MTD in the network increases, the size of the policy search space for the IL and DACC architectures increase exponentially, consequently increasing the solution space. To address this issue, in the CLDI architecture, there is a single set of weights, and therefore a single policy π and a search space $\Pi^{CLDI} = \{\pi | \pi : \mathcal{A}_i \times \mathcal{O}_i \rightarrow [0, 1],\ i = 1, \dots N_U\}$ that does not increase in size with the number of MTD. Both the policy and the critic are trained on the edge and an updated set of weights is periodically broadcast to the MTD, thus reducing the computational burden required to train a neural network on the devices. Moreover, the policy on the edge is trained on data from all MTD leading to improved sample efficiency. Hence, instead of solving (5.11), the CLDI architecture looks for solutions to

$$\pi^* = \arg \min_{\pi \in \Pi^{CLDI}} E_{\mathbf{s} \sim \mathbb{P}(\mathbf{s}), \pi} \left[\sum_{t=0}^{\infty} \gamma^t c_{CLDI}(\mathbf{s}_t, \mathbf{a}_t) \middle| \mathbf{s}_0 = \mathbf{s} \right], \tag{5.31}$$

where the CLDI cost function is given by

$$c_{CLDI}(\mathbf{s}, \mathbf{a}) = \frac{1}{N_U} \sum_{i=1}^{N_U} x_i (P_{ON} + p_i) + (1 - x_i) P_{OFF} + \omega_i \left(b_i + \mu_i \xi_i \right), \tag{5.32}$$

which is the average cost function of the MTD. It is worth highlighting that the CLDI cost is an average of the costs of all MTD, thus, the shared policy is updated to increase the average

performance of all MTD, as opposed to the IL and the DACC architecture where the policy of each MTD is updated to optimize its local performance. Both the policy and value function networks are stored and trained on the edge following Algorithm 5.1 using the cost function defined in (5.32). The devices have a copy of the policy network, but they do not train it, they just use it for decision-making. In this architecture, the devices must append the buffer state information to every transmitted packet, and thus, the networks can be trained on the edge node, where the network must send the updated weights back to the MTD periodically.

5.5 Numerical Experiments

In this section, the performance of the proposed architectures is evaluated through computer simulations. In order to provide a frame of reference, we also simulate the performance of a baseline employing a reactive HARQ protocol with power boosting. The details of the baseline are described in Appendix III, Section 1. We consider that there are two BS and eight subcarriers serving a circular area with a 300 m radius. We generate 1000 realizations of this scenario, where at each realization we place both the BS and the MTD in a random location within the circular area. At each realization the learning algorithms start from scratch (e.g. the weights of the agents are randomly initialized at the beginning of each realization) and runs for 15000 TTI. Then, we compare the average performances, along with their variances, with respect to the average delay experienced by the network, the number of dropped packets, the average power spent, and the number of collisions.

5.5.1 Results

We compare the baseline and the architectures proposed in Section 5.4 in terms of the average network delay, power, dropped packets, and collisions during 15000 TTI. We evaluate the network delay through the holding cost, as the average network delay is proportional to the number of packets held in the devices' buffer. We consider that devices with different mean packet arrival rates and latency constraints are being serviced by the same cellular network. For each realization, the packet arrival rate of each MTD is uniformly sampled from $\{40, 60, 80\}$

Table 5.1 Parameters used in the simulations

Parameter	Value	Parameter	Value
f_S	10^5 symbols/s	L	100 bytes
R	300 m	Δ_t	10 ms
N_U	{2560, 7680} users	δ_i	U ({4, 8, 12}) packets
N_B	2 BS	λ_i	U ({40, 60, 80}) packets/s
N_S	8 subcarriers	γ	0.99
N_P	64 preambles	P_{ON}	320 milliwatts
α	3.5	P_{OFF}	0 milliwatts
B	25 packets	$f_{\max}$	10 Hz
T	200 TTI		

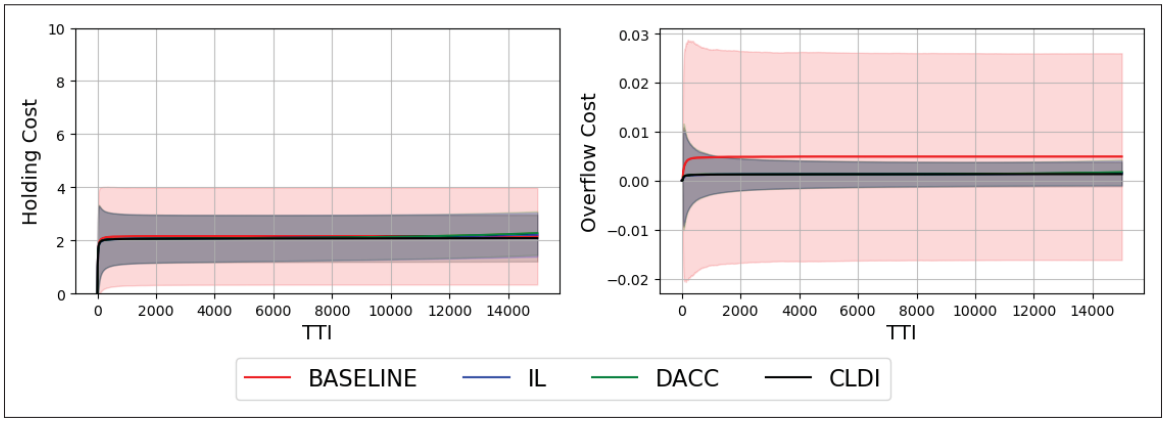

Figure 5.4 Simulation results showing the holding costs and overflow costs with 2560 MTD in the simulated area for the three proposed architectures and the baseline, where IL stands for the independent learners, DACC for distributed actor with central critic and CLDI for central learning with decentralized inference

packets per second and the latency constraint is uniformly sampled from $\{4, 8, 12\}$ queued packets. Notice that in all the plots the x-axis shows the TTI. In the holding cost plot, the y-axis shows the cumulative average of the number of packets in the buffer at a given TTI. The y-axis in the overflow cost plots show the cumulative average value of ζ_i. Furthermore, the y-axis in the power cost plots shows the cumulative average of the power spent by MTD in milliwatts. Finally, the y-axis in the collisions' plot shows the cumulative sum of collisions up to the given TTI. As shown in Fig. 5.4, with 2560 users, the average holding cost between all four approaches is

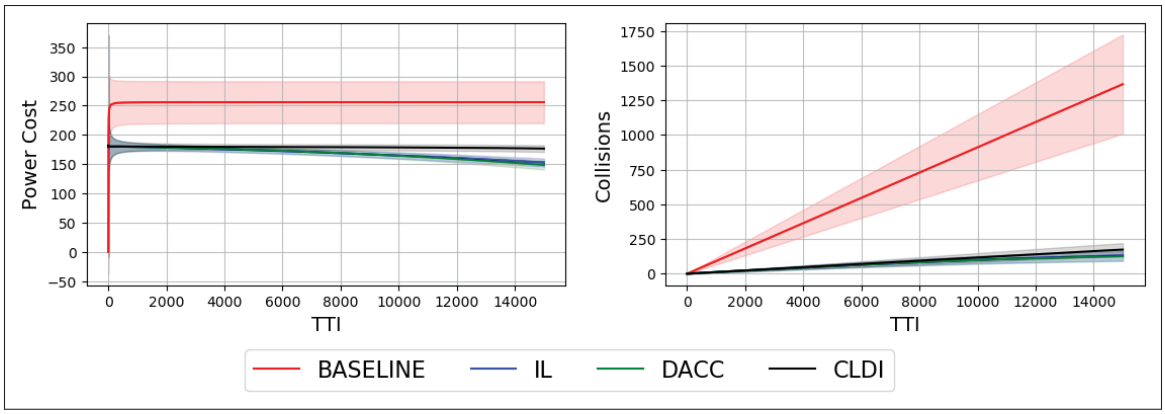

Figure 5.5 Simulation results showing the power costs and the number of collisions with 2560 MTD in the simulated area for the three proposed architectures and the baseline, where IL stands for the independent learners, DACC for distributed actor with central critic and CLDI for central learning with decentralized inference

roughly the same. However, we notice that the baseline presents a significantly higher variance than the proposed architectures. Furthermore, the average network delay is below four, which is the smallest latency constraint in the network, within at least one standard deviation. With respect to overflown packets, also in Fig. 5.4, on average the baseline approach drops slightly more packets than the proposed architectures, but again with significantly more variance. With respect to the power consumption, as shown in Fig. 5.5, the three proposed architectures spend on average roughly 70% of the power spent by the baseline. Moreover, as mentioned in Section 5.4, the CLDI algorithm tends to converge faster as it is trained on observations from every device in the network and has to search for a policy in a notably small policy search space. This is confirmed by the fact that, as the simulation advances in time and the IL and DACC algorithms train on more data, they achieve similar performance levels as CLDI, while using less power. The performance improvement of the proposed architectures compared to the baseline is even more significant when it comes to the number of collisions, as shown in Fig. 5.5. On average, the reinforcement learning based solutions experience 15% of the baseline's collisions during the same period of time.

Moreover, in all investigated architectures, the holding cost performance, when averaged over users with the same delay constraint, follows the same trend as when averaged over all users

(shown in Fig. 5.4). Therefore, we can conclude that in a scenario with 2560 MTD, in average, all the architectures satisfy the delay constraints. However, the baseline approach presents larger performance fluctuations, as shown by the larger standard deviation in Fig. 5.4.

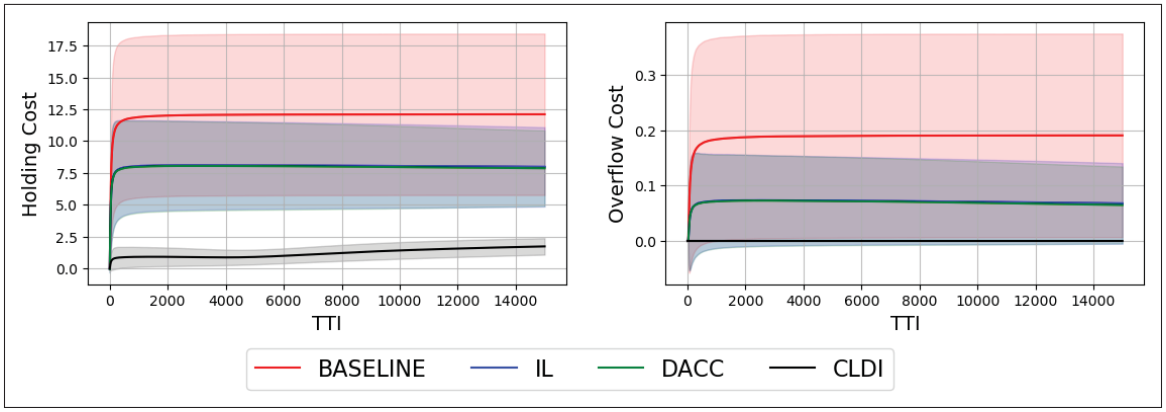

Figure 5.6 Simulation results showing the holding costs and overflow costs with 7680 MTD in the simulated area for the three proposed architectures and the baseline, where IL stands for the independent learners, DACC for distributed actor with central critic and CLDI for central learning with decentralized inference

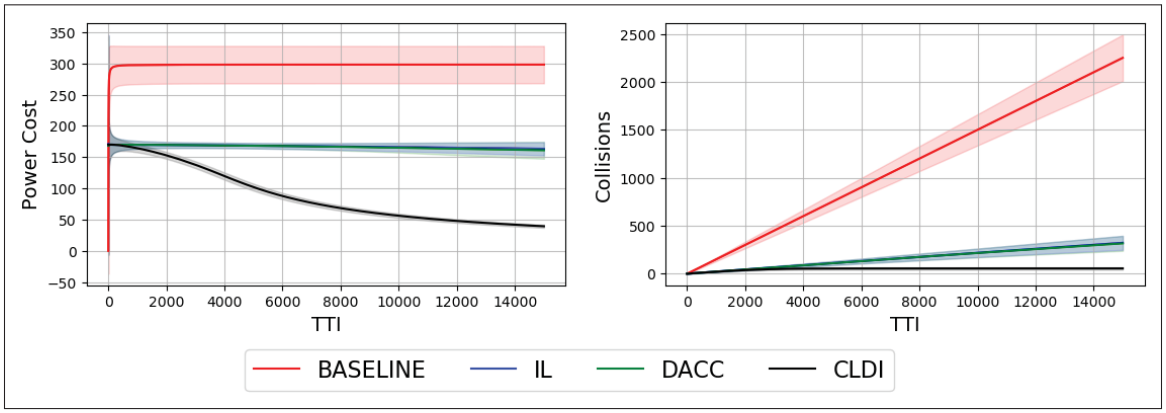

Figure 5.7 Simulation results showing the power costs and the number of collisions with 7680 MTD in the simulated area for the three proposed architectures and the baseline, where IL stands for the independent learners, DACC for distributed actor with central critic and CLDI for central learning with decentralized inference

As illustrated in Fig. 5.6, when the number of users is increased to 7680, the average holding cost of the CLDI architecture converges to 2 packets, while the IL and DACC converge to 8

Table 5.2 Overhead and Performance Tradeoffs for $N_U = 2560$

Algorithm	DL Overhead	UL Overhead	Collisions	Power Cost	Holding Cost
Baseline	-	-	1364 col.	255.54 mW	2.15 packets
IL	-	-	131 col.	168.68 mW	2.11 packets
DACC	1.6 kbits/s	1.6 kbits/s	122 col.	168.06 mW	2.12 packets
CLDI	20.496 kbits/s	1.6 kbits/s	174 col.	178.81 mW	2.07 packets

packets and the baseline to 12 packets. From this result, we conclude that as the number of users increases the lack of collaboration between the MTD in the IL and DACC architectures starts to impact the average network delay, while CLDI performance stays around the same as for 2560 users. Also in Fig. 5.6, the average overflow cost of CLDI still remains around 0, while the IL and DACC estabilize around 0.7 and the baseline at 0.19. With regards to the average power costs at convergence, the CLDI architecture spends 16.66% of the power spent by the baseline, while the IL and DACC spend 52%, as seen in Fig. 5.7. The significant decrease in the power spent by CLDI is explained by the centralized training, which makes more training data available, since CLDI has 7680 new data points for each TTI while the other architectures have only 1, which points to a cooperative behavior arising among the MTD. This is also reflected in the collisions performance, where CLDI experiences around 2.25% of the baseline's collisions and IL and DACC experience around 14%.

Furthermore, similar to the 2560 MTD case, in all architectures investigated, all devices converge to roughly the same average holding cost, regardless of the delay constraint. Thus, in the 7680 MTD scenario, only the CLDI architecture maintains an average holding cost below the delay constraints for devices with $\delta_i = 4$, $\delta_i = 8$ and $\delta_i = 12$. In the IL and DACC architectures, in average, only devices with $\delta_i = 8$ and $\delta_i = 12$ satisfy their constraints. Finally, when the baseline architecture is employed, on average, none of the MTD is able to satisfy its constraint. This confirms that the CLDI architecture scales better than the others in densely deployed scenarios.

Table 5.3 Overhead and Performance Tradeoffs for $N_U = 7680$

Algorithm	DL Overhead	UL Overhead	Collisions	Power Cost	Holding Cost
Baseline	-	-	2253 col.	297.6154 mW	12.01 packets
IL	-	-	322 col.	166.98 mW	8.025 packets
DACC	1.6 kbits/s	1.6 kbits/s	317 col.	166.25 mW	7.95 packets
CLDI	20.496 kbits/s	1.6 kbits/s	55 col.	87.81 mW	1.21 packets

5.5.2 Tradeoffs

In this subsection, we analyze the advantages and disadvantages of each of the proposed architectures, and discuss possible application scenarios.

The IL architecture does not require a central edge entity to work, and therefore it cuts all the necessary overhead associated to data transmission between MTD and BS. However, each MTD has to perform training and inference of its DNN, which can be computationally expensive. Moreover, as each MTD is trained in a fully distributed manner, without sharing any information, there is no chance of cooperation arising. Both DACC and CLDI architectures require MTD to transmit information about their number of packets currently in the buffers. On the other hand, since part of the training for DACC, and all the training for CLDI is performed in the edge, some of the computational burden is offloaded, thus saving power and easing the computation requirements of MTD. In this work, we use 16 bit floating point numbers to encode the state information, action, and network weights. Furthermore, we consider any extra data exchange that is not the payload to be overhead. Thus, in the uplink direction, the overhead of the DACC and CLDI architectures is given by $\frac{16}{\Delta_t}$. Regarding the downlink overhead, in the DACC architecture the network must send the critic value in every TTI, and therefore, the overhead is also $\frac{16}{\Delta_t}$. Meanwhile, in the CLDI architecture, the network must send all the weights of the DNN to the MTD every 200 TTI. Tables 5.2 and 5.3 show the average performance of each architecture and its respective overhead. As shown in Section 5.5.1, for a smaller user density, the IL and DACC architectures slightly outperform CLDI. However, for a higher density of MTD, the CLDI architecture is able to leverage data from observations collected from all MTD, and thanks to

the centralized training, the MTD work together to use the network resources more equitably, resulting in tremendous power savings, small average delays, and a minimal number of dropped packets and collisions. Therefore, we conclude that for cellular networks designed to serve a smaller number of MTD, the IL and DACC architectures, depending on whether the the devices have enough computational power to train their DNN and how much overhead is tolerated, are recommended. However, for cellular networks designed to support a massive number of low-cost devices, the CLDI architecture is deemed more suitable.

5.6 Conclusions

In this paper, we proposed a system model for mMTC networks using grant-free transmission and formulated it as an average power minimization problem subject to delay constraints. Based on the related literature, we conclude that static access protocols are inefficient to handle the optimization problem and proposed three reinforcement learning based architectures to solve the optimization problem in a distributed fashion. The architectures have different degrees of centralization and overhead . Furthermore, we simulated the three architectures and compared their performance among against a static access policy baseline based on the reactive HARQ protocol with power boosting. Finally, we showed that all three learnable architectures outperform the static baseline and we proceeded to analyze the tradeoffs between the architectures.

CONCLUSION AND RECOMMENDATIONS

6.1 Conclusions

This thesis studies the modelling and optimization of multiple access technology for 5G NR and next-generation cellular networks. We focus mainly on mMTC and URLLC applications since they have the most distinct QoS requirements and operating characteristics compared to previous cellular standards. Furthermore, we identify NOMA and grant-free access as the most promising technologies to satisfy the requirements of the new services.

Chapter two formulated the joint power and subcarrier allocation optimization problems of the sum rate and the fairness for a system utilizing SCMA. We proved that both problems are NP-Hard, meaning that there is no polynomial-time algorithm capable of solving the problem optimally. We propose two novel algorithms, based on successive convex approximations and the relaxation of integer constraints, that consists of optimally solving a sequence of subproblems. We used numerical simulations to show that this approach reaches better performance than heuristic-based algorithms proposed in the literature. Also, as the algorithm depends on the CSI, we analyzed the performance deterioration of both algorithms when only outdated CSI is available. An exciting development since the publication of this paper was made in (Cheraghy, Chen, Tang, Wu & Li, 2021), where the authors formulate a multi-objective optimization problem aiming to optimize both the sum rate and the fairness.

Chapter three analyzed the problem of grant-free access SCMA networks dedicated to mMTC services. We proposed an analytical model to derive closed-form expressions for the probability of success of a transmission attempt, and the area spectral efficiency using results from the theory of interference functionals on Poisson networks (Schilcher *et al.*, 2016). Moreover, we compared the performance of the aforementioned system with one using OMA for an increased density between users and BSs. We show that in the OMA scenario, the area spectral efficiency

saturates after a specific value of the relative density between users and BSs. On the other hand, the area spectral efficiency increases with an increase in the relative density in the SCMA system, thus, showing that SCMA based systems can better support mMTC services than OMA. The work in (Lai *et al.*, 2021) builds upon the model developed in chapter three by including the impact of transmit power control and the limitations of the MPA receiver.

Chapter four considered the modelling of massive MIMO systems serving URLLC applications on the mmWave bands. We formulated a model based on stochastic geometry and derived approximate closed-form expressions for the latent access failure probability for systems utilizing a reactive and K-repetition HARQ protocol. We validated the analytical results using numerical simulations, and we identified the limitations of the proposed model. Additionally, we investigated the impact of the number of BS antennas on the system's reliability. We noticed that all other parameters being the same, increasing the number of BS antennas above a certain point has minimal impact on the reliability performance. We concluded that this saturation of the performance gain is because, after a certain number of BS antennas, the probability of having a LOS link becomes the main performance bottleneck. We also studied the maximum density of users that could be supported for a given number of BS antennas and QoS requirements, thus quantifying the gain obtained using massive antenna arrays. Finally, we concluded that mmWave massive MIMO alone is not enough to satisfy the QoS requirements of the most strict URLLC applications (user-plane latency under 1 ms and reliability greater than $1 - 10^{-6}$).

Chapter five is concerned with the distributed link adaptation problem in grant-free mMTC applications. We proposed a model for the link adaptation problem as the average power minimization under user-specific transmission delay constraints. We formulated the problem as a POSG that must be solved in a distributed fashion. We proposed three algorithms based on MARL with different degrees of centralization and compared their performance to a reactive HARQ protocol with power-boosting. We showed that our MARL solutions could significantly

lower power consumption and average network delay compared to the reactive HARQ baseline in a more robust manner. Specifically, the CLDI architecture can satisfy the QoS requirements even under high user density scenarios. Finally, we analyzed the tradeoffs between the three proposed architectures concerning the amount of overhead required by each of them, thus concluding that to obtain the higher performance of the CLDI architecture, one must pay the price by increasing the system's overhead.

6.2 Future Work

This section presents future research paths worth pursuing, drawing from the results obtained in this thesis and the literature review presented in chapter one.

6.2.1 The Multi-Antenna NOMA Controversy

During the last decade, NOMA became one of the most active research fields within the wireless research community, and many researchers believe it will play a vital role in 5G NR standards. As of today, NOMA technologies have played a minor role in the standardized cellular systems, as an optional feature of LTE Advanced (LTE-A) named multiuser superposition transmission (MUST). The main reason for this is that NOMA requires each user to fully decode the messages of other users (typically through SIC or other MUD techniques), which results in a multiplexing gain erosion, and rate and spectral efficiency loss, rendering it inefficient for large numbers of users in multi-antenna settings, as shown in (Clerckx *et al.*, 2021). This resulted in a shift of attention to rate splitting multiple access (RSMA). RSMA is also a NOMA technique, albeit it has a much smaller body of literature than PD-NOMA and SCMA and seeks to bridge the gap between space-division multiple access (SDMA) and NOMA. While in NOMA, the receiver must fully decode the interference, the receiver treats multiple access interference as noise in SDMA (Mao, Clerckx & Li, 2018). In RSMA, the receiver decodes part of the multiuser

interference and treats the rest as noise. Thus it is a generalization of the NOMA and SDMA competing paradigms.

The uplink and downlink RSMA systems' optimization is investigated in (Yang, Chen, Saad, Xu & Shikh-Bahaei, 2020) and (Yang, Chen, Saad & Shikh-Bahaei, 2021), respectively. The authors in (Mao, Clerckx & Li, 2019) study the RSMA coordinated multi-point problem, while the authors in Yu, Kim & Park (2019) evaluate RSMA's performance for the downlink of cloud radio access networks. Despite this growing body of literature, not much attention was given to designing RSMA systems for the uplink in mMTC and URLLC networks and obtaining good stochastic geometry models for these systems. Therefore, we envision the following possible topics for future works:

- Propose stochastic geometry models of RSMA networks to enable the mathematical characterization of the performance of large networks.
- Extending the work done in the third chapter of this thesis by evaluating the scalability and area spectral efficiency gains of RSMA compared to SCMA, NOMA, and MU-MIMO in mMTC applications.
- Formulating spatiotemporal models for RSMA systems for URLLC applications, similar to the work developed in the fourth chapter of this thesis.

6.2.2 Grant-Free 5G NR Uplink on the Unlicensed Spectrum

The operation on the unlicensed spectrum bands is considered a key enabler of several 5G NR applications, such as industrial internet of things, airborne communications, augmented and virtual reality, and urban V2X communications (Lu *et al.*, 2019). The main challenge existing in transmitting on the unlicensed bands is the coexistence with other wireless standards. For instance, in the 5.925 to 7.125 GHz bands, the 5G NR users must perform dynamic frequency selection (DFS) to avoid interfering with radar signals that operate in this band. Moreover, the 5G NR unlicensed users must also employ power control to minimize the interference caused to

other services operating on the same spectrum (Hirzallah, Krunz, Kecicioglu & Hamzeh, 2020). In this vein, the system proposed in Chapter five can be easily extended to incorporate such interference constraints in the distributed link adaptation problem.

6.2.3 Queueing Dynamics and HARQ Integration into Spatiotemporal Models of Grant-Free Networks

The work developed in Chapter four and (Liu *et al.*, 2020) consider the impact of different HARQ protocols on the reliability and the user-plane latency of grant-free URLLC service. Both cases consider the single-packet arrival model, where a single packet arrives at the transmitting queues of the UEs at $t = 0$. This setting is helpful to compare distinct HARQ protocols. However, it provides limited insight into the performance of real systems due to the limited packet arrival model considered in these works. On the other hand, the authors in (Gharbieh *et al.*, 2018; Gharbieh, ElSawy, Bader & Alouini, 2017; Gharbieh, ElSawy, Emara, Yang & Alouini, 2020) consider a sophisticated discrete-time Markov chain to model a general packet arrival process and an iterative algorithm to obtain the average buffer size, average waiting time in the queue, and the stability regions of uplink grant-free access systems. However, they do not consider the impact of HARQ on the performance. Therefore, there is a clear gap in the literature regarding the performance evaluation of grant-free access systems. Integrating the complex queueing dynamics by modelling the packet arrival dynamics and the performance metrics from (Gharbieh *et al.*, 2018, 2017, 2020) with the HARQ protocol's impact on the performance would be an interesting future work to pursue.

APPENDIX I

APPENDIX OF CHAPTER 2

1. Proof of Theorem 1

To prove that both problems are NP-hard, we show that the subcarrier assignment subproblem can be reduced in polynomial time to the hypergraph assignment problem (HAP) which is shown to be NP-hard in (Borndörfer & Heismann, 2015).

We start by briefly introducing the HAP. The HAP takes as input a bipartite graph $\mathcal{G} = \mathcal{V} \cup \mathcal{U}$ such that $\mathcal{V} \cap \mathcal{U} = \emptyset$, a set of hyperedges $\mathcal{E}$, and a cost function $c : \mathcal{E} \rightarrow \mathbb{R}$. In addition to that, we have that $|e \cap \mathcal{V}| \geq 1$ and $|e \cap \mathcal{U}| \geq 1 \; \forall \; e \in \mathcal{E}$.

A hyperassignment is a set $\mathcal{H} \subseteq \mathcal{E}$ such that every element $v \in \mathcal{V} \cup \mathcal{U}$ appears exactly once in $\mathcal{H}$. The output of the HAP is an optimal hyperassignment $\mathcal{H}^* = \min\{c(\mathcal{H}) | \mathcal{H}$ is an hyperassignment of $\mathcal{G}\}$.

Now consider the problem $\mathbf{P}_{\textbf{Max-SR}}$ in the HAP context, with a fixed power allocation matrix $\mathbf{P}$. Let $\mathcal{U} = \{SC_1, \cdots, SC_K\}$ and $\mathcal{V} = \{U_{1,1} \cdots U_{1,N}, U_{2,1}, \cdots U_{2,N}, \cdots U_{J,N}\}$ be the vertex set of available subcarriers and allocated subcarriers, respectively. Notice that SC_k denotes the k-th available subcarrier, while $U_{j,i}$ denotes the i-th subcarrier allocated to user j, with $1 \leq i \leq N$. In this context, a hyperassignment determines which subcarriers are allocated to each user. For instance, a hyperedge $e = \{SC_1, U_{1,1}, U_{2,2}\}$ indicates that users 1 and 2 are allocated to the first subcarrier. As at most N subcarriers can be allocated to each user, every hyperassignment satisfies (2.11). Notice that the subcarrier allocation matrix $\mathbf{F}$ corresponds to the hyperedge incidence matrix of the hypergraph, for instance, the hyperedge $e = \{SC_1, U_{1,1}, U_{2,2}\}$ would result in $\mathbf{f}_1 = \begin{bmatrix} 1 & 1 & 0 & \cdots & 0 \end{bmatrix}$, where $\mathbf{f}_1$ is the first row of $\mathbf{F}$. Furthermore, consider the hyperedge set $\mathcal{E} = \{e \in 2^{\mathcal{U} \cup \mathcal{V}} | \quad 1 < |e| \leq d_f + 1\}$ and let $F_{\mathcal{H}} \in \mathbb{B}^{K \times J}$ be the incidence matrix of a hypermatch $\mathcal{H} \subseteq \mathcal{E}$. As $|e| \leq d_f + 1 \; \forall \; e \in \mathcal{E}$ constraint (2.12) is always satisfied.

Furthermore, the cost function is given as

$$c(\mathcal{H}) = \sum_{k\in\mathcal{K}} \ln\left(1 + \frac{\sum\limits_{j\in\mathcal{J}} |h_{k,j}|^2 f_{k,j} p_{k,j}}{\sigma_n^2}\right).$$

So, solving $\mathbf{P}_{\textbf{Max-SR}}$ with $\mathbf{P}$ fixed, is equivalent to solving an HAP, therefore, $\mathbf{P}_{\textbf{Max-SR}}$ is NP-hard.

Finally, we also conclude $\mathbf{P}_{\textbf{Max-Min}}$ is NP-hard using the same HAP formulation, but using the cost function

$$c(\mathcal{H}) = \min_{j\in\mathcal{J}} \sum_{k\in\mathcal{K}} \ln\left(1 + \frac{|h_{k,j}|^2 f_{k,j} p_{k,j}}{\sigma_n^2 + \sum\limits_{i=1}^{j-1} |h_{k,i}|^2 f_{k,i} p_{k,i}}\right).$$

APPENDIX II

APPENDIX OF CHAPTER 4

1. Proof of Lemma 5

The probability of success in (4.21) can be expanded to

$$\begin{aligned} & \mathbb{P}\left(\mathrm{SINR}_m \geq \gamma \left| \bar{C}, x_0 \in LOS_m, N_m = n \right.\right) \\ = \; & \mathbb{P}\left\{ |g_0|^2 \geq \frac{\gamma}{\rho K}\left[\sigma^2 + I\right] \middle| \bar{C}, x_0 \in LOS_m, N_m = n \right\} \\ = \; & \exp\left(-\frac{\gamma\sigma^2}{\rho K}\right) \mathcal{L}_I\left(s|\bar{C}, x_0 \in LOS_m, N_m = n\right), \end{aligned} \tag{A II-1}$$

where $s = \frac{\gamma}{\rho K}$, $I = \sum\limits_{x_i \in \Phi_I} \rho \left|g_i\right|^2 F_K\left(\frac{\pi}{2}\left(\theta_0 - \theta_i\right)\right)$ is the interference on the typical user's transmission and $\mathcal{L}_I\left(s|\bar{C}, x_0 \in LOS_m, N_m = n\right)$ is the Laplace transform of the interference conditioned on the user not experiencing preamble collision, them having a LOS path, and there being n interferers in the cell.

The Laplace transform of the interference can be derived as

$$\begin{aligned} & \mathcal{L}_I\left(s|\bar{C}, x_0 \in LOS_m, N_m = n\right) \\ = \; & E_{g_i,\theta_i}\left\{\exp\left[-s\sum_{x_i \in \Phi_I} \rho\left|g_i\right|^2 F_K\left(\frac{\pi}{2}\left(\theta_0 - \theta_i\right)\right)\right]\right\} \\ = \; & \prod_{x_i \in \Phi_I} E_{g_i,\theta_i}\left\{\exp\left[-s\rho\left|g_i\right|^2 F_K\left(\frac{\pi}{2}\left(\theta_0 - \theta_i\right)\right)\right]\right\} \\ = \; & \prod_{x_i \in \Phi_I} E_{\theta_i}\left[\frac{1}{1 + s\rho F_K\left(\frac{\pi}{2}\left(\theta_0 - \theta_i\right)\right)}\right]. \end{aligned} \tag{A II-2}$$

Unfortunately, obtaining a closed-form expression for the expectation in (A II-2) is not mathematically tractable. Therefore, we first obtain a suitable approximation to the Fejer kernel. Due to the Fejer kernel property in (4.10), as the number of antennas increases most of the energy is

concentrated on the main lobe as shown in Fig. 4.2. Hence, we choose to approximate it as

$$F_K(x) \approx f_K(x) = \begin{cases} -\frac{K^3 x^2}{4} + K & \text{, if } x \in \left\{-\frac{2}{K}, \frac{2}{K}\right\} \\ 0 & \text{, otherwise.} \end{cases} \tag{A II-3}$$

The quadratic approximation in (A II-3) renders the derivation of the expectation in (A II-2) tractable. Furthermore, it ensures that $f_K(x) = 0$ whenever $x \notin \left(-\frac{2}{K}, \frac{2}{K}\right)$, i.e., the contributions of the signals arriving from directions outside of the main lobe to the interference is zero, and that $F_K(0) = f_K(0) = K$. Hence,

$$\begin{aligned} & \prod_{x_i \in \Phi_I \cap \theta_i \in \left(-\frac{2}{K}, \frac{2}{K}\right)} E_{\theta_i}\left[\frac{1}{1 + s\rho F_K\left(\frac{\pi}{2}(\theta_0 - \theta_i)\right)}\right] \\ \overset{(a)}{=} & \prod_{x_i \in \Phi_I \cap \theta_i \in \left(-\frac{2}{K}, \frac{2}{K}\right)} \frac{\tanh^{-1}\left(\sqrt{\frac{\gamma}{1+\gamma}}\right)}{\sqrt{\gamma(1+\gamma)}} \\ \overset{(b)}{=} & \sum_{n'=0}^{n} \binom{n}{n'} \left(\frac{2}{K}\right)^{n'} \left(1 - \frac{2}{K}\right)^{n-n'} \left[\frac{\tanh^{-1}\left(\sqrt{\frac{\gamma}{1+\gamma}}\right)}{\sqrt{\gamma(1+\gamma)}}\right]^{n'}, \end{aligned} \tag{A II-4}$$

where (a) is obtained from $\int \frac{1}{1-x^2} dx = \tanh^{-1}(x)$. While step (b) comes from the fact that the interferers' angles are uniformly distributed, given that there are n interferers in the cell, the number of interferers within the typical user's main lobe direction follows a binomial distribution with $n' \sim Binomial\left(\frac{2}{K}\right)$. Thus, the conditional success probability can be obtained by summing the marginal distribution weighted by n''s probability mass function (PMF) This completes the proof.

2. Proof of Lemma 6

In order for a K-repetition HARQ transmission attempt to be successful at least one of the repetitions must be successfully decoded. Therefore, the probability that the m-th retransmission attempt is successful, conditioned on no preamble collisions, a LOS path and n interferers, can

be obtained as the complement probability that all repetitions fail

$$\begin{aligned}
& \mathbb{P}\left(\bigcup_{l=1}^{K_{rep}} \mathrm{SINR}_{m,l} \geq \gamma \,\middle|\, \bar{C}, x_0 \in LOS_m, N_m = n\right) \\
= \;& 1 - \mathbb{P}\left(\bigcap_{l=1}^{K_{rep}} \mathrm{SINR}_{m,l} < \gamma \,\middle|\, \bar{C}, x_0 \in LOS_m, N_m = n\right) \\
\overset{(a)}{=} \;& 1 - \prod_{l=1}^{K_{rep}} \left[1 - \mathbb{P}\left(\mathrm{SINR}_{m,l} \geq \gamma \,\middle|\, \bar{C}, x_0 \in LOS_m, N_m = n\right)\right] \\
\overset{(b)}{=} \;& 1 - \left[1 - \mathbb{P}\left(\mathrm{SINR}_{m} \geq \gamma \,\middle|\, \bar{C}, x_0 \in LOS_m, N_m = n\right)\right]^{K_{rep}} \\
\overset{(c)}{=} \;& \sum_{l=1}^{K_{rep}} \binom{K_{rep}}{l} (-1)^{l+1} \mathbb{P}\left(\mathrm{SINR}_{m} \geq \gamma \,\middle|\, \bar{C}, x_0 \in LOS_m, N_m = n\right)^{l}, \qquad \text{(A II-5)}
\end{aligned}$$

where step (a) follows from the fact that the set of interferers is different from one repetition to the next, as a new subcarrier is randomly selected for every repetition by each UE, making the SINRs on distinct repetitions mutually independent. Also, as the SINR of every repetition is affected by an interferer process having the same intensity, the probability of success of each repetition is equal, which justifies step (b). Finally, step (c) is obtained from the binomial expansion of the power term. If we work from (A II-5) and follow the same steps derived in Appendix 1, we obtain (4.27), which completes the proof.

APPENDIX III

APPENDIX OF CHAPTER 5

1. Baseline Algorithm

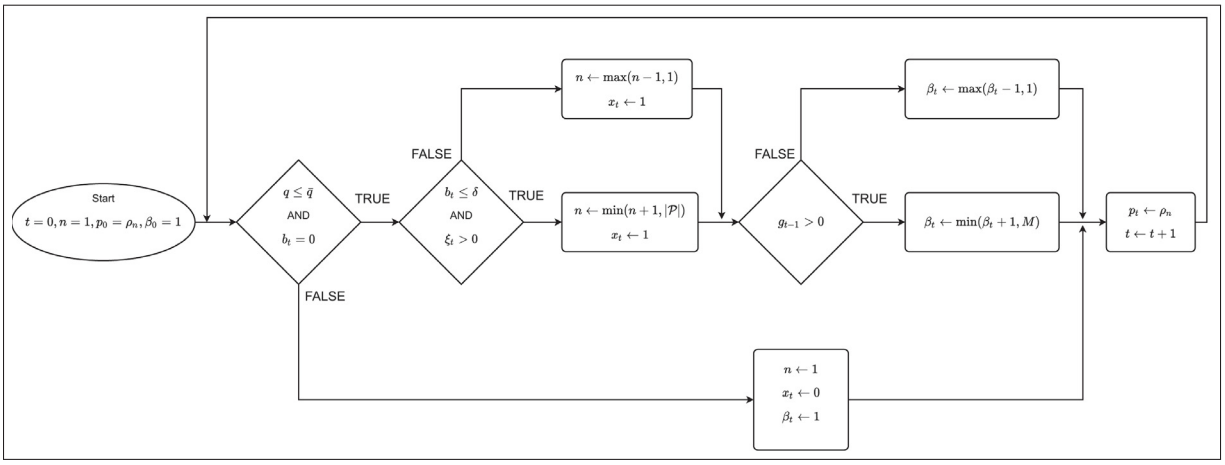

Figure-A III-1 Flowchart of the baseline algorithm

Firstly, each device with packets in the buffer to transmit draws a random number $q \sim U([0, 1])$, and if $q \leq \bar{q}$, where $\bar{q}$ is a congestion control threshold, the device tries to access the channel. This is done to avoid congestion by having all devices trying to access the channel at the same time. Furthermore, if the MTD is currently violating its delay constraints or if there was a dropped packet in the last TTI, the device ramps up its power. Moreover, if at least one packet was successfully transmitted on the last TTI, the MTD assumes it is facing a good channel condition, and it then increases the transmission modulation order. Otherwise, it assumes a bad channel and decreases it. The algorithm is described by the flowchart in Fig. III-1.

2. DNN Architecture and Parameters

One of the requirements is that the DNN must be shallow and relatively small to keep a light memory footprint on the devices and to reduce the computational complexity of the training and inference. We consider a GRU (Cho, van Merriënboer, Bahdanau & Bengio, 2014) connected to a two-layer perceptron. As the observations of the MTD are temporally correlated (through

Table-A III-1 Number of Weights in the DNN

Layer	Number of Weights
GRU	$3[32^2 + 32(4 + N_B N_S) + 32]$
Fully Connected Layers	$2(32^2 + 32)$
Policy Network Head	$66M\|\mathcal{P}\|N_S$
Value Function Network Head	64

the number of packets in the buffer, and the channel gains) we include a GRU in the input to extract information from sequences of states. We employ GRU as it has been shown that they have comparable performance to the more commonly used long short term memory (LSTM) units while being more computationally efficient (Chung, Gülçehre, Cho & Bengio, 2014). In our model, we consider a GRU with $N_B N_S + 4$ inputs, where $N_B N_S$ inputs take the channel state information, and the remaining four are the number of packets in the buffer (b_i), the number of arriving packets (l_i), the goodput on the previous TTI (g_i) and the number of overflown packets in the previous TTI (ξ_i). The GRU unit has 32 output values, while both of the linear layers have 32 inputs and 32 outputs. Finally, the actor head has 32 inputs and $2M|\mathcal{P}|N_S$ outputs (one for each possible action), while the critic head has 32 inputs and one output (the critic value). Table III-1 summarize the number of weights needed for each stage of the network[1]. The networks are trained using an adaptive moment estimation (ADAM) optimizer (Kingma & Ba, 2017) with a learning rate of 7×10^{-4}. At each DNN network update, the weights are trained over 4 PPO epochs with 10 minibatches per epoch. To avoid large gradient updates that make the optimization unstable, the gradients are clipped such that $\|\nabla J_{\mathbf{w}}\| \leq 0.5$. A value loss coefficient $k_1 = 0.5$ and an entropy loss coefficient $k_2 = 0.01$ are used.

[1] We used the values in (Dey & Salem, 2017) to compute the number of weights needed by a GRU.

AUTHOR'S PUBLICATIONS

The author's Ph.D. research output contributed to the following published and submitted research papers.

Escribano, F. J., Wagemakers, A., Kaddoum, G. & Evangelista, J. V. C. (2019). Design and Performance Analysis of an Index Time-Frequency Modulation Scheme for Optical Communications. *IEEE Journal of Selected Topics in Signal Processing*, 13(6), 1403-1416.

Escribano, F. J., Wagemakers, A., Kaddoum, G. & Evangelista, J. V. C. (2020). A Spatial Time-Frequency Hopping Index Modulated Scheme in Turbulence-free Optical Wireless Communication Channels. *IEEE Transactions on Communications*, 68(7), 4437-4450.

Evangelista, J. V. C., Sattar, Z., Kaddoum, G. & Chaaban, A. (2019a). Fairness and Sum-Rate Maximization via Joint Subcarrier and Power Allocation in Uplink SCMA Transmission. *IEEE Transactions on Wireless Communications*, 18(12), 5855-5867.

Evangelista, J. V., Sattar, Z. & Kaddoum, G. (2019b, Nov). Analysis of Contention-Based SCMA in mMTC Networks. *2019 IEEE Latin-American Conference on Communications (LATINCOM)*, pp. 1-6.

Evangelista, J. V., Kaddoum, G. & Sattar, Z. (2021a). Reliability and User-Plane Latency Analysis of mmWave Massive MIMO for Grant-Free URLLC Applications. *arXiv preprint arXiv:2107.08151, Submitted to the IEEE Transactions on Communications*.

Evangelista, J. V., Sattar, Z., Kaddoum, G., Selim, B. & Sarraf, A. (2021b). Intelligent Link Adaptation for Grant-Free Access Cellular Networks: A Distributed Deep Reinforcement Learning Approach. *arXiv preprint arXiv:2107.04145, Submitted to the IEEE Transactions on Wireless Communications*.

Sattar, Z., Evangelista, J. V. C., Kaddoum, G. & Batani, N. (2017, Feb). Analysis of the cell association for decoupled wireless access in a two tier network. *2017 IEEE 28th Annual International Symposium on Personal, Indoor, and Mobile Radio Communications (PIMRC)*, pp. 1-6.

Sattar, Z., Evangelista, J. V. C., Kaddoum, G. & Batani, N. (2019). Spectral Efficiency Analysis of the Decoupled Access for Downlink and Uplink in Two-Tier Network. *IEEE Transactions on Vehicular Technology*, 68(5), 4871-4883.

Sattar, Z., De Carvalho Evangelista, J. V., Kaddoum, G. & Batani, N. (2020a). Full-Duplex Two-Tier Heterogeneous Network With Decoupled Access: Cell Association, Coverage, and Spectral Efficiency Analysis. *IEEE Access*, 8, 172982-172995.

Sattar, Z., Evangelista, J. V. C., Kaddoum, G. & Batani, N. (2020b). Antenna Array Gain and Capacity Improvements of Ultra-Wideband Millimeter Wave Systems Using a Novel Analog Architecture Design. *IEEE Wireless Communications Letters*, 9(3), 289-293.

Selim, B., Alam, M. S., Evangelista, J. V. C., Kaddoum, G. & Agba, B. L. (2020). NOMA-Based IoT Networks: Impulsive Noise Effects and Mitigation. *IEEE Communications Magazine*, 58(11), 69-75.

BIBLIOGRAPHY

3GPP. (2016). *Discussion on the feasibility of advanced MU-detector*.

3GPP. (2017a). *Grant-free transmission for UL URLLC* (Report n°38.213).

3GPP. (2017b). *5G; Study on Scenarios and Requirements for Next Generation Access Technologies* (Report n°38.913).

3GPP. (2017). *TR 38.192 - Study on New Radio (NR) access technology*.

3GPP. (2018a). *Physical layer procedures for control* (Report n°38.213).

3GPP. (2018b). *Study on New Radio (NR) access technology* (Report n°38.912).

3GPP. (2020). *Study on scenarios and requirements for next generation access technologies* (Report n°36.913).

3GPP. (2021a). *5G NR User Equipment (UE) radio transmission and reception; Part 3: Range 1 and Range 2 Interworking operation with other radios* (Report n°38.101).

3GPP. (2021b). *5G NR Physical channels and modulation* (Report n°38.211).

Abedi, M. R., Mokari, N., Javan, M. R. & Jorswieck, E. A. (2018). Single or Multiple Frames Content Delivery for Next-Generation Networks? *ArXiv e-prints*, arXiv:1802.06910.

Abreu, R., Jacobsen, T., Berardinelli, G., Pedersen, K., Kovács, I. Z. & Mogensen, P. (2018). Power control optimization for uplink grant-free URLLC. *IEEE Wireless Communications and Networking Conference*, pp. 1-6.

Adhikary, A., Dhillon, H. S. & Caire, G. (2015). Massive-MIMO meets HetNet: Interference coordination through spatial blanking. *IEEE Journal on Selected Areas in Communications*, 33(6), 1171–1186.

Afify, L. H., ElSawy, H., Al-Naffouri, T. Y. & Alouini, M.-S. (2016). A unified stochastic geometry model for MIMO cellular networks with retransmissions. *IEEE Transactions on Wireless Communications*, 15(12), 8595–8609.

Agrawal, A., Verschueren, R., Diamond, S. & Boyd, S. (2018). A Rewriting System for Convex Optimization Problems. *Journal of Control and Decision*, 5(1), 42–60.

Ahlswede, R. (1973, Sept). Multi-way communication channels. *2nd International Symposium on Information Theory*, pp. 23–51.

Altman, E. (1999). *Constrained Markov Decision Processes*. Chapman and Hall.

Americas, G. (2020). *Understanding mmWave Spectrum for 5G Networks*. 5G Americas.

Andrews, J. G., Bai, T., Kulkarni, M. N., Alkhateeb, A., Gupta, A. K. & Heath, R. W. (2017). Modeling and Analyzing Millimeter Wave Cellular Systems. *IEEE Transactions on Communications*, 65(1), 403-430.

Au, K., Zhang, L., Nikopour, H., Yi, E., Bayesteh, A., Vilaipornsawai, U., Ma, J. & Zhu, P. (2014, Dec). Uplink contention based SCMA for 5G radio access. *IEEE Globecom Workshops*, pp. 900-905.

Au, K., Zhang, L., Nikopour, H., Yi, E., Bayesteh, A., Vilaipornsawai, U., Ma, J. & Zhu, P. (2014, Dec). Uplink contention based SCMA for 5G radio access. *IEEE Globecom Workshops*, pp. 900-905.

Baccelli, F. & Błaszczyszyn, B. (2009). *Stochastic geometry and wireless networks*. Now Publishers Inc.

Baddeley, A., Bárány, I. & Schneider, R. (2007). Spatial Point Processes and their Applications. In Weil, W. (Ed.), *Stochastic Geometry: Lectures given at the C.I.M.E. Summer School held in Martina Franca, Italy, September 13–18, 2004* (pp. 1–75). Berlin, Heidelberg: Springer Berlin Heidelberg.

Bao, J., Ma, Z., Xiao, M., Ding, Z. & Zhu, Z. (2017). Performance Analysis of Uplink SCMA with Receiver Diversity and Randomly Deployed Users. *IEEE Trans. Veh. Technol.*, PP(99), 1-1.

Bjornson, E., Larsson, E. & Lozano, A. (2021, Dec). *16. 6G and the Physical Layer (with Angel Lozano)*. Wireless Future. Retrieved from: https://open.spotify.com/show/0RDeni3rDUx5HnZWJGACqO.

Björnson, E., Hoydis, J. & Sanguinetti, L. (2018). Massive MIMO Has Unlimited Capacity. *IEEE Transacions on Wireless Communications*, 17(1), 574-590.

Bockelmann, C., Pratas, N., Nikopour, H., Au, K., Svensson, T., Stefanovic, C., Popovski, P. & Dekorsy, A. (2016). Massive machine-type communications in 5G: physical and MAC-layer solutions. *IEEE Communications Magazine*, 54(9), 59-65.

Borndörfer, R. & Heismann, O. (2015). The Hypergraph Assignment Problem. *Discret. Optim.*, 15(C), 15–25.

Boyd, S. & Vandenberghe, L. (2004). *Convex Optimization*. New York, NY, USA: Cambridge University Press.

Cai, D., Fan, P. & Mathiopoulos, P. T. (2017). A Tight Lower Bound for the Symbol Error Performance of the Uplink Sparse Code Multiple Access. *IEEE Communication Letters*, 6(2), 190-193.

Chen, Z., Ding, Z., Dai, X. & Zhang, R. (2017). An optimization perspective of the superiority of NOMA compared to conventional OMA. *IEEE Transactions on Signal Processing*, 65(19), 5191–5202.

Cheraghy, M., Chen, W., Tang, H., Wu, Q. & Li, J. (2021). Joint Rate and Fairness Improvement Based on Adaptive Weighted Graph Matrix for Uplink SCMA With Randomly Distributed Users. *IEEE Transactions on Communications*, 69(5), 3106-3118.

Chisci, G., ElSawy, H., Conti, A., Alouini, M.-S. & Win, M. Z. (2019). Uncoordinated massive wireless networks: Spatiotemporal models and multiaccess strategies. *IEEE/ACM Transactions on Networking*, 27(3), 918–931.

Cho, K., van Merriënboer, B., Bahdanau, D. & Bengio, Y. (2014, Oct). On the Properties of Neural Machine Translation: Encoder–Decoder Approaches. *Proceedings of SSST-8, Eighth Workshop on Syntax, Semantics and Structure in Statistical Translation*, pp. 103–111.

Choi, J. (2015). Minimum Power Multicast Beamforming With Superposition Coding for Multiresolution Broadcast and Application to NOMA Systems. *IEEE Transactions on Communications*, 63(3), 791-800.

Choi, J. (2004, Aug.). Low density spreading for multicarrier systems. *8th IEEE International Symposium on Spread Spectrum Techniques and Applications*.

Chung, J., Gülçehre, Ç., Cho, K. & Bengio, Y. (2014). Empirical Evaluation of Gated Recurrent Neural Networks on Sequence Modeling. *arXiv e-prints*, abs/1412.3555, 1–9.

Claus, C. & Boutilier, C. (1998). The Dynamics of Reinforcement Learning in Cooperative Multiagent Systems. *Proceedings of the Fifteenth National/Tenth Conference on Artificial Intelligence/Innovative Applications of Artificial Intelligence*, pp. 746–752.

Clerckx, B., Mao, Y., Schober, R., Jorswieck, E. A., Love, D. J., Yuan, J., Hanzo, L., Li, G. Y., Larsson, E. G. & Caire, G. (2021). Is NOMA Efficient in Multi-Antenna Networks? A Critical Look at Next Generation Multiple Access Techniques. *IEEE Open Journal of the Communications Society*, 2, 1310-1343.

Cover, T. (1972). Broadcast channels. *IEEE Transactions on Information Theory*, 18(1), 2-14.

Cover, T. M. & Thomas, J. A. (2006). *Elements of Information Theory*. Wiley-Interscience.

Cui, J., Fan, P., Lei, X., Ma, Z. & Ding, Z. (2017, June). Downlink Power Allocation in SCMA with Finite-Alphabet Constraints. *IEEE 85th Veh. Technol. Conf.*, pp. 1-5.

Dabiri, M. & Saeedi, H. (2018). Dynamic SCMA Codebook Assignment Methods: A Comparative Study. *IEEE Communication Letters*, 22(2), 364-367.

Dahlman, E., Parkvall, S. & Skold, J. (2018). *5G NR: The Next Generation Wireless Access Technology* (ed. 1st). USA: Academic Press, Inc.

Dey, R. & Salem, F. M. (2017, Aug). Gate-variants of Gated Recurrent Unit (GRU) neural networks. *IEEE 60th International Midwest Symposium on Circuits and Systems*, pp. 1597-1600.

Di, B., Bayat, S., Song, L. & Li, Y. (2015, Dec.). Radio Resource Allocation for Downlink Non-Orthogonal Multiple Access (NOMA) Networks Using Matching Theory. *IEEE Global Communications Conference*, pp. 1-6.

Di, B., Song, L. & Li, Y. (2016, May). Radio resource allocation for uplink sparse code multiple access (SCMA) networks using matching game. *IEEE International Conf. on Communications*, pp. 1-6.

Diamond, S. & Boyd, S. (2016). CVXPY: A Python-Embedded Modeling Language for Convex Optimization. *Journal of Machine Learning Research*, 17(83), 1–5.

Ding, J., Qu, D., Jiang, H. & Jiang, T. (2019). Success Probability of Grant-Free Random Access With Massive MIMO. *IEEE Internet Things J.*, 6(1), 506-516.

Ding, Z., Yang, Z., Fan, P. & Poor, H. V. (2014). On the Performance of Non-Orthogonal Multiple Access in 5G Systems with Randomly Deployed Users. *IEEE Signal Processing Letters*, 21(12), 1501-1505.

Ding, Z., Peng, M. & Poor, H. V. (2015). Cooperative Non-Orthogonal Multiple Access in 5G Systems. *IEEE Communication Letters*, 19(8), 1462-1465.

Ding, Z., Adachi, F. & Poor, H. V. (2016a). The Application of MIMO to Non-Orthogonal Multiple Access. *IEEE Transactions on Wireless Communications*, 15(1), 537-552.

Ding, Z., Fan, P. & Poor, H. V. (2016b). Impact of User Pairing on 5G Nonorthogonal Multiple-Access Downlink Transmissions. *IEEE Transactions on Vehicular Technology*, 65(8), 6010-6023.

Ding, Z., Fan, P. & Poor, H. V. (2017). Random beamforming in millimeter-wave NOMA networks. *IEEE Access*, 5, 7667–7681.

Domahidi, A., Chu, E. & Boyd, S. (2013). ECOS: An SOCP solver for embedded systems. *European Control Conference*, pp. 3071-3076.

El-Taha, M. & Stidham Jr., S. (2012). *Sample-Path Analysis of Queueing Systems*. Springer Science & Business Media.

ElSawy, H. & Hossain, E. (2014). On stochastic geometry modeling of cellular uplink transmission with truncated channel inversion power control. *IEEE Transactions on Wireless Communications*, 13(8), 4454–4469.

Ericsson. (2015). *Ericsson Mobility Report*. Retrieved from: https://www.ericsson.com/assets/local/mobility-report/documents/2015/ericsson-mobility-report-june-2015.pdf.

Evangelista, J. V. C., Sattar, Z. & Kaddoum, G. (2019a). Analysis of Contention-Based SCMA in mMTC Networks. *IEEE Latin-American Conference on Communications*, pp. 1-6.

Evangelista, J. V. C., Sattar, Z., Kaddoum, G. & Chaaban, A. (2019b). Fairness and Sum-Rate Maximization via Joint Subcarrier and Power Allocation in Uplink SCMA Transmission. *IEEE Transactions on Wireless Communications*, 18(12), 5855-5867.

Evangelista, J. V. C., Sattar, Z., Kaddoum, G., Selim, B. & Sarraf, A. (2021, Jul). Intelligent Link Adaptation for Grant-Free Access Cellular Networks: A Distributed Deep Reinforcement Learning Approach.

Foerster, J., Nardelli, N., Farquhar, G., Afouras, T., Torr, P. H. S., Kohli, P. & Whiteson, S. (2017). Stabilising Experience Replay for Deep Multi-Agent Reinforcement Learning. *ICML 2017: Proceedings of the Thirty-Fourth International Conference on Machine Learning*, pp. 1146–1155. Retrieved from: http://arxiv.org/abs/1702.08887.

Foerster, J. N., Assael, Y. M., de Freitas, N. & Whiteson, S. (2016). Learning to Communicate with Deep Multi-Agent Reinforcement Learning. (Nips), 1–9. Retrieved from: http://arxiv.org/abs/1605.06676.

Foerster, J., Farquhar, G., Afouras, T., Nardelli, N. & Whiteson, S. (2018). Counterfactual multiagent policy gradients. *Neural Information Processing Systems*, pp. 2974–2982.

Ford, R., Zhang, M., Mezzavilla, M., Dutta, S., Rangan, S. & Zorzi, M. (2017). Achieving Ultra-Low Latency in 5G Millimeter Wave Cellular Networks. *IEEE Communications Magazine*, 55(3), 196-203.

Forney Jr., G. D. & Wei, L.-F. (1989). Multidimensional Constellations-Part I : Introduction , Figures of Merit, and Generalized Cross Constellations. *IEEE Journal on Selected Areas in Communications*, I(6), 877–892.

Gao, Y. & Dai, L. (2019). Random Access: Packet-Based or Connection-Based? *IEEE Transactions on Wireless Communications*, 18(5), 2664-2678.

Gharbieh, M., ElSawy, H., Bader, A. & Alouini, M.-S. (2017). Spatiotemporal Stochastic Modeling of IoT Enabled Cellular Networks: Scalability and Stability Analysis. *IEEE Transactions on Communications*, 65(8), 3585-3600.

Gharbieh, M., ElSawy, H., Yang, H.-C., Bader, A. & Alouini, M.-S. (2018). Spatiotemporal model for uplink IoT traffic: Scheduling and random access paradox. *IEEE Transactions on Wireless Communications*, 17(12), 8357–8372.

Gharbieh, M., ElSawy, H., Emara, M., Yang, H.-C. & Alouini, M.-S. (2020). Grant-Free Opportunistic Uplink Transmission in Wireless-Powered IoT: A Spatio-Temporal Model. *IEEE Transactions on Communications*, 69(2), 991-1006.

Goldsmith, A. (2005). *Wireless Communications*. New York, NY, USA: Cambridge University Press.

Goodfellow, I., Bengio, Y. & Courville, A. (2016). *Deep Learning* (ed. 1st). MIT Press. Retrieved from: http://www.deeplearningbook.org.

Gradshteyn, I. & Ryzhik, I. (2007). *Table of Integrals, Series and Products* (ed. 7). Elsevier Academic Press.

Haenggi, M. (2012). *Stochastic geometry for wireless networks*. Cambridge University Press.

Haenggi, M. (2013). *Stochastic Geometry for Wireless Networks*. Cambridge University Press.

Hasan, M., Hossain, E. & Niyato, D. (2013). Random access for machine-to-machine communication in LTE-advanced networks: issues and approaches. *IEEE Communications Magazine*, 51(6), 86-93.

Heusse, M., Rousseau, F., Berger-Sabbatel, G. & Duda, A. (2003). Performance Anomaly of 802.11b. *IEEE International Conference on Computer Communications*, pp. 836–843.

Hirzallah, M., Krunz, M., Kecicioglu, B. & Hamzeh, B. (2020). 5G New Radio Unlicensed: Challenges and Evaluation. *IEEE Transactions on Cognitive Communications and Networking*, 1-1.

Hmamouche, Y., Benjillali, M., Saoudi, S., Yanikomeroglu, H. & Renzo, M. D. (2021). New Trends in Stochastic Geometry for Wireless Networks: A Tutorial and Survey. *Proceedings of the IEEE*, 109(7), 1200-1252.

Hong, M., Wang, X., Razaviyayn, M. & Luo, Z.-Q. (2017). Iteration complexity analysis of block coordinate descent methods. *Mathematical Programming*, 163(1), 85–114.

Hoymann, C., Astely, D., Stattin, M., Wikstrom, G., Cheng, J., Hoglund, A., Frenne, M., Blasco, R., Huschke, J. & Gunnarsson, F. (2016). LTE release 14 outlook. *IEEE Communications Magazine*, 54(6), 44-49.

Huang, R., Wong, V. W. S. & Schober, R. (2019). Throughput Optimization in Grant-Free NOMA with Deep Reinforcement Learning. *IEEE Global Communications Conference*, pp. 1-6.

ITU. (2015). *IMT Vision–Framework and overall objectives of the future development of IMT for 2020 and beyond*.

Jacobsen, T., Abreu, R., Berardinelli, G., Pedersen, K., Mogensen, P., Kovács, I. Z. & Madsen, T. K. (2017, Jan). System level analysis of uplink grant-free transmission for URLLC. *IEEE Globecom Workshops*, pp. 1–6.

Jacquelin, A., Vilgelm, M. & Kellerer, W. (2019). Grant-Free Access with Multipacket Reception: Analysis and Reinforcement Learning Optimization. *Conference on Wireless On-demand Network Systems and Services*, pp. 83-90.

Jiang, N., Deng, Y., Kang, X. & Nallanathan, A. (2018a). Random Access Analysis for Massive IoT Networks Under a New Spatio-Temporal Model: A Stochastic Geometry Approach. *IEEE Transactionc on Communications*, 66(11), 5788-5803.

Jiang, N., Deng, Y., Nallanathan, A., Kang, X. & Quek, T. Q. S. (2018b). Analyzing Random Access Collisions in Massive IoT Networks. *IEEE Transactions on Wireless Communications*, 17(10), 6853-6870.

Karadag, G., Gul, R., Sadi, Y. & Coleri Ergen, S. (2019). QoS-Constrained Semi-Persistent Scheduling of Machine-Type Communications in Cellular Networks. *IEEE Transactions on Wireless Communications*, 18(5), 2737-2750.

Kim, J., Yi, J. & Bahk, S. (2020). Uplink Channel Access Enhancement for Cellular Communication in Unlicensed Spectrum. *IEEE Access*, 8, 216386-216397.

Kim, J., Lee, G., Kim, S., Taleb, T., Choi, S. & Bahk, S. (2021). Two-Step Random Access for 5G System: Latest Trends and Challenges. *IEEE Networks Magazine*, 35(1), 273-279.

Kingma, D. P. & Ba, J. (2017). Adam: A Method for Stochastic Optimization.

Lai, K., Lei, J., Deng, Y., Wen, L. & Chen, G. (2021). Analyzing Uplink Grant-free Sparse Code Multiple Access System in Massive IoT Networks. *arXiv preprint arXiv:2103.10241*, 1–14.

Lan, T., Kao, D., Chiang, M. & Sabharwal, A. (2010, Mar.). An Axiomatic Theory of Fairness in Network Resource Allocation. *Proc. IEEE INFOCOM*, pp. 1-9.

Larsson, E. G., Edfors, O., Tufvesson, F. & Marzetta, T. L. (2014). Massive MIMO for next generation wireless systems. *IEEE Communications Magazine*, 52(2), 186-195.

Laya, A., Alonso, L. & Alonso-Zarate, J. (2014). Is the Random Access Channel of LTE and LTE-A Suitable for M2M Communications? A Survey of Alternatives. *IEEE Communications Surveys and Tutorials*, 16(1), 4-16.

Le, M. T. P., Ferrante, G. C., Quek, T. Q. S. & Di Benedetto, M. (2018). Fundamental Limits of Low-Density Spreading NOMA With Fading. *IEEE Transactions on Wireless Communications*, 17(7), 4648-4659.

Lee, G., Sung, Y. & Seo, J. (2015). Randomly-directional beamforming in millimeter-wave multiuser MISO downlink. *IEEE Transactions on Wireless Communications*, 15(2), 1086–1100.

Lee, N., Morales-Jimenez, D., Lozano, A. & Heath, R. W. (2014). Spectral efficiency of dynamic coordinated beamforming: A stochastic geometry approach. *IEEE Transactions on Wireless Communications*, 14(1), 230–241.

Li, Z., Chen, W., Wei, F., Wang, F., Xu, X. & Chen, Y. (2016, July). Joint codebook assignment and power allocation for SCMA based on capacity with Gaussian input. *IEEE/CIC International Conf. on Communications in China*, pp. 1-6.

Lim, S., Kim, N. & Park, H. (2017). Uplink SCMA System With Multiple Antennas. *IEEE Transactions on Vehicular Technologies*, 66(8), 6982-6992.

Liu, J., Sheng, M., Liu, L., Shi, Y. & Li, J. (2017). Modeling and Analysis of SCMA Enhanced D2D and Cellular Hybrid Network. *IEEE Transactions on Communications*, 65(1), 173-185.

Liu, J., Wu, G., Zhang, X., Fang, S. & Li, S. (2020). Modeling, Analysis, and Optimization of Grant-Free NOMA in Massive MTC via Stochastic Geometry. *arxiv e-prints*, 4389–4402.

Liu, L., Larsson, E. G., Yu, W., Popovski, P., Stefanovic, C. & de Carvalho, E. (2018). Sparse Signal Processing for Grant-Free Massive Connectivity: A Future Paradigm for Random Access Protocols in the Internet of Things. *IEEE Signal Processing Magazine*, 35(5), 88-99.

Liu, L., Sheng, M., Liu, J., Wang, X. & Li, J. (2018). Success Probability and Area Spectral Efficiency in SCMA Wireless Networks. *IEEE Transactions on Vehicular Technologies*, 67(8), 7764-7768.

Liu, Y., Deng, Y., Zhou, H., Elkashlan, M. & Nallanathan, A. (2021). A General Deep Reinforcement Learning Framework for Grant-Free NOMA Optimization in mURLLC. *arXiv preprint arXiv:2101.00515*, 1–31.

Liu, Y., Pan, G., Zhang, H. & Song, M. (2016). On the capacity comparison between MIMO-NOMA and MIMO-OMA. *IEEE Access*, 4, 2123–2129.

Lowe, R., Wu, Y., Tamar, A., Harb, J. & Abbeel, P. (2017). Multi-Agent Actor-Critic for Mixed Cooperative-Competitive Environments. *Neural Information Processing Systems*, pp. 6379–6390.

Lu, L., Li, G. Y., Swindlehurst, A. L., Ashikhmin, A. & Zhang, R. (2014). An Overview of Massive MIMO: Benefits and Challenges. *IEEE Journal on Selected Topics in Signal Processing*, 8(5), 742-758.

Lu, W. & Di Renzo, M. (2015, Nov). Stochastic geometry modeling of cellular networks: Analysis, simulation and experimental validation. *Proceedings of the 18th ACM International Conference on Modeling, Analysis and Simulation of Wireless and Mobile Systems*, pp. 179–188.

Lu, X., Petrov, V., Moltchanov, D., Andreev, S., Mahmoodi, T. & Dohler, M. (2019). 5G-U: Conceptualizing Integrated Utilization of Licensed and Unlicensed Spectrum for Future IoT. *IEEE Communications Magazine*, 57(7), 92-98.

Lu, X., Salehi, M., Haenggi, M., Hossain, E. et al. (2021). Stochastic geometry analysis of spatial-temporal performance in wireless networks: A tutorial. *arXiv preprint arXiv:2102.00588*, 1–49.

Luo, L., Li, L. & Su, X. (2017, Jan). Optimization of resource allocation in relay assisted multi-user SCMA uplink network. *International Conf. on Computing, Networking and Communications*, pp. 282-286.

Machina Research. (2015). *M2M growth necessitates a new approach to network planning and optimisation*.

Madani, O., Hanks, S. & Condon, A. (1999). On the Undecidability of Probabilistic Planning and Infinite-Horizon Partially Observable Markov Decision Problems. *AAAI '99/IAAI '99*, pp. 541–548.

Mahmood, N. H., Abreu, R., Böhnke, R., Schubert, M., Berardinelli, G. & Jacobsen, T. H. (2019). Uplink Grant-Free Random Access Solutions for URLLC services in 5G New Radio.

Maldonado, R., Rosa, C. & Pedersen, K. I. (2020). Latency and Reliability Analysis of Cellular Networks in Unlicensed Spectrum. *IEEE Access*, 8, 49412-49423.

Mao, Y., Clerckx, B. & Li, V. O. (2018). Rate-splitting multiple access for downlink communication systems: bridging, generalizing, and outperforming SDMA and NOMA. *EURASIP journal on wireless communications and networking*, 2018(1), 1–54.

Mao, Y., Clerckx, B. & Li, V. O. K. (2019, May). Rate-Splitting Multiple Access for Coordinated Multi-Point Joint Transmission. *IEEE International Conference on Communications Workshops*, pp. 1-6.

Marsden, J. E., Hoffman, M. J. et al. (1993). *Elementary classical analysis*. Macmillan.

Marzetta, T. L., Larsson, E. G., Yang, H. & Ngo, H. Q. (2016). *Fundamentals of Massive MIMO*. Cambridge University Press.

Mastronarde, N. & van der Schaar, M. (2013). Joint Physical-Layer and System-Level Power Management for Delay-Sensitive Wireless Communications. *IEEE Transactions on Mobile Computing*, 12(4), 694-709.

Mastronarde, N., Modares, J., Wu, C. & Chakareski, J. (2016). Reinforcement Learning for Energy-Efficient Delay-Sensitive CSMA / CA Scheduling. *IEEE Global Communications Conference*, pp. 1–7.

Matignon, L., Laurent, G. J. & Le Fort-Piat, N. (2012). Independent Reinforcement Learners in Cooperative Markov Games: A Survey Regarding Coordination Problems. *Knowl. Eng. Rev.*, 27(1), 1-–31.

McEliece, R. J., MacKay, D. J. C. & Cheng, J.-F. (1998). Turbo decoding as an instance of Pearl's 'belief propagation' algorithm. *IEEE Journal on Selected Areas in Communications*, 16(2), 140-152.

Mezzavilla, M., Zhang, M., Polese, M., Ford, R., Dutta, S., Rangan, S. & Zorzi, M. (2018). End-to-end simulation of 5G mmWave networks. *IEEE Communications Surveys & Tutorials*, 20(3), 2237–2263.

Mnih, V., Badia, A. P., Mirza, M., Graves, A., Lillicrap, T., Harley, T., Silver, D. & Kavukcuoglu, K. (2016, 6). Asynchronous Methods for Deep Reinforcement Learning. *Proceedings of Machine Learning Research*, pp. 1928–1937.

Mokdad, A., Azmi, P., Mokari, N., Moltafet, M. & Ghaffari-Miab, M. (2019). Cross-Layer Energy Efficient Resource Allocation in PD-NOMA Based H-CRANs: Implementation via GPU. *IEEE Transactions on Mobile Computing*, 18(6), 1246-1259.

Moltafet, M., Azmi, P., Mokari, N., Javan, M. R. & Mokdad, A. (2018). Optimal and Fair Energy Efficient Resource Allocation for Energy Harvesting-Enabled-PD-NOMA-Based HetNets. *IEEE Transactions on Wireless Communications*, 17(3), 2054-2067.

Moltafet, M., Mokari, N., Javan, M. R., Saeedi, H. & Pishro-Nik, H. (2018a). A New Multiple Access Technique for 5G: Power Domain Sparse Code Multiple Access (PSMA). *IEEE Access*, 6, 747-759.

Moltafet, M., Yamchi, N. M., Javan, M. R. & Azmi, P. (2018b). Comparison Study Between PD-NOMA and SCMA. *IEEE Transactions on Vehicular Technologies*, 67(2), 1830-1834.

Nesterov, Y. and Nemirovskii, A. (1994). *Interior-Point Polynomial Algorithms in Convex Programming*. Society for Industrial and Applied Mathematics.

Neyman, A. & Sorin, S. (2003). *Stochastic Games and Applications*. Kluwer Academic Publishers.

Nguyen, T. M., Jeong, Y., Quek, T. Q., Tay, W. P. & Shin, H. (2013). Interference alignment in a Poisson field of MIMO femtocells. *IEEE Transactions on Wireless Communications*, 12(6), 2633–2645.

Nikopour, H. & Baligh, H. (2013, Sept). Sparse code multiple access. *IEEE 24th Annual International Symposium on Personal, Indoor, and Mobile Radio Communications*, pp. 332-336.

Nikopour, H., Yi, E., Bayesteh, A., Au, K., Hawryluck, M., Baligh, H. & Ma, J. (2014, Dec). SCMA for downlink multiple access of 5G wireless networks. *IEEE Global Communications Conference*, pp. 3940-3945.

Nocedal, J. & Wright, S. J. (2006). *Numerical Optimization* (ed. second). New York, NY, USA: Springer.

Oliehoek, F. A. & Amato, C. (2016). *A Concise Introduction to Decentralized POMDPs*. Springer Publishing Company, Incorporated.

Omidshafiei, S., Pazis, J., Amato, C., How, J. P. & Vian, J. (2017). Deep Decentralized Multi-task Multi-Agent Reinforcement Learning under Partial Observability. *International Conference on Machine Learning*, 70, 2681–2690.

Parida, P. & Das, S. S. (2014, Dec.). Power allocation in OFDM based NOMA systems: A DC programming approach. *2014 IEEE Globecom Workshops*, pp. 1026-1031.

Patzold, M. (2012). *Mobile Radio Channels*. Wiley Publishing.

Proakis, J. G. (2007). *Digital Communications*. McGraw-Hill.

Puterman, M. L. (2014). *Markov decision processes: discrete stochastic dynamic programming*. John Wiley & Sons.

Qian, L. P. & Zhang, Y. J. (2010). S-MAPEL: Monotonic optimization for non-convex joint power control and scheduling problems. *IEEE Transaction on Wireless Communications*, 9(5), 1708-1719.

Qian, L. P., Wu, Y., Zhou, H. & Shen, X. (2017). Joint Uplink Base Station Association and Power Control for Small-Cell Networks With Non-Orthogonal Multiple Access. *IEEE Transactions on Wireless Communications*, 16(9), 5567-5582.

Rangan, S., Rappaport, T. S. & Erkip, E. (2014). Millimeter-Wave Cellular Wireless Networks: Potentials and Challenges. *IEEE Proceedings*, 102(3), 366-385.

Rappaport, T. S., Sun, S., Mayzus, R., Zhao, H., Azar, Y., Wang, K., Wong, G. N., Schulz, J. K., Samimi, M. & Gutierrez, F. (2013). Millimeter Wave Mobile Communications for 5G Cellular: It Will Work! *IEEE Access*, 1, 335-349.

Razaviyayn, M., Hong, M. & Luo, Z.-Q. (2013). A Unified Convergence Analysis of Block Successive Minimization Methods for Nonsmooth Optimization. *SIAM Journal on Optimization*, 23(2), 1126-1153.

Razaviyayn, M. (2014). *Successive Convex Approximation : Analysis and Applications*. (Ph.D. thesis, University of Minnesota, Minneapolis, MN).

Roh, W., Seol, J.-Y., Park, J., Lee, B., Lee, J., Kim, Y., Cho, J., Cheun, K. & Aryanfar, F. (2014). Millimeter-wave beamforming as an enabling technology for 5G cellular communications: Theoretical feasibility and prototype results. *IEEE communications magazine*, 52(2), 106–113.

Sattar, Z., Evangelista, J. V. C., Kaddoum, G. & Batani, N. (2017, Feb). Analysis of the cell association for decoupled wireless access in a two tier network. *IEEE 28th Annual International Symposium on Personal, Indoor, and Mobile Radio Communications*, pp. 1-6.

Sattar, Z., Evangelista, J. V. C., Kaddoum, G. & Batani, N. (2019a). Antenna Array Gain and Capacity Improvements of Ultra-Wideband Millimeter Wave Systems Using a Novel Analog Architecture Design. *IEEE Wireless Commun. Lett.*, 9(3), 289-293.

Sattar, Z., Evangelista, J. V. C., Kaddoum, G. & Batani, N. (2019b). Spectral Efficiency Analysis of the Decoupled Access for Downlink and Uplink in Two-Tier Network. *IEEE Transactions on Vehicular Technology*, 68(5), 4871-4883.

Schilcher, U., Toumpis, S., Haenggi, M., Crismani, A., Brandner, G. & Bettstetter, C. (2016). Interference Functionals in Poisson Networks. *IEEE Transactions on Information Theory*, 62(1), 370-383.

Schulman, J., Wolski, F., Dhariwal, P., Radford, A. & Klimov, O. (2005). Proximal Policy Optimization Algorithms. *arXiv*, pp. 1–12.

Schulman, J., Levine, S., Abbeel, P., Jordan, M. & Moritz, P. (2015, 6). Trust Region Policy Optimization. *International Conference on Machine Learning*, pp. 1889–1897.

Serrano, S. A. (2015). *Algorithms for unsymmetric cone optimization and an implementation for problems with the exponential cone*. (Ph.D. thesis, Stanford University, Institute for Computational and Mathematical Engineering).

Shental, O., Zaidel, B. M. & Shitz, S. S. (2017, June). Low-density code-domain NOMA: Better be regular. *2017 IEEE International Symposium on Information Theory*, pp. 2628-2632.

Singh, B., Tirkkonen, O., Li, Z. & Uusitalo, M. A. (2018). Contention-Based Access for Ultra-Reliable Low Latency Uplink Transmissions. *IEEE Communication Letters*, 7(2), 182-185.

Song, H., Cui, Q., Gu, Y., Stüber, G. L., Li, Y., Fei, Z. & Guo, C. (2019). Cooperative LBT Design and Effective Capacity Analysis for 5G NR Ultra Dense Networks in Unlicensed Spectrum. *IEEE Access*, 7, 50265-50279.

Sun, Q., Han, S., I, C. L. & Pan, Z. (2015). On the Ergodic Capacity of MIMO NOMA Systems. *IEEE Wireless Communication Letters*, 4(4), 405-408.

Sun, Y., Ng, D. W. K., Ding, Z. & Schober, R. (2016, Dec.). Optimal Joint Power and Subcarrier Allocation for MC-NOMA Systems. *IEEE Global Communications Conference*, pp. 1-6.

Sutton, R. S. & Barto, A. G. (2018). *Reinforcement Learning: An Introduction* (ed. 2nd). Cambridge (Mass.): The MIT Press.

Taherzadeh, M., Nikopour, H., Bayesteh, A. & Baligh, H. (2014, Sept). SCMA Codebook Design. *IEEE 80th Veh. Technol. Conf.*, pp. 1-5.

Tanbourgi, R., Dhillon, H. S. & Jondral, F. K. (2015). Analysis of joint transmit–receive diversity in downlink MIMO heterogeneous cellular networks. *IEEE Transactions on Wireless Communications*, 14(12), 6695–6709.

Thornburg, A., Bai, T. & Heath, R. W. (2016). Performance Analysis of Outdoor mmWave Ad Hoc Networks. *IEEE Transactions on Signal Processing*, 64(15), 4065-4079.

Vaezi, M., Baduge, G. A. A., Liu, Y., Arafa, A., Fang, F. & Ding, Z. (2019). Interplay between NOMA and other emerging technologies: A survey. *IEEE Transactions on Cognitive Communications and Networking*, 5(4), 900–919.

van de Beek, J. & Popovic, B. M. (2009, Nov.). Multiple Access with Low-Density Signatures. *IEEE Global Telecommunications Conference*, pp. 1-6.

Vilgelm, M., Schiessl, S., Al-Zubaidy, H., Kellerer, W. & Gross, J. (2018, May). On the Reliability of LTE Random Access: Performance Bounds for Machine-to-Machine Burst Resolution Time. *IEEE International Conference on Communications*, pp. 1-7.

Wang, B., Wang, K., Lu, Z., Xie, T. & Quan, J. (2015, June). Comparison study of non-orthogonal multiple access schemes for 5G. *IEEE International Symposium on Broadband Multimedia Systems and Broadcasting*, pp. 1-5.

Watkins, C. J. C. H. & Dayan, P. (1992). Q-learning. *Machine Learning*, 8(3-4), 279–292.

Wei, F. & Chen, W. (2017). Low Complexity Iterative Receiver Design for Sparse Code Multiple Access. *IEEE Transactions on Communications*, 65(2), 621-634.

Wei, Z., Ng, D. W. K. & Yuan, J. (2016, Dec.). Power-Efficient Resource Allocation for MC-NOMA with Statistical Channel State Information. *2016 IEEE Global Communications Conference*, pp. 1-7.

Wei, Z., Yang, L., Ng, D. W. K., Yuan, J. & Hanzo, L. (2019). On the performance gain of NOMA over OMA in uplink communication systems. *IEEE Transactions on Communications*, 68(1), 536–568.

Xue, T., Qiu, L. & Li, X. (2016, Sept). Resource Allocation for Massive M2M Communications in SCMA Network. *IEEE 84th Veh. Technol. Conf.*, pp. 1-5.

Yang, Z., Lei, X., Ding, Z., Fan, P. & Karagiannidis, G. K. (2017). On the Uplink Sum Rate of SCMA System With Randomly Deployed Users. *IEEE Communication Letters*, 6(3), 338-341.